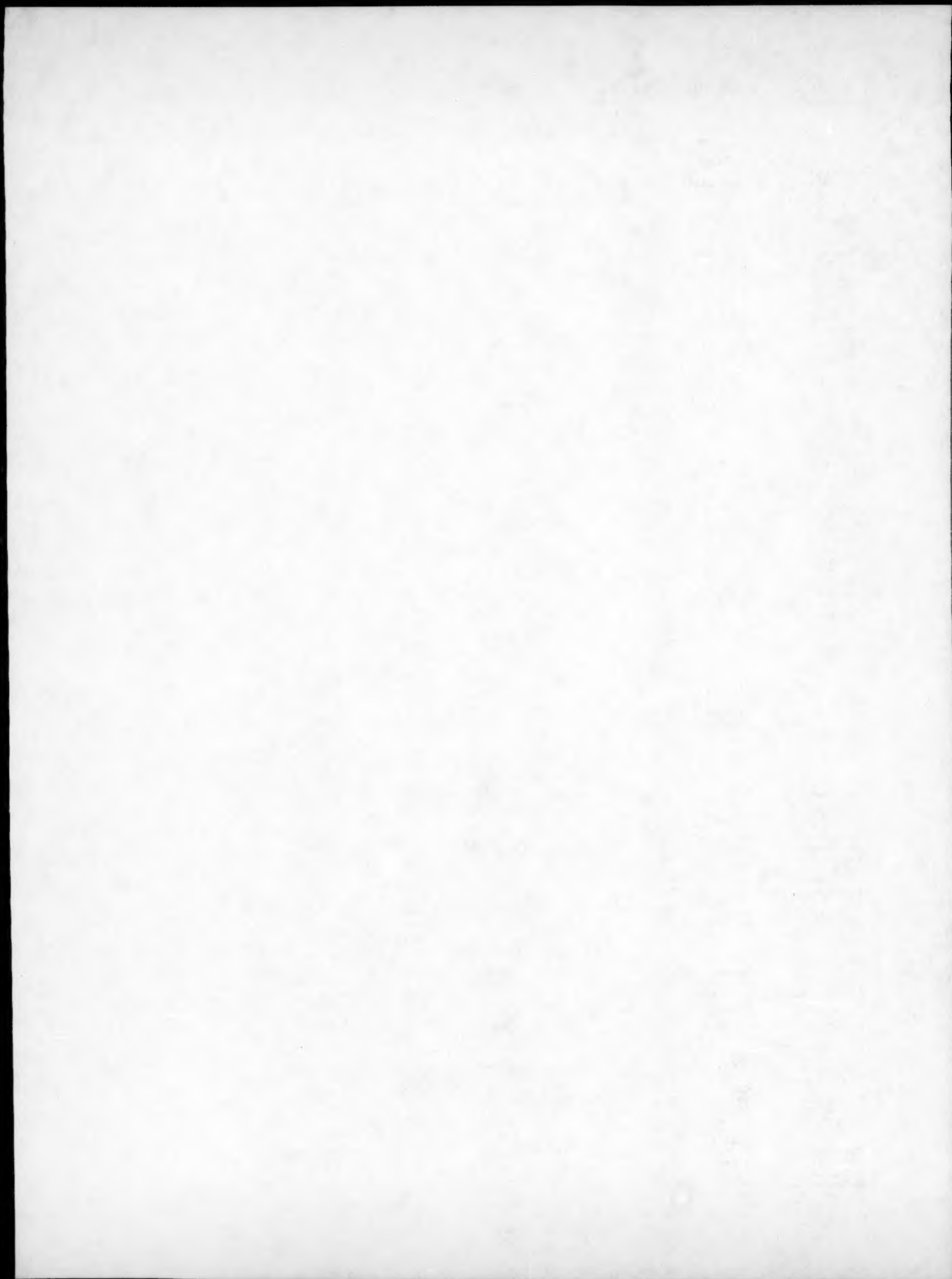


Combined Author Index

- Aaronson, H.I. 1381-1384A
1385-1397A
1399-1407A
1703-1715A
1095-1100A
742A
Aballe, M. 2139-2152A
Abbas, M. 1523-1527A
Abbaschian, G.J. 2063-2073A
Abdel-Hamid, A.A. 349-351A
Abe, H. 617-620A
Abis, S. 209-216B
Adachi, K. 945-959A
Adachi, M. 221-229A
Adams, B.L. 2199-2207A
513-517A
Adamson, M.G. 2090-2093A
Adler, P.H. 1725-1737A
Adler, P.N. 635-643A
Agarwal, R.K. 615-620B
Agren, J. 607-615A
617-620A
2083-2084A
Aifantis, E.C. 1637-1640A
Akers, F. 647-656B
Akselsen, O.M. 1529-1538A
Alam, M. 565-574B
Allemand, C.D. 1851-1863A
Allen, S.M. 2239-2247A
Altstetter, C.J. 2086-2090A
An, T.S. 331-337A
An, Z.Z. 331-337A
Angers, R. 37-44A
Ankem, S. 2209-2226A
Antolovich, S.D. 173-180A
Apelian, D. 2049-2062A
Arai, K.I. 1295-1299A
Arnberg, L. 1657-1664A
2077-2080A
Arsenault, R.J. 379-389A
Asaki, Z. 639-645B
367-373B
Awakura, Y. 621-627B
19-28B
41-50B
- Badini, C. 1665-1669A
Baile, C.W. 1057-1063A
1211-1215A
267-270B
Ballester, A. 2127-2137A
Banerji, A. 405-413B
Barnes, H.L. 1075-1080A
Barrailler, V. 479-485B
Batterham, R.J. 259-265B
Bautista, R.G. 1421-1428A
Bayuzick, R.J. 973-981A
307-316B
781-790A
Benderaky, L.A. 2117-2125A
Benlyamani, M. 647-656B
Bentley, A.P. 1593-1600A
Bernstein, I.M. 1633-1637A
Bertram, L.A. 357-365B
Biancaniello, F.S. 2117-2125A
Bibby, M. 587-600B
Bird, J.E. 1537-1546A
Blanchard, W.K. 1081-1086A
Blander, M. 805-815B
Bobowiec, P. 195-203A
Boettinger, W.J. 2117-2125A
781-790A
923-932A
231-241A
Bowman, R.R. 173-180A
Boyd, W.K. 1601-1610A
Briant, C.L. 2084-2086A
Bricknell, R.H. 583-591A
Brimacombe, J.K. 1493-1503A
677-685B
1061-1066A
665-676B
347-356B
Brown, E.L. 31-38A
Buschow, K.H.J. 777-780A
Bustos, A.A. 677-685B
Butler, E.P. 163-167A
- 1673-1675A
823-832A
267-270B
1481-1483A
1985-1993A
1647-1656A
1955-1966A
1977-1984A
137-149A
- Caceres, C.H. 1673-1675A
Cahoon, J.R. 823-832A
Calvo, F.A. 267-270B
Cameron, T.B. 1481-1483A
Cantor, B. 1985-1993A
Carlson, O.N. 1647-1656A
1955-1966A
1977-1984A
Carter, J.P. 137-149A
- Cassagne, T.B. 703-710A
Cathles, L.M. 405-413B
Chan, A.H. 491-496B
Chan, K.S. 1739-1750A
Chandrasekaran, M. 2153-2161A
Chang, K.-M. 1685-1692A
Chang, S.C. 1485-1487A
Chang, Y.A. 133-148B
1104-1106A
1361-1372A
1373-1380A
1241-1245A
785-799B
2227-2237A
51-80B
415-423B
65-72A
107-114A
Cheng, J.-J.A. 2049-2062A
Chhabra, R.P. 355-358A
Cho, E.H. 745-753B
Cho, S.-J. 2175-2182A
Chou, T.-W. 1051-1055A
1547-1559A
1995-2006A
711-716A
717-725A
1361-1372A
1373-1380A
1632-1633A
1001-1009A
2107-2116A
2035-2047A
791-798A
503-514B
1250-1253A
Colinet, C. 777-780A
Collier, J.P. 651-661A
Colmenares, C.A. 911-914A
Colwell, J.A. 1065-1074A
Corbett, J.M. 1611-1623A
Courtney, T.H. 1165-1171A
Couture, A. 37-44A
Covino, B.S., Jr. 137-149A
Craven, S.M. 351-355A
Cruells, M. 443-448B
Curreri, P.A. 2301-2303A
1121-1130A
- Daehn, G.S. 2295-2298A
Dahmen, U. 807-814A
Dai, L. 799-806A
Dalyuk, S. 663-668A
Darmann, C. 1301-1312A
Dayananda, M.A. 362-364A
983-990A
189-194A
de Fontaine, D. 1671-1683A
de Jonckere, A. 1131-1138A
Dean, D.C. 595-574B
Decker, R.F. 5-30A
Dharwadkar, H.N. 553-564B
Diebold, T.P. 374A
Doherty, R.D. 2049-2062A
Dowling, J.M. 1611-1623A
Driscoll, T.J. 137-149A
Droste, W. 833-844B
Dubke, M. 119-131B
Dugas, H. 1250-1253A
Dunlap, J.W. 205-213A
Dunlop, G.L. 45-52A
Dunn, G.J. 1851-1863A
1865-1871A
657-663B
339-347A
Durand, F. 349-351A
Dutrizac, J.E. 5-17B
- Eagar, T.W. 735-744B
879-885B
887-901B
601-607B
1851-1863A
1885-1871A
781-790A
405-413B
2093-2097A
1921-1934A
Edwards, G.R. 374A
El-Kaddah, N. 687-693B
El-Rahaiby, S.K. 307-316B
Elliott, J.F. 1461-1469A
147-157B
400B
2093-2097A
833-844B
1381-1384A
1385-1397A
1399-1407A
- Era, H. 621-633A
Ernst, S.C. 2227-2237A
Espil, F. 443-448B
Evans, N.D. 1421-1428A
973-981A
1935-1947A
549-559A
271-280A
- Eylon, D. 315-323A
1447-1453A
77-85B
229-231B
687-693B
2239-2247A
1809-1823A
2187-2198A
815-822A
2163-2173A
379-389A
1121-1130A
703-710A
357-365B
914-918B
961-966A
861-867A
869-875A
243-252A
889-898A
1935-1947A
549-559A
271-280A
797-804B
317-322B
397-399B
491-496B
535-540B
541-545B
415-423B
799-806A
967-972A
923-932A
1751-1755A
- Fang, K. 315-323A
Fang, T.-T. 1447-1453A
Farias, L.R. 77-85B
229-231B
687-693B
2239-2247A
1809-1823A
2187-2198A
815-822A
2163-2173A
379-389A
1121-1130A
703-710A
357-365B
914-918B
961-966A
861-867A
869-875A
243-252A
889-898A
1935-1947A
549-559A
271-280A
797-804B
317-322B
397-399B
491-496B
535-540B
541-545B
415-423B
799-806A
967-972A
923-932A
1751-1755A
- Fautrelle, Y. 315-323A
Ference, T.G. 1447-1453A
Fernández Guíllarmet, 77-85B
1809-1823A
2187-2198A
815-822A
2163-2173A
379-389A
1121-1130A
703-710A
357-365B
914-918B
961-966A
861-867A
869-875A
243-252A
889-898A
1935-1947A
549-559A
271-280A
797-804B
317-322B
397-399B
491-496B
535-540B
541-545B
415-423B
799-806A
967-972A
923-932A
1751-1755A
- Fruehan, R.J. 797-804B
317-322B
397-399B
491-496B
535-540B
541-545B
415-423B
799-806A
967-972A
923-932A
1751-1755A
- Fuerstenau, M.C. 491-496A
Fukatsu, N. 1876-1877A
Fultz, B. 791-798B
Funkbusch, A.W. 771-776B
Funkbusch, P.D. 307-316B
- Gabb, T.P. 491-496A
497-505A
507-512A
1885-1890A
2075-2077A
2249-2253A
669-678A
1876-1877A
791-798B
771-776B
307-316B
- Gayda, J. 491-496A
497-505A
507-512A
1885-1890A
2075-2077A
2249-2253A
669-678A
1876-1877A
791-798B
771-776B
307-316B
- Gedeon, S.A. 491-496A
497-505A
507-512A
1885-1890A
2075-2077A
2249-2253A
669-678A
1876-1877A
791-798B
771-776B
307-316B
- Gerin, F. 1671-1683A
Gerlach, U. 435-442A
German, R.M. 205-213A
903-906A
553-564B
461-469B
419-428A
347-356B
- Ghosh, A. 1665-1669A
Ghosh, D.N. 317-322B
Giamei, A.F. 657-663B
687-702A
1625-1629A
742-745A
587-600B
1131-1138A
183-167A
657-663B
915-921A
739-741A
1529-1538A
1797-1807A
1250-1253A
691-696A
45-52A
87-103B
725-733B
449-459B
695-703B
- Gianoglio, C. 1665-1669A
Glaws, P.C. 317-322B
Gleitner, C. 657-663B
Goel, N.C. 687-702A
Gokhale, A.M. 1625-1629A
742-745A
587-600B
1131-1138A
183-167A
657-663B
915-921A
739-741A
1529-1538A
1797-1807A
1250-1253A
691-696A
45-52A
87-103B
725-733B
449-459B
695-703B
- Goldak, J. 587-600B
Goldstein, J.I. 1131-1138A
183-167A
657-663B
915-921A
739-741A
1529-1538A
1797-1807A
1250-1253A
691-696A
45-52A
87-103B
725-733B
449-459B
695-703B
- Gougeon, M. 657-663B
Grabke, H.J. 915-921A
Gregor, R.B. 739-741A
Gronq, Ø. 1529-1538A
1797-1807A
1250-1253A
691-696A
45-52A
87-103B
725-733B
449-459B
695-703B
- Gruziecki, J.E. 1250-1253A
Guimarães, J.R.C. 691-696A
Gustafsson, G. 45-52A
Guthrie, R.L.L. 87-103B
725-733B
449-459B
695-703B
- Gutierrez, E.M. 695-703B
- Ha, K.F. 331-337A
Haasen, P. 742A
Hack, J.E. 1739-1750A
Hahn, G.T. 1561-1572A
Hall, E.L. 1685-1692A
407-417A
- Hall, I.W. 1075-1080A
Hammond, C. 93-106A
Han, J.K. 2097-2098A
415-423B
425-432B
Hanada, S. 1409-1420A
Handa, M. 2031-2034A
Hannula, S.-P. 1757-1767A
Hansen, N. 253-259A
Harrison, R. 357-365B
Hawbolt, E.B. 1493-1503A
Hayes, P.C. 375-381B
383-393B
Headley, T.J. 2107-2116A
2035-2047A
983-990A
1891-1905A
1081-1086A
507-512A
247-257B
29-39B
645-650A
Hetherington, M.G. 1629-1632A
Hicks, P.D. 1837-1849A
Hillert, M. 1878-1879A
741A
Hino, M. 755-761B
913-914B
Hintz, M.B. 1081-1086A
Hirato, T. 19-28B
Hirono, S. 69-76B
41-50B
791-798A
933-944A
1485-1487A
621-633A
399-405A
1421-1428A
973-981A
215-220A
1505-1515A
1573-1575A
House, R. 587-600B
Howe, J.M. 593-605A
Hsiao, C.-M. 711-716A
717-725A
133-146B
1104-1108A
1373-1380A
1561-1572A
1885-1890A
407-417A
2084-2086A
575-586B
Hwang, N.-M. 1429-1431A
Hyzak, J.M. 1876-1877A
- Huang, Q. 115-120A
Huang, S.-C. 1323-1334A
261-269A
1353-1359A
115-120A
1657-1664A
2077-2080A
77-85B
229-231B
281-289B
261-269A
1323-1334A
2031-2034A
323-329B
1409-1420A
1433-1439A
- Hussain, M.M. 1429-1431A
Hwang, N.-M. 1876-1877A
- Igo, Y. 115-120A
Ida, Y. 1323-1334A
Ikuta, I. 261-269A
Im, H.B. 1353-1359A
Imai, T. 115-120A
Inoue, A. 1657-1664A
2077-2080A
77-85B
229-231B
281-289B
261-269A
1323-1334A
2031-2034A
323-329B
1409-1420A
1433-1439A
- Ishida, T. 229-231B
Ishihara, J. 281-289B
Ito, Y. 1323-1334A
Iwai, T. 2031-2034A
Iyengar, G.N.K. 323-329B
Izum, O. 1409-1420A
1433-1439A
- Jacob, K.T. 1102-1104A
763-770B
323-329B
1223-1228A
755-775A
Jakovics, J.P. 1629-1632A
Jenowski, G.M. 1891-1905A
Jardine, F.S.J. 1985-1993A
Jata, K.V. 1011-1026A
Jayaraman, N. 2291-2294A
Jayaraman, R. 1493-1503A
Jensen, D.J. 253-259A
Jia, W.X. 331-337A
Jiran, E. 1102-1104A
Jones, R.H. 1229-1240A
Jönsson, B. 807-815A
Judin, V.-P. 259-265B
1573-1575A
- Kaiser, D.L. 147-157B
400B
845-859B
- Kajioka, H. 147-157B
400B
845-859B

Kajiware, S. Kaku, Y. Kang, S.-J.L.	1693-1702A 171-177B 2175-2182A 325-330A 1429-1431A 425-432B 159-162B	Lichter, B.D. Lin, C.S. Lin, H.J. Lin, I.J. Lin, J.-C.	703-710A 933-944A 215-220A 433-442B 1361-1372A 1241-1245A 765-769B	Nagamori, M. Nakamura, T. Nakiboglu, F.	913-914B 503-514B 339-346B 375-381B 383-393B 1577-1583A 93-106A	Richards, G.G. Richardson, B.C. Risbud, S.H.	677-685B 1479-1481A 561-566A 1479-1481A 727-737A						
Kang, T.K. Kasama, A. Kasner, M.E. Kato, H. Kato, M. Kaufman, M.J. Keefe, P.W. Keene, B.J. Keller, H. Keller, H. Kemori, N. Kerr, H.W. Kerr, W.R. Kidd, M. Kikuchi, S. Kim, C.H.	2093-2097A 823-832A 1949-1953A 575-581A 651-661A 159-162B 497-501B 111-117B 1611-1623A 2298-2300A 771-776B 221-229A 745-746A 1173-1178A 1157-1164A 967-972A 29-39B 1157-1164A 1353-1359A 2097-2098A 967-972A 1577-1583A 19-28B 231-232B 2007-2016A 1217-1221A 1027-1034A 2107-2116A 231-241A 232-234B 609-610B 2255-2263A 1447-1453A 1865-1890A 367-373B 1757-1767A 2265-2270A 2271-2277A 171-177B 351-355A 31-36A 1493-1503A 1165-1171A 903-911B 1517-1527A 2295-2298A 2099-2102A 1461-1469A 1471-1477A 1825-1835A 705-724B 443-450A 639-645B 1529-1536A 745-746A 1173-1178A 1915-1919A	Lin, M.L. Liu, C. Liu, Y. Lovey, F.C. Lucke, K. Luhman, T. Lynch, D.C. Lytle, F.W. Lyudkovsky, G.	601-607B 679-684A 685-690A 1433-1439A 2153-2161A 1301-1312A 739-741A 235-238B 817-827B 739-741A 1267-1275A	MacCrone, R.K. Mackert, J.R., Jr. Majima, H.	911-914A 746-749A 69-76B 621-627B 19-28B 41-50B 503-514B 247-257B 1277-1285A 2209-2226A 107-114A 451-460A 2017-2029A 1797-1807A 991-1000A 1657-1664A 2077-2080A 845-859B 1313-1322A 725-733B 2301-2303A 515-521B 1787-1795A 1139-1148A 159-162B 163-170B 877-887A 1087-1094A 1223-1228A 1035-1041A 1043-1050A 1703-1715A 443-450A 217-227B 1523-1527A 1287-1294A 370-374A 791-798A 159-162B 163-170B 159-162B 1035-1041A 1787-1795A 261-269A 491-496A 497-505A 507-512A 1301-1312A 358-360A 1441-1445A 53-63A 115-120A 845-859B 367-385A 189-194A 587-600B 914-918B 185-196B 197-207B 1949-1953A 1751-1755A 1481-1483A 360-362A 914-918B 575-596B 967-972A 243-252A 537-547A 1157-1164A 791-796B 365-366A 861-868B 869-877B 523-526B 529-533B 395-397B 915-921A 487-490B 1447-1453A	Nardi, V.C. Neal, D.F. Neumann, J.P. Ngai, T.L. Ni, R. Nieh, T.G. Nishi, Y. Nishida, M. Nishida, Y. Nitta, M. Nityanand, N. Nix, W.D.	1577-1583A 93-106A 1484-1485A 1241-1245A 315-323A 121-126A 901-903A 1505-1515A 833-844B 367-373B 247-257B 121-126A 281-293A 151-162A 163-170B 829-832B 629-637B 443-448B	Rodrigues, P.M.B. Romanowska-Haftek, E. Romig, A.D., Jr. Rosenfield, A.R. Rosenstein, A.H. Rothman, M.F. Ruano, O.A.	1967-1975A 2107-2116A 2035-2047A 791-798A 151-162A 1087-1094A 1517-1527A				
Kim, H.J. Kim, J.I. Kim, S.-H. Kim, Y.-H. Kim, Y.G. Kim, Y.H. Kimmerle, W.L. Kinoshita, M. Kipourou, G.J. Kirkbride, R. Kleppa, O.J. Kluh, R.L. Knorovsky, G.A. Knott, J.F. Ko, H.C. Kobayashi, Y. Kola, R.R. Korn, Y. Kondo, Y. Korhonen, M.A. Kou, S. Kozuka, Z. Kramer, D.P. Krauss, G. Kuban, M.B. Kubisch, D.G. Kubo, K. Kum, D.W. Kumar, M. Kundrat, D.M.	1157-1164A 967-972A 29-39B 1157-1164A 1353-1359A 2097-2098A 967-972A 1577-1583A 19-28B 231-232B 2007-2016A 1217-1221A 1027-1034A 2107-2116A 231-241A 232-234B 609-610B 2255-2263A 1447-1453A 1865-1890A 367-373B 1757-1767A 2265-2270A 2271-2277A 171-177B 351-355A 31-36A 1493-1503A 1165-1171A 903-911B 1517-1527A 2295-2298A 2099-2102A 1461-1469A 1471-1477A 1825-1835A 705-724B 443-450A 639-645B 1529-1536A 745-746A 1173-1178A 1915-1919A	Malinsky, I. Manley, B. Marder, A.R. Margolin, H. Martins, G.P. Mason, J.T. Masumoto, T. Matsumiya, T. Matsuo, M. Mazumdar, D. McCay, M.H. McCune, R.A. McEvily, A.J. McKelliget, J. McLean, A. McMinn, A. McNallan, M.J. McNelly, T.R. Menon, E.S.K. Meyers, M.A. Meyrick, G. Michal, G.M. Michael, D.J. Miglin, M.T. Miller, W.A. Mills, K.C. Mills, M.E. Minakawa, K. Minemura, T. Miner, R.V.	911-914A 746-749A 69-76B 621-627B 19-28B 41-50B 503-514B 247-257B 1277-1285A 2209-2226A 107-114A 451-460A 2017-2029A 1797-1807A 991-1000A 1657-1664A 2077-2080A 845-859B 1313-1322A 725-733B 2301-2303A 515-521B 1787-1795A 1139-1148A 159-162B 163-170B 877-887A 1087-1094A 1223-1228A 1035-1041A 1043-1050A 1703-1715A 443-450A 217-227B 1523-1527A 1287-1294A 370-374A 791-798A 159-162B 163-170B 159-162B 1035-1041A 1787-1795A 261-269A 491-496A 497-505A 507-512A 1301-1312A 358-360A 1441-1445A 53-63A 115-120A 845-859B 367-385A 189-194A 587-600B 914-918B 185-196B 197-207B 1949-1953A 1751-1755A 1481-1483A 360-362A 914-918B 575-596B 967-972A 243-252A 537-547A 1157-1164A 791-796B 365-366A 861-868B 869-877B 523-526B 529-533B 395-397B 915-921A 487-490B 1447-1453A	Nogi, K. Notis, M.R. Núñez, C. Ogino, K. Oguchi, M. Oh, J.M. Ohashi, T. Ohira, T. Ohmori, K. Ohno, R. Oka, M. Okabayashi, K. Okamoto, H. Oktay, E. Oliveras, J. Olson, D.L.	163-170B 1657-1664A 1087-1094A 799-806A 843-852A 1295-1299A 291-305B 1113-1120A 1203-1209A 1113-1120A 541-545B 629-637B 374A 1797-1807A 1725-1737A 1949-1953A 735-744B 1809-1823A 53-63A 115-120A 527-535A 853-859A 1179-1189A 1725-1737A 1517-1527A 87-103B 397-399B	Sadoway, D.R. Sakai, T. Sakuma, Y. Salcedo, M. Sam, D.D. Samuel, A.M. Samuel, F.H.	231-232B 1313-1322A 617-620A 449-459B 513-517A 1671-1683A 1671-1683A 73-91A	Sanchez, J.M. Sankaran, S. Sarreal, J.A. Sasaki, Y. Sastri, P. Sato, K. Savage, W.F. Schaler, J.V. Schaefer, R.J. Schaefer, S.C. Schlesinger, M.E. Schmid, R. Schoen, J.W. Schulte, R.L. Schwenker, S.W. Schwerdtfeger, K. Schwitzgebel, G. Scott, T.E. Seetharaman, S. Sellamuthu, R.	189-194A 911-914A 2063-2073A 307-316B 105-110B 69-76B 727-737A 137-149A 217-2125A 515-521B 235-238B 817-827B 1361-1372A 785-789B 1335-1346A 635-643A 271-280A 497-501B 119-131B 791-798B 527-535A 853-859A 1179-1189A 179-184B 419-428A 347-356B 395-397B	Sharma, I.G. Shatynski, S.R. Shechtman, D. Shen, T.H. Sherby, O.D. Shewmon, P. Shibata, Y. Shiiki, M. Shimizu, M. Shimizu, Y. Shull, R.D. Siewert, T.A. Sigworth, G.K. Singh, J. Sjödén, O. Slane, J.A. Smegill, J.G. Smith, E.F., III Smith, G.C. Smith, G.D.W. Smith, H.H. Smith, J.F. Smith, K.A.	911-914A 2117-2125A 1347-1351A 1517-1527A 2295-2298A 1523-1527A 111-117B 639-645B 621-633A 1323-1334A 575-581A 1797-1807A 349-351A 65-72A 179-184B 1287-1294A 923-932A 339-347A 1593-1600A 1629-1632A 370-374A 1647-1656A 914-918B 185-196B	Smith, R.R. Sohn, H.Y. Sommer, F. Sommerville, I.D. Socia, G.B. Sosinsky, D.J. Southwick, P.D. Speyer, R.F. Spitzer, K.H. Spitzig, W.A. Srivastava, S.K. St. John, D.H. Staffansson, L.-I. Starke, E.A., Jr. Stefanescu, D.M. Stengel, A.F. Stephens, J.J. Stone, B.C. Strum, M. Stüwe, H.P. Suga, Y. Sun, W.-P. Suzuki, T.	429-434A 51-60B 791-796B 331-337B 519-525A 331-337B 1267-1275A 561-566A 1479-1481A 119-131B 527-535A 853-859A 1179-1189A 1537-1546A 375-381B 383-393B 179-184B 1011-1026A 1121-1130A 1043-1050A 281-293A 2227-2237A 537-547A 1455-1459A 1313-1322A 216-220A 617-620A

Swanson, R.E.	1633-1637A	Winter, P.L.	307-313A
Swindeman, R.W.	1027-1034A	Witcomb, M.J.	807-814A
Szekely, J.	665-676B	Wolke, I.	663-668A
	487-490B	Woodward, R.L.	307-313A
	695-703B	Wright, M.G.	429-434A
	735-744B	Wright, R.N.	519-525A
	1139-1148A		399-405A
	687-693B	Wu, S.-T.	633-841A
Szklarska-Smialowska, Z.	2255-2263A		
		Xu, B.-J.	711-716A
Taberlet, E.	687-693B		
Takada, J.	221-229A	Yaguchi, H.	2080-2083A
Takahashi, I.	2031-2034A		2017-2029A
Takasugi, T.	1433-1439A	Yamamoto, S.	221-229A
Tanabe, T.	367-373B	Yang, J.-M.	1547-1559A
Tanaka, S.	449-459B	Yao, S.	171-177B
Tangri, K.	697-702A	Yoon, D.N.	2175-2182A
Tantevee, T.	217-227B		325-330A
Tarby, S.K.	829-832B		1429-1431A
Tavlarides, L.L.	615-620B		1915-1919A
Tewari, S.N.	2279-2290A	Yoshihiro, A.	901-903A
	2291-2294A	You, Y.-Z.	1104-1106A
	2099-2102A		
Thomas, G.	2163-2173A	Zanner, F.J.	357-365B
Thomas, J.F., Jr.	2227-2237A	Zbib, H.M.	1637-1640A
Thompson, A.W.	2249-2253A	Zedalis, M.S.	2187-2198A
	451-472A	Zhang, T.-Y.	717-725A
	1789-1786A	Zimmels, Y.	433-442B
	1633-1637A		
Thorvaldsson, T.	45-52A		
Tien, J.K.	651-661A		
	1577-1583A		
	151-162A		
Toaz, M.W.	549-559A		
Todd, J.A.	1191-1202A		
Toguri, J.M.	547-552B		
	755-761B		
	913-914B		
	339-346B		
Tomita, Y.	1203-1209A		
Tomono, M.	111-117B		
Tomota, Y.	537-547A		
Topor, L.	1217-1221A		
Trivedi, R.	991-1000A		
Tseng, D.	697-702A		
Tsuchida, N.	523-528B		
	529-533B		
Tsukihashi, F.	535-540B		
	541-545B		
Tumuluru, M.D.	295-306A		
Udupa, A.R.	914-918B		
	185-196B		
Ueshima, Y.	845-859B		
Unnam, J.	899-901A		
Upadhyay, K.	197-207B		
	271-279B		
Utgard, T.	547-552B		
	339-346B		
Uz, M.	1955-1966A		
Vaidyanathan, S.	2090-2093A		
Van Der Schaaf, P.J.	1441-1445A		
Van Gent, A.	1441-1445A		
Van Tendeloo, G.	2153-2161A		
Vandermeer, R.A.	1717-1723A		
Varin, R.A.	1967-1975A		
Venkatasubramanian, R.	382-384A		
Venkatraman, M.	1484-1485A		
Verhoeven, J.D.	991-1000A		
Vinels, J.	629-637B		
Vogelsang, M.	379-389A		
Voigt, R.C.	491-496A		
Wada, H.	238-239B		
	391-398A		
	1585-1592A		
Wagoner, R.H.	1632-1633A		
	1001-1009A		
Wang, H.	1051-1055A		
Wang, Y.H.	2265-2270A		
	2271-2277A		
Wang, Z.	107-114A		
Warren, G.W.	29-39B		
Wasynczuk, J.A.	2163-2173A		
Wayman, C.M.	65-72A		
	1505-1515A		
Wayman, M.L.	429-434A		
Webster, D.	2007-2016A		
Weiss, B.Z.	1885-1890A		
Weiss, I.	1935-1947A		
	549-559A		
Weissberger, S.	433-442B		
Welsch, G.E.	1935-1947A		
Westmacott, K.H.	807-814A		
Wiedemann, K.E.	899-901A		
Wilkinson, D.S.	1873-1875A		
Williams, D.B.	163-167A		
Wilson, D.V.	367-370A		



Combined Subject Index

- Abatement (pollution)**
See Pollution abatement
- Abrasion resistance**
Wear Resistance of Quenched and Tempered AISI 4137H Steel. 295-306A
- Absolute pressure**
See Pressure
- Absolute viscosity**
See Viscosity
- Acid cleaning**
See Pickling
- Acid leaching**
See also Hydrochloric acid leaching
Extraction Equilibria in the System $\text{GaCl}_3\text{—AlCl}_3\text{—HCl—H}_2\text{O—Tributyl Phosphate}$. 259-265B
Acidic Rate- and Flow-Controlled Dissolution of Uraninite Ores. 405-413B
- Acid pickling**
See Pickling
- Actinide metals**
See Uranium
- Activated sintering**
The Effect of the Binder Phase Melting Temperature on Enhanced Sintering. 903-906A
- Activity (chemical)**
Measurements of Oxygen Pressure in a Copper Flash Smelting Furnace by an EMF Method. 111-117B
Activity Coefficient of Oxygen in Copper—Tellurium Melts. 171-177B
Activity of Arsenic in Molten Lead. 235-238B
Arsenic Activities in Molten Copper and Copper Sulfide Melts. 755-761B
A Modified Interaction Parameter Formalism for Non-Dilute Solutions. 1211-1215A
An Ambiguity in the Definition of the Activity Coefficient at Infinite Dilution. 1484-1485A
- Activity coefficients**
See Activity (chemical)
- Additives**
See Master alloys
- Adsorption**
Potentiometric Studies on the Adsorption of $\text{Au}(\text{CN})_2^-$ and $\text{Ag}(\text{CN})_2^-$ Onto Activated Carbon. 523-528B
Studies on Role of Oxygen in the Adsorption of $\text{Au}(\text{CN})_2^-$ and $\text{Ag}(\text{CN})_2^-$ Onto Activated Carbon. 529-533B
- Age hardening**
See Precipitation hardening
- Agglomerating**
See Agglomeration
- Agglomeration**
Agglomeration of Particles During Roasting of Zinc Sulfide Concentrates. 647-656B
- Aggregation**
See Agglomeration
- Aging**
See also Aging (artificial)
Strain aging
Transformation Sequence in a Cu—Al—Ni Shape Memory Alloy at Elevated Temperatures. 65-72A
- Aging (artificial)**
The Kinetics of Carbide Precipitation in Silicon—Aluminum Steels. 1287-1294A
- Agitation**
See Electromagnetic stirring
- Air gaps**
The Air-Gap Formation Process at the Casting/Mold Interface and the Heat Transfer Mechanism Through the Gap. 833-844B
- Air pollution**
Theoretical and Experimental Study of the Removal of Dust Particles From Flue Gases Using Two-Phase Steam—Water Droplet Mixtures. 665-676B
Removal of SO_2 With Oxygen in the Presence of $\text{Fe}(\text{III})$. 745-753B
- Aircomatic welding**
See Gas metal arc welding
- Aircraft components, Materials substitution**
Mechanical Properties and Microstructure of Al—Li—Cu—Mg—Zr Die Forgings. 2007-2016A
- Aircraft equipment**
See Aircraft components
- Alfven waves**
See Magnetohydrodynamics
- Alkali metal alloys**
See Lithium base alloys
- Alkali metals**
See Cesium
Lithium
Potassium
- Alkaline earth metal alloys**
See Magnesium base alloys
Strontium
- Alkaline earth metal compounds**
See also Lime
- Alkaline earth metal compounds, Thermal properties**
Legendre Polynomial Expansions of Thermodynamic Properties of Binary Solutions. 1057-1063A
- Alkaline earth metals**
See Calcium
Magnesium
Strontium
- Allotropic transformation**
The β -to- α Phase Transformation in a Uranium Alloy. 1717-1723A
- Allotropic transformation, Size effects**
The Alpha \rightleftharpoons Gamma Transformation in Iron Powders. 37-44A
- Alloy cast iron**
See Chromium iron
- Alloy powders, Microstructure**
Microstructural Characterization of Rapidly Solidified Al—Li—Co Powders. 73-91A
Microstructure and Stability of Melt Spun Inconel 713LC. 173-180A
An Analysis of the Microstructure of Rapidly Solidified Al—8Fe Powder. 781-790A
Dendritic Microstructure in Argon Atomized Superalloy Powders. 2099-2102A
- Alloy steels**
See also Austenitic stainless steels
Boron steels
Carbon manganese steels
Chromium molybdenum steels
Chromium molybdenum vanadium steels
Chromium steels
Duplex stainless steels
Electrical steels
Ferritic stainless steels
High strength low alloy steels
High strength steels
Low alloy steels
Manganese steels
Molybdenum steels
Nickel chromium molybdenum steels
Nickel chromium steels
Nickel steels
Resulfurized steels
Silicon manganese steels
Silicon steels
Stainless steels
Vanadium steels
- Alloy steels, Mechanical properties**
New Considerations on Tempered Martensite Embrittlement. 745-746A
- Alloying elements, Diffusion**
Measurement of Segregation and Distribution Coefficients in MAR-M200 and Hafnium-Modified MAR-M200 Superalloys. 419-428A
- Alloys**
See Alloy steels
Casting alloys
Dispersion hardening alloys
Ferrous alloys
Magnetic alloys
Master alloys
Precipitation hardening alloys
Superalloys
- Alpha annealing**
See Annealing
- Alphatizing**
See Annealing
- Alumina**
See Aluminum oxide
- Aluminizing**
CVD Aluminide Nickel. 215-220A
- Aluminum, Alloying elements**
Directional Solidification and Annealing of $\text{Mn}_{55}\text{Al}_{45}$ Alloys. 1247-1249A
Effect of Aluminum Content on Low Temperature Tensile Properties in Cryogenic Fe/Mn/Al/Nb/C Steels. 2097-2098A
- Aluminum, Binary systems**
The Aluminum—Strontium Phase Diagram. 1250-1253A
- Aluminum, Crystal lattices**
Serrated Grain Boundary Formation During High Temperature Fatigue. 1100-1102A
- Aluminum, Extraction**
On the Separation of TiCl_4 From AlCl_3 . 232-234B
Extraction Equilibria in the System $\text{GaCl}_3\text{—AlCl}_3\text{—HCl—H}_2\text{O—Tributyl Phosphate}$. 259-265B
Electrocapillarity in the Aluminum Reduction Cell. 547-552B
The Vapor—Liquid Equilibria of the Aluminum Chloride—Titanium Tetrachloride System. 609-610B
- Aluminum, Microstructure**
Deformation and Recrystallization Textures in Commercially Pure Aluminum. 253-259A

Aluminum

- Aluminum, Reactions (chemical)**
Solubility and Activity of Oxygen in Liquid Nickel in Equilibrium With α - Al_2O_3 and NiO x (1 + x) Al_2O_3 . 763-770B
- Aluminum, Solubility**
Alloying Behavior of Co_3Ti . 1433-1439A
- Aluminum, Ternary systems**
Discussion of "The Grain Refining of Aluminum and Phase Relationships in the Al—Ti—B System" and Reply. 349-351A
- Aluminum base alloys, Casting**
Numerical Simulation of Solidification in an Aluminum Casting. 209-216B
The Air-Gap Formation Process at the Casting/Mold Interface and the Heat Transfer Mechanism Through the Gap. 833-844B
Development of Al—Ti—C Grain Refiners Containing TiC. 2127-2137A
- Aluminum base alloys, Composite materials**
An *In Situ* HREM Study of Dislocation Generation at Al/SiC Interfaces in Metal Matrix Composites. 379-389A
The Effect of Thermal Exposure on the Microstructure and Fiber/Matrix Interface of an $\text{Al}_2\text{O}_3/\text{Al}$ Composite. 1075-1080A
Structure-Performance Maps of Polymeric, Metal, and Ceramic Matrix Composites. 1547-1559A
- Aluminum base alloys, Corrosion**
The Effect of Cathodic Polarization on the Corrosion Fatigue Behavior of a Precipitation Hardened Aluminum Alloy. 339-347A
Effect of Notch Root Radius on Stress Intensity in Mode I and Mode III Loading. 1633-1637A
- Aluminum base alloys, Diffusion**
The Effect of Solidification Rate on Microsegregation. 2063-2073A
- Aluminum base alloys, Heat treatment**
Lithium Depletion During Heat Treatment of Aluminum—Lithium Alloys. 635-643A
- Aluminum base alloys, Mechanical properties**
Unloading Yield Effects in Aluminum Alloys. 121-126A
Correlation Between Creep Stress Exponent and Ductility in Al—10 At.% Zn. 365-366A
Dependence of Total Elongations of Superplastic Materials on m. 685-690A
Tensile Properties of Directionally Solidified Al—4Cu Alloys With Columnar and Equiaxed Grains. 823-832A
Influence of Soaking Treatments on Hot Ductility of Al—4.85Mg Alloys Containing Manganese. 833-841A
Fatigue Crack Growth and Fracture Toughness Behavior of an Al—Li—Cu Alloy. 1011-1026A
Rolling Contact Deformation of 1100 Aluminum Disks. 1561-1572A
The Influence of Load Ratio on Fatigue Crack Growth in 7090-T6 and IN9021-T4 P/M Aluminum Alloys. 1787-1795A
The Effect of Hot-Rolling on Chill-Cast Al— Al_3Cu , and Unidirectionally Solidified Al— Al_3Ni Eutectic Alloys. 1985-1993A
Mechanical Properties and Microstructure of Al—Li—Cu—Mg—Zr Die Forgings. 2007-2016A
Characterization and Modeling of the High Temperature Flow Behavior of Aluminum Alloy 2024. 2227-2237A
- Aluminum base alloys, Metal working**
On the Directionality of Strain Localization When Stretching Aluminum Alloy Sheets in Biaxial Tension. 367-370A
- Aluminum base alloys, Microstructure**
The Influence of Iron and Chromium on the Microstructure of Cast Al—Si—Mg Alloys. 45-52A
Microstructural Characterization of Rapidly Solidified Al—Li—Co Powders. 73-91A
- Aluminum base alloys, Phases (state of matter)**
The Aluminum—Strontium Phase Diagram. 1250-1253A
Compositional Analysis of the Icosahedral Phase in Rapidly Quenched Al—Mn and Al—V Alloys. 1657-1664A
On the Microstructure of Rapidly Solidified Al—15Mn Ribbons: Effect of Annealing in the Temperature Range 300–600°C. 1671-1683A
Icosahedral and Decagonal Phase Formation in Al—Mn Alloys. 2117-2125A
Growth of Silicon Particles in an Aluminum Matrix. 2139-2152A
- Aluminum base alloys, Powder technology**
An Analysis of the Microstructure of Rapidly Solidified Al—8Fe Powder. 781-790A
- Aluminum base alloys, Structural hardening**
Metallographic and Differential Scanning Calorimetry Analyses of Precipitation and Recrystallization in an Al—Mn Alloy. 593-605A
Decomposition Characteristics of Al—Mn—Zr Alloys Rapidly-Quenched From the Melt. 799-806A
Superplasticity in a Thermomechanically Processed High-Magnesium, Al—Mg Alloy. 1035-1041A
The Influence of Thermomechanical Processing Variables on Superplasticity in a High-Magnesium, Al—Mg Alloy. 1043-1050A
Precipitation and Ostwald Ripening in Dilute Aluminum Base-Zr—V Alloys. 2187-2198A
- Aluminum base alloys, Welding**
Three-Dimensional Convection in Laser Melted Pools. 2265-2270A
Computer Simulation of Convection in Moving Arc Weld Pools. 2271-2277A
- Aluminum compounds**
See also Aluminum oxide
- Aluminum compounds, Crystal lattices**
L₁₂-Type Ni—Al—Cr Alloys Processed by Rapid Solidification. 1685-1692A
- Aluminum compounds, Diffusion**
Carbon Segregation to Grain Boundaries in Rapidly Solidified Ni_3Al . 2084-2086A
- Aluminum compounds, Mechanical properties**
Fracture of Fe_3Al . 2298-2300A
- Aluminum killed steels, Mechanical properties**
Flow Behavior of an Aluminum-Killed Steel After Tensile Pre-straining and Strain-Aging. 1573-1575A
- Aluminum killed steels, Phase transformations**
The Dissolution of Cementite in a Low Carbon Steel During Isothermal Annealing at 700°C. 617-620A
- Aluminum oxide, Composite materials**
The Effect of Thermal Exposure on the Microstructure and Fiber/Matrix Interface of an $\text{Al}_2\text{O}_3/\text{Al}$ Composite. 1075-1080A
- Ambient pressure**
See Pressure
- Amorphous materials**
See Metallic glasses
- Analyzing**
See Depth profiling
Differential thermal analysis
Mathematical analysis
Numerical analysis
Stress analysis
- Androforming**
See Stretch forming
- Anisotropy**
A Model for Yielding in Anisotropic Metals. 107-114A
- Annealing**
See also Homogenizing
Isothermal annealing
Spheroidizing
Factors Affecting the Final Grain Size of Decarburized Lamination Steels. 1277-1285A
The Study of Desulfurization Kinetics in Grain Oriented 3% Silicon Iron. 1347-1351A
- Antimony, Impurities**
A Kinetic Model for the Vacuum Refining of Inductively Stirred Copper Melts. 87-103B
Thermodynamics of Gaseous SbS. 913-914B
- Arc discharges**
See Electric arcs
- Arc plasma welding**
See Plasma arc welding
- Arc welding**
See also Gas metal arc welding
Gas tungsten arc welding
Plasma arc welding
Submerged arc welding
Computer Modeling of Heat Flow in Welds. 587-600B
Computer Simulation of Convection in Moving Arc Weld Pools. 2271-2277A
- Arc welds**
See Welded joints
- Arcs (electric)**
See Electric arcs
- Argon arc welding**
See Gas tungsten arc welding
- Armor, Microstructure**
Microstructural Analysis of Residual Projectiles—a New Method to Explain Penetration Mechanisms. 435-442A
- Armor plate**
See Armor
- Arsenic, Binary systems**
Activity of Arsenic in Molten Lead. 235-238B
- Arsenic, Impurities**
A Kinetic Model for the Vacuum Refining of Inductively Stirred Copper Melts. 87-103B
Arsenic Activities in Molten Copper and Copper Sulfide Melts. 755-761B
- Artificial aging**
See Aging (artificial)
- Artillery shells**
See Projectiles
- Atmospheric pollution**
See Air pollution
- Atomic diffusion**
See Diffusion
- Atomization**
See Atomizing
- Atomizing**
Dendritic Microstructure in Argon Atomized Superalloy Powders. 2099-2102A
- Austenite**
See also Retained austenite
- Austenite, Chemical analysis**
The Chemical Composition of Precipitated Austenite in 9Ni Steel. 967-972A
- Austenite, Diffusion**
Determination of the Interdiffusion Coefficients in the Fe—Ni and Fe—Ni—P Systems Below 900°C. 1131-1138A
- Austenitic stainless steels, Corrosion**
Dissolution Behavior of 304 Stainless Steel in HNO_3/HF Mixtures. 137-149A

- High Temperature Corrosion of Superalloys in an Environment Containing Both Oxygen and Chlorine. 1087-1094A
Liquid Cesium Tellurium-Induced Fatigue Embrittlement of Cold-Worked 316 Stainless Steel. 2090-2093A
- Austenitic stainless steels, Crystal lattices**
Changes in the Subboundary Mesh Size With Creep Strain in 304 Stainless Steel. 2093-2097A
- Austenitic stainless steels, Mechanical properties**
Influence of Prestrain History on Fracture Toughness Properties of Steels. 473-489A
Low Temperature Impact Properties of Phosphorus and Sulfur Doped and Sensitized Type 304 Stainless Steel. 663-668A
- Austenitic stainless steels, Microstructure**
On the Kinetics of the Spreading of Extrinsic Grain Boundary Dislocations. 1967-1975A
- Austenitic stainless steels, Oxidation**
Stability of the Chromia Layer on Steels in Flowing Nonequilibrium $H_2-H_2O-CH_4-CO$ Mixtures at 950°C. 915-921A
- Austenitic stainless steels, Phase transformations**
Phase Transformation of Austenitic Stainless Steels as a Result of Cathodic Hydrogen Charging. 1593-1600A
- Austenitic stainless steels, Structural hardening**
Strain Aging and Load Relaxation Behavior of Type 316 Stainless Steel at Room Temperature. 1757-1767A
- Austenitic stainless steels, Welding**
Solidification and Solidification Cracking in Nitrogen-Strengthened Austenitic Stainless Steels. 727-737A
Metal Vapors in Gas Tungsten Arcs. I. Spectroscopy and Monochromatic Photography. 1851-1883A
Metal Vapors in Gas Tungsten Arcs. II. Theoretical Calculations of Transport Properties. 1865-1871A
- Austenitizing**
Retained Carbide Distribution in Intercritically Austenitized 52100 Steel. 31-36A
- Auto oxidation**
See Oxidation
- Autodiffusion**
See Diffusion
- Autogenous smelting**
See Flash smelting
- A15 compounds, Mechanical properties**
High-Temperature Plastic Deformation of Two V—Ga Alloys With A15 Structure. 519-525A
- A15 compounds, Superconductivity**
The Effect of High Temperature Plastic Flow on the Superconducting Transition in A15 Compounds. 399-405A
- Bacterial corrosion**
Biotechnology/Materials: the Growing Interface. 5-30A
- Bacterial leaching**
Biotechnology/Materials: the Growing Interface. 5-30A
- Bainite, Crystal growth**
Discussion of "The Bainite Reaction in Fe—Si—C Alloys: the Primary Stage" and "The Bainite Reaction in Fe—Si—C Alloys: the Secondary Stage". 1095-1100A
Lower Bainite With Midrib in Hypereutectoid Steels. 1113-1120A
- Ball mills**
An Analysis of Radial Segregation for Different Sized Spherical Solids in Rotary Cylinders. 247-257B
- Balling**
See Agglomeration
- Basic converters**
Theoretical and Experimental Study of the Removal of Dust Particles From Flue Gases Using Two-Phase Steam—Water Droplet Mixtures. 665-676B
Soda Slag System for Hot Metal Dephosphorization. 797-804B
- Basic electric furnaces**
See Electric furnaces
- Basic oxygen furnaces**
See Basic converters
- Basic oxygen processes**
See Oxygen steel making
- Basic oxygen steel making**
See Oxygen steel making
- Batch type furnaces**
See Basic converters
Bottom blown converters
Copper converters
Rotary converters
Top blown converters
Vacuum arc furnaces
- Bauschinger effect**
Grain Boundary Contribution to the Bauschinger Effect in β -Brass Bicyrystals. 2017-2029A
- BCC metals, Diffusion**
On the Effective Hydrogen Permeability in Metastable β Titanium Alloy, Niobium and 2.25Cr—1Mo Ferritic Steel. 2086-2090A
- Bearing steels, Heat treatment**
Retained Carbide Distribution in Intercritically Austenitized 52100 Steel. 31-36A
- Beehive kilns**
See Kilns
- Bendability**
See Formability
- Beryllium bronzes, Phase transformations**
Martensitic Transformation of Cu—2Be Alloys Induced by Explosive Cladding. 1865-1890A
- Beryllium copper**
See Beryllium bronzes
- Binary systems**
A Modified Regular-Solution Model for Terminal Solutions. 1878-1879A
- Binary systems, Phases (state of matter)**
A Theoretical Evaluation of Chemical Ordering and Glass Transition in Liquid Mg—Sn Alloys. 607-615A
Study of the Enthalpies of Formation in the Gd—Ni System. 777-780A
Thermodynamics of the Mn—P System. 777-783B
An HVEM Study of an Unusual Ordering Reaction in Platinum—Carbon. 807-814A
Effect of Small Additions of Silver on the Eutectic Temperature in the Lead—Tin System. 829-832B
The Aluminum—Strontium Phase Diagram. 1250-1253A
Magnetic Contributions to the Thermodynamic Functions of Alloys and the Phase Equilibria of Fe—Ni System Below 1200K. 1361-1372A
A Thermodynamic Analysis of the Phase Equilibria of the Fe—Ni System Above 1200K. 1373-1380A
Direct Use of the Chemical Potential Function in Thermodynamic Modeling of Alloy Phase Diagrams. 1471-1477A
The Vanadium—Nitrogen System: a Review. 1647-1656A
- Binary systems, Thermal properties**
Calorimetric and Emf Studies on Liquid Li—Sn Alloys. 791-796B
- Biochemistry**
Biotechnology/Materials: the Growing Interface. 5-30A
- Bismuth, Impurities**
A Kinetic Model for the Vacuum Refining of Inductively Stirred Copper Melts. 87-103B
- Bismuth, Physical properties**
Interfacial Tension and Flotation Characteristics of Liquid Metal—Sodium Flux Systems. 339-346B
- Blades**
See Turbine blades
- Blast furnace chemistry**
Structural Effects in the Reaction Between Carbon Dioxide and Coke Doped With Various Potassium Bearing Catalytic Precursors. 565-574B
Reduction of Lead Minerals by CO/CO_2 Gas Mixtures: Application of the Grain Model. 575-586B
An Investigation of the Critical Influence of Potassium on the Reduction of Wustite. 657-663B
- Blast furnace practice**
Development of an Analytical Equation for Calculation of the Blast Furnace Fuel Rate. 705-724B
- Blast furnace slags**
The Reaction of $SiO(g)$ With Liquid Slags. 397-399B
- Blast furnace slags, Solubility**
PbO Solubility in Lead-Blast Furnace Slags. 817-827B
- Blast furnaces**
The Settling of Metallic Lead From Lead Blast Furnace Slag. 267-270B
- Blowholes**
An Ice-Water Model Study on Formation of Blowhole-Free Skin With Reference to Solidification of Steel. 553-564B
- Blowing**
A Multi-Phase Model for Plumes in Powder Injection Refining Processes. 77-85B
Heat Flow in Copper Converters. 677-685B
Mixing Models for Gas Stirred Metallurgical Reactors. 725-733B
- Blunging**
See Mixing
- Body centered cubic metals**
See BCC metals
- BOF**
See Basic converters
- Boiling water reactors**
Relative Stress Corrosion Susceptibilities of Alloys 690 and 600 in Simulated Boiling Water Reactor Environments. 877-887A
- Bonding**
See Explosive bonding
- Bonding strength**
A Relationship Between Indigenous Impurity Elements and Protective Oxide Scale Adherence Characteristics. 923-932A
- Boron, Alloying additive**
The Microstructure and Mechanical Properties of a Modified 2.25Cr—1Mo Steel. 1027-1034A
Effects of Decarburization and Normalizing Heat Treatment in Boron-Silicon Iron Alloys. 1353-1359A
- Boron, Diffusion**
Carbon Segregation to Grain Boundaries in Rapidly Solidified Ni_3Al . 2084-2086A
- Boron, Solubility**
The Solubility of Boron in Iron. 1481-1483A
- Boron, Ternary systems**
Discussion of "The Grain Refining of Aluminum and Phase Relationships in the Al—Ti—B System" and Reply. 349-351A
Balance of Distribution of Some Transition Metals Between the $(M', M'')B$ and $(M', M'')_2B$ Phases. 1665-1669A

Boron intensified steels

Boron intensified steels

See Boron steels

Boron steels, Welding

A Comparative Study of the Heat Affected Zone (HAZ) Properties of Boron Containing Low Carbon Steels. 1529-1536A

BOS process

See Oxygen steel making

Bottom blown converters

Model Study of Mixing and Mass Transfer Rates of Slag-Metal in Top and Bottom Blown Converters. 461-469B
Mixing Models for Gas Stirred Metallurgical Reactors. 725-733B

Boundaries

See Grain boundaries
Grain sub boundaries

Brasses, Corrosion

Further Observations of SCC in α - β Brass: Considerations Regarding the Appearance of Crack Arrest Markings During SCC. 1081-1086A

Brasses, Crystal lattices

Deformation of Martensite in a Polycrystalline Cu—Zn—Al Alloy. 945-959A

Brasses, Mechanical properties

Grain Boundary Contribution to the Bauschinger Effect in β -Brass Bicrystals. 2017-2029A

Brasses, Metal working

Effect of Stress—Strain-Law Transients on Formability. 1001-1009A

Brasses, Metallography

Modulated Microstructures in β Cu—Zn—Al. 2153-2161A

Brasses, Phase transformations

Microstructural Effects of Martensitic Transformation Cycling of a Cu—Zn—Al Alloy: Vestigial Structures in the Parent Phase. 195-203A

Brazing

See Vacuum brazing

Brick kilns

See Kilns

Brittle fracture

Size Effects on the Microscopic Cleavage Stress, σ_F , in Martensitic Microstructures. 231-241A
Fracture Behavior in Medium-Carbon Martensitic Silicon- and Nickel-Steels. 1173-1178A
Hydrogen-Induced Subcritical Crack Growth of a 12Cr—1Mo Ferritic Stainless Steel. 1229-1240A

Brittleness

See also Temper brittleness
Fracture of Fe₃Al. 2298-2300A

Bromides, Thermal properties

Legendre Polynomial Expansions of Thermodynamic Properties of Binary Solutions. 1057-1063A

Bronzes

See Eryllium bronzes

Bullets

See Projectiles

Burdening

See Blast furnace practice

Cadmium base alloys, Crystal growth

Nonlinear Regression Analysis of Superimposed DSC Crystallization Peaks. 1479-1481A

Cesium

See Cesium

Calcining

See Roasting

Calcium, Diffusion

Measurement of Tracer Diffusivities of Ca⁴⁵ and Fe⁵⁹ in Silica Saturated FeO—CaO—SiO₂ Melts With the Porous Frit Technique. 497-501B

Calcium, Impurities

The Gaseous Reduction of Solid Calcicostites in CO/CO₂ and H₂/H₂O Gas Mixtures. 375-381B
The Effect of Sulfur on the Gaseous Reduction of Solid Calcicostites. 383-393B

Calcium compounds

See Lime

Calcium oxide

See Lime

Calorimeters

A Straightforward New Procedure for Determining Crystallization Kinetics by Heating Rate DSC. 561-566A

Calorimetry

Nonlinear Regression Analysis of Superimposed DSC Crystallization Peaks. 1479-1481A

Capillarity

An Analysis of the Surface Menisci in a Mixture of Liquid and Deformable Grains. 325-330A

Capillary tubes

Experimental Studies on Drop Formation at the Tip of Melting Rods. 471-477B

Carbides

See also Silicon carbide
Tungsten carbide

Retained Carbide Distribution in Intercritically Austenitized 52100 Steel. 31-36A

Carbides, Composition effects

Influence of Alloy Chemistry on Carbide Precipitation in a Nickel Base Superalloy. 2075-2077A

Carbides, Crystal growth

Thermodynamics of the Fe—Mo—C System at 985K. 391-398A
The Microstructure and Mechanical Properties of a Modified 2.25Cr—1Mo Steel. 1027-1034A
Discussion of "The Bainite Reaction in Fe—Si—C Alloys: the Primary Stage" and "The Bainite Reaction in Fe—Si—C Alloys: the Secondary Stage". 1095-1100A
Microstructure—Mechanical Property Relationships in Isothermally Transformed Vanadium Steels. 1191-1202A
The Kinetics of Carbide Precipitation in Silicon—Aluminum Steels. 1287-1294A

Carbides, Thermal properties

Thermodynamic Properties of Carbides in 2.25Cr—1Mo Steel at 985K. 1585-1592A
Gibbs Free Energies of Formation of Molybdenum Carbide and Tungsten Carbide From 1173-1573K. 2031-2034A

Carbon, Alloying additive

On the Microstructure and Mechanical Behavior of Melt-Spun Fe—24Ni—0.5C Ribbons: Effect of Austenite Grain Size. 127-136A
Dendritic Microstructure in Argon Atomized Superalloy Powders. 2099-2102A

Carbon, Binary systems

An HVEM Study of an Unusual Ordering Reaction in Platinum—Carbon. 807-814A

Carbon, Diffusion

A Simplified Treatment of Carbon Diffusion in Compound Welds Having an Intermediate Layer. 2083-2084A
Carbon Segregation to Grain Boundaries in Rapidly Solidified Ni₃Al. 2084-2086A

Carbon, Impurities

The Effects of Interstitials and Hydrogen-Interstitial Interactions on Low Temperature Hardening and Embrittlement in Vanadium, Niobium, and Tantalum. 1179-1189A

Carbon, Quaternary systems

Phase Relationships in the Iron-Rich Fe—Cr—Ni—C System at Solidification Temperatures. 1461-1469A

Carbon, Quinary systems

Phase Relationships in the Fe—Cr—Mn—Ni—C System at Solidification Temperatures. 1825-1835A

Carbon, Reactions (chemical)

Reduction of Phosphate Ore by Carbon. II. Rate Limiting Steps. 869-877B

Carbon, Solubility

Thermodynamics of the Fe—Mo—C System at 985K. 391-398A
Thermotransport of Carbon in Two-Phase V—C and Nb—C Alloys. 1955-1966A

Carbon, Sorption

Potentiometric Studies on the Adsorption of Au(CN)₂⁻ and Ag(CN)₂⁻ Onto Activated Carbon. 523-528B
Studies on Role of Oxygen in the Adsorption of Au(CN)₂⁻ and Ag(CN)₂⁻ Onto Activated Carbon. 529-533B

Carbon, Ternary systems

Thermodynamics of the Fe—Mo—C System at 985K. 391-398A
Thermodynamics of the Si—C—O System for the Production of Silicon Carbide and Metallic Silicon. 503-514B
Direct Use of the Chemical Potential Function in Thermodynamic Modeling of Alloy Phase Diagrams. 1471-1477A

Carbon compounds

See Carbides
Carbon dioxide
Carbon monoxide
Tungsten carbide

Carbon dioxide, Reactions (chemical)

Interfacial Rates of Reaction of CO₂ With Liquid Iron Silicates, Silica-Saturated Manganese Silicates, and Some Calcium Iron Silicates. 307-316B
Structural Effects in the Reaction Between Carbon Dioxide and Coke Doped With Various Potassium Bearing Catalytic Precursors. 565-574B
Reduction of Lead Minerals by CO/CO₂ Gas Mixtures: Application of the Grain Model. 575-586B
Reactions of Fe—Cr and Ni—Cr Alloys in CO/CO₂ Gases at 850 and 950°C. 1065-1074A

Carbon manganese steels, Corrosion

A Study of the Hydrogen-Induced Degradation of Two Steels Differing in Sulfur Content. 2255-2263A

Carbon manganese steels, Mechanical properties

High Temperature Ductility Loss in Carbon—Manganese and Niobium-Treated Steels. 1995-2006A

Carbon manganese steels, Welding

A Model for the Silicon—Manganese Deoxidation of Steel Weld Metals. 1797-1807A

Carbon monoxide, Reactions (chemical)

Reduction of Lead Minerals by CO/CO₂ Gas Mixtures: Application of the Grain Model. 575-586B
Reactions of Fe—Cr and Ni—Cr Alloys in CO/CO₂ Gases at 850 and 950°C. 1065-1074A

Carbon steels

See also Aluminum killed steels
Carbon manganese steels

- Carbon steels, Crystal growth**
Effect of Copper Precipitation on the Development of Recrystallization Textures Through Continuous Annealing of Low-Carbon Sheet Steel. 621-633A
Lower Bainite With Midrib in Hypereutectoid Steels. 1113-1120A
Grain Growth in Capped Steel. 1907-1913A
- Carbon steels, Diffusion**
Analysis of Solute Distribution in Dendrites of Carbon Steel With δ/γ Transformation During Solidification. 845-859B
- Carbon steels, Mechanical properties**
A Model for Yielding in Anisotropic Metals. 107-114A
Effects of the Prior Austenite Grain Size on the Ductility of Fully Pearlitic Eutectoid Steel. 461-472A
Hydrogen Degradation of Spheroidized AISI 1020 Steel. 1485-1487A
Instabilities During Tension of Thin Voided Viscoplastic Sheets. 1637-1640A
Microstructural Effects on the Cleavage Fracture Stress of Fully Pearlitic Eutectoid Steel. 1769-1786A
- Carbon steels, Metal working**
Effect of Stress—Strain-Law Transients on Formability. 1001-1009A
- Carbon steels, Phase transformations**
The Dissolution of Cementite in a Low Carbon Steel During Isothermal Annealing at 700°C. 617-620A
The Kinetics of Ferrite Nucleation at Austenite Grain Edges in Fe—C and Fe—C—X Alloys. 1399-1407A
- Carbon steels, Phases (state of matter)**
Development of Ferrous Laminated Composites With Unique Microstructures by Control of Carbon Diffusion. 1517-1527A
- Carbon steels, Welding**
The Diffusion Bonding of Zr—2.5Nb to Steel. 429-434A
- Carbothermic reactions**
Application of Thermodynamic and Kinetic Principles in the Reduction of Metal Oxides by Carbon in a Plasma Environment. 197-207B
- Carburization**
See Carburizing
- Carburization (corrosion)**
Stability of the Chromia Layer on Steels in Flowing Nonequilibrium H_2 — H_2O — CH_4 —CO Mixtures at 950°C. 915-921A
- Carburizing**
Reactions of Fe—Cr and Ni—Cr Alloys in CO/CO₂ Gases at 850 and 950°C. 1065-1074A
- Carrier concentration**
See Carrier density
- Carrier density**
Thermodynamic Properties and Defect Structure of Semiconducting Compound Phases: Tin Telluride. 1241-1245A
- Case carburizing**
See Carburizing
- Case hardening**
See Carburizing
- Cast iron**
See also Chromium iron
Nodular iron
- Cast iron, Casting**
Heat and Moisture Transfer in Sand Molds Containing Water. 903-911B
- Cast iron, Crystal growth**
Misra Technique Applied to Solidification of Cast Iron. 358-360A
Microstructural Variations Induced by Gravity Level During Directional Solidification of Near-Eutectic Iron—Carbon Type Alloys. 1121-1130A
- Cast iron, Mechanical properties**
The Interaction of Hydrogen With the Interface of Al₂O₃ Particles in Iron. 2183-2186A
- Casting**
See Continuous casting
Ingot casting
Melt spinning
Permanent mold casting
Rheocasting
Sand casting
- Casting alloys, Microstructure**
The Influence of Iron and Chromium on the Microstructure of Cast Al—Si—Mg Alloys. 45-52A
- Casting defects**
See also Blowholes
An Ice-Water Model Study on Formation of Blowhole-Free Skin With Reference to Solidification of Steel.
The Air-Gap Formation Process at the Casting/Mold Interface and the Heat Transfer Mechanism Through the Gap. 553-564B
833-844B
- Castings**
See also Continuous cast shapes
- Castings, Crystal growth**
Numerical Simulation of Solidification in an Aluminum Casting. 209-216B
- Cathodic coatings (oxide)**
See Oxide coatings
- Cathodic polarization**
The Effect of Cathodic Polarization on the Corrosion Fatigue Behavior of a Precipitation Hardened Aluminum Alloy. 339-347A
- Cavitation**
Superplasticity in a Thermomechanically Processed High-Magnesium, Al—Mg Alloy. 1035-1041A
- The Influence of Thermomechanical Processing Variables on Superplasticity in a High-Magnesium, Al—Mg Alloy. 1043-1050A
- Cells**
See Electrolytic cells
- Cementite**
The Dissolution of Cementite in a Low Carbon Steel During Isothermal Annealing at 700°C. 617-620A
- Cerium, Chemical analysis**
Research on Determination of the Rare-Earth Content in Metal Phases of Steel. 315-323A
- Cesium, Environment**
Liquid Cesium Tellurium-Induced Fatigue Embrittlement of Cold-Worked 316 Stainless Steel. 2090-2093A
- CGF forging process**
See Forging
- Chalcocite, Reduction (chemical)**
Lime-Enhanced Reduction of Sulfide Concentrates: a Thermodynamic Discussion. 185-196B
- Chalcogenides**
See Sulfides
Tellurides
- Chalcopyrite, Reduction (chemical)**
The Leaching of Chalcopyrite With Ferric Chloride. 19-28B
Intrinsic Kinetics of the Oxidation of Chalcopyrite Particles Under Isothermal and Nonisothermal Conditions. 51-60B
Lime-Enhanced Reduction of Sulfide Concentrates: a Thermodynamic Discussion. 185-196B
Discussion of "Lime-Enhanced Reduction of Sulfide Concentrates: a Thermodynamic Discussion" and Authors' Reply. 914-918B
- Chemical analysis**
See Depth profiling
- Chemical attack**
See Preferential attack (corrosion)
- Chemical cleaning**
See Pickling
- Chemical kinetics**
See Reaction kinetics
- Chemical properties**
See Heat of formation
- Chemical tests**
See Depth profiling
- Chemistry**
See Biochemistry
Physical chemistry
Surface chemistry
Thermochemistry
- Chlorides, Environment**
High Temperature Corrosion of Superalloys in an Environment Containing Both Oxygen and Chlorine. 1067-1094A
- Chlorides, Refining**
The Vapor—Liquid Equilibria of the Aluminum Chloride—Titanium Tetrachloride System. 609-610B
- Chlorides, Synthesis**
On the Separation of TiCl₄ From AlCl₃. 232-234B
- Chlorides, Thermal properties**
Legendre Polynomial Expansions of Thermodynamic Properties of Binary Solutions. 1057-1063A
- Chlorination**
The Formation of Volatile Corrosion Products During the Mixed Oxidation—Chlorination of Cobalt at 650°C. 1223-1228A
- Chlorine**
Leaching Kinetics of Natural Cobalt Triarsenide in Chlorine Solutions. 629-637B
- Chromium, Alloying additive**
The Influence of Iron and Chromium on the Microstructure of Cast Al—Si—Mg Alloys. 45-52A
L₁ Type Ni—Al—Cr Alloys Processed by Rapid Solidification. 1685-1692A
- Chromium, Alloying elements**
The Kinetics of the Nitrogen Reaction With Liquid Iron—Chromium Alloys. 317-322B
Comparison of Solution Models for Nonmetallic Solutes in Binary Liquid Alloys: Nitrogen in Fe—Cr and Fe—Ni. 785-789B
Roles of Dislocations and Grain Boundaries in Martensite Nucleation. 1693-1702A
- Chromium, Diffusion**
Interdiffusion in the Ni—Cr—Co—Mo System at 1300°C. 963-990A
- Chromium, Extraction**
Application of Thermodynamic and Kinetic Principles in the Reduction of Metal Oxides by Carbon in a Plasma Environment. 197-207B
- Chromium, Quaternary systems**
Phase Relationships in the Iron-Rich Fe—Cr—Ni—C System at Solidification Temperatures. 1461-1469A
- Chromium, Quinary systems**
Phase Relationships in the Fe—Cr—Mn—Ni—C System at Solidification Temperatures. 1825-1835A
- Chromium, Solubility**
Alloying Behavior of Co₃Ti. 1433-1439A
- Chromium, Ternary systems**
Direct Use of the Chemical Potential Function in Thermodynamic Modeling of Alloy Phase Diagrams. 1471-1477A

Chromium

- Balance of Distribution of Some Transition Metals Between the (M' , M'')B and (M' , M'')₂B Phases. 1665-1669A
- Chromium compounds, Thermal properties**
Standard Enthalpies of Formation of $TiSi_2$ and VS_2 by High-Temperature Calorimetry. 1217-1221A
- Chromium etc., Mechanical properties**
Microstructure and Creep Behavior of a Niobium Alloyed Cast Heat-Resistant 28% Chromium Steel. 691-696A
- Chromium molybdenum nickel steels**
See Nickel chromium molybdenum steels
- Chromium molybdenum steels**
See also Chromium molybdenum vanadium steels
Nickel chromium molybdenum steels
- Chromium molybdenum steels, Corrosion**
Sulfide Stress Cracking Susceptibility of Nickel Containing Steels. 1601-1610A
- Chromium molybdenum steels, Diffusion**
On the Effective Hydrogen Permeability in Metastable β Titanium Alloy, Niobium and 2.25Cr—1Mo Ferritic Steel. 2086-2090A
- Chromium molybdenum steels, Mechanical properties**
Wear Resistance of Quenched and Tempered AISI 4137H Steel. 295-306A
Dependence of Total Elongations of Superplastic Materials on m. 685-690A
The Microstructure and Mechanical Properties of a Modified 2.25Cr—1Mo Steel. 1027-1034A
Effect of Microstructure on Strength and Toughness of Heat-Treated Low Alloy Structural Steels. 1203-1209A
- Chromium molybdenum steels, Phases (state of matter)**
Thermodynamic Properties of Carbides in 2.25Cr—1Mo Steel at 985K. 1585-1592A
- Chromium molybdenum steels, Structural hardening**
Effect of Tempering Temperature on the Work-Hardening Rate of Five HSLA Steels. 307-313A
- Chromium molybdenum vanadium steels, Mechanical properties**
Dependence of Total Elongations of Superplastic Materials on m. 685-690A
- Chromium nickel molybdenum steels**
See Nickel chromium molybdenum steels
- Chromium nickel steels**
See Nickel chromium steels
- Chromium ores, Reduction (chemical)**
Application of Thermodynamic and Kinetic Principles in the Reduction of Metal Oxides by Carbon in a Plasma Environment. 197-207B
- Chromium steels**
See also Austenitic stainless steels
Chromium molybdenum steels
Chromium molybdenum vanadium steels
Duplex stainless steels
Ferritic stainless steels
Nickel chromium molybdenum steels
Nickel chromium steels
Stainless steels
- Chromium steels, Mechanical properties**
The C.L. m — δ Equation of Superplasticity. 679-684A
- Chromium steels, Phases (state of matter)**
Development of Ferrous Laminated Composites With Unique Microstructures by Control of Carbon Diffusion. 1517-1527A
- Chromium vanadium steels**
See Chromium molybdenum vanadium steels
- Circuits**
See Integrated circuits
- Clad metals, Mechanical properties**
Superplasticity of a Stainless Steel Clad Ultrahigh Carbon Steel. 2295-2298A
- Cleaning**
See also Gas scrubbing
Pickling
Surface Oxide on fcc Iron—Nickel Alloys. 163-167A
- Cleavage**
Microstructural Effects on the Cleavage Fracture Stress of Fully Pearlitic Eutectoid Steel. 1769-1786A
- Coating**
See Aluminizing
Vapor deposition coating
- Coatings**
See Oxide coatings
Protective coatings
- Cobalt, Alloying additive**
Microstructural Characterization of Rapidly Solidified Al—Li—Co Powders. 73-91A
The Effect of Alloying Additions on the Superplastic Properties of Ti—6Al—4V. 93-106A
- Cobalt, Alloying elements**
Nucleation, Growth, and Overall Transformation Kinetics of Grain Boundary Allotriomorphs of Proeutectoid α in Ti—3.2 at.% Co and Ti—6.6 at.% Cr Alloys. 1703-1715A
- Cobalt, Corrosion**
The Formation of Volatile Corrosion Products During the Mixed Oxidation—Chlorination of Cobalt at 650°C. 1223-1228A
- Cobalt, Diffusion**
Interdiffusion in the Ni—Cr—Co—Mo System at 1300°C. 983-990A
- Cobalt, Extraction**
Leaching Kinetics of Natural Cobalt Triarsenide in Chlorine Solutions. 629-637B
- Cobalt, Reactions (chemical)**
Rates of Dissolution of Solid Iron, Cobalt, Nickel, and Silicon in Liquid Copper and Diffusion Rate of Iron From Liquid Cu—Fe Alloy Into Liquid Copper. 291-305B
- Cobalt, Recovering**
Diffusivity of Cobalt and Nickel Compounds as a Function of Concentration and Temperature. 425-432B
- Cobalt, Ternary systems**
Balance of Distribution of Some Transition Metals Between the (M' , M'')B and (M' , M'')₂B Phases. 1665-1669A
- Cobalt base alloys, Corrosion**
High Temperature Corrosion of Superalloys in an Environment Containing Both Oxygen and Chlorine. 1087-1094A
- Cobalt base alloys, Magnetic properties**
Directional Solidification and Characterization of Near Eutectic Sm_2Co_{17}/Co Alloys. 1149-1155A
- Cobalt base alloys, Powder technology**
The Critical Grain Size for Liquid Flow Into Pores During Liquid Phase Sintering. 1915-1919A
- Cobalt compounds, Oxidation**
Oxidation of Cobalt Sulfide. 367-373B
- Cobalt compounds, Solubility**
Alloying Behavior of Co_3Ti . 1433-1439A
- Coercive force**
Directional Solidification and Annealing of $Mn_{55}Al_{45}$ Alloys. 1247-1249A
- Coercive force, Microstructural effects**
Directional Solidification and Characterization of Near Eutectic Sm_2Co_{17}/Co Alloys. 1149-1155A
Grain Growth Characteristics and Magnetic Properties of Rapidly Quenched Silicon Steel Ribbons. 1295-1299A
- Coercivity**
See Coercive force
- Coils (strip), Crystal growth**
Grain Growth in Capped Steel. 1907-1913A
- Coke, Reactions (chemical)**
Structural Effects in the Reaction Between Carbon Dioxide and Coke Doped With Various Potassium Bearing Catalytic Precursors. 565-574B
- Coke breeze**
See Coke
- Cold cracking (welds)**
See Weld defects
- Cold ductility**
See Ductility
- Cold formability**
See Formability
- Cold forming**
See Cold working
- Cold reduction**
See Cold working
- Cold shortness**
See Brittleness
- Cold working**
See also Stretch forming
Deformation of Martensite in a Polycrystalline Cu—Zn—Al Alloy. 945-959A
The Processing and Properties of Heavily Cold Worked Directionally Solidified Ni—W Eutectic Alloys. 1165-1171A
- Columbium**
See Niobium
- Columbium base alloys**
See Niobium base alloys
- Columbium compounds**
See Niobium compounds
- Columnar structure, Alloying effects**
Microstructural Characterization of Rapidly Solidified Al—Li—Co Powders. 73-91A
- Compacting**
See also Hot isostatic pressing
An Empirical Model for Hot Isostatic Pressing of Metal Powders. 1977-1984A
- Compacts**
See Powder compacts
Sintered compacts
- Compliance (elasticity)**
See Modulus of elasticity
- Composite materials**
See also Fiber composites
- Composite materials, Microstructure**
An In Situ HVEM Study of Dislocation Generation at Al/SiC Interfaces in Metal Matrix Composites. 379-389A
- Compression strength**
See Compressive strength

- Compressive modulus**
See Modulus of elasticity
- Compressive strength**
High-Temperature Plastic Deformation of Two V—Ga Alloys With A15 Structure. 519-525A
- Compressive strength, Microstructural effects**
Orientation and Temperature Dependence of Some Mechanical Properties of the Single-Crystal Nickel-Base Superalloy René N4: III. Tension—Compression Anisotropy. 507-512A
- Compressive yield strength**
See Compressive strength
- Computer programs**
Announcement of a Computer Program for the Analysis of Compositionally Broadened X-Ray Diffraction Peaks. Orienting Grains With {110} Surface Traces. 899-901A
961-966A
- Computer simulation**
Numerical Simulation of Solidification in an Aluminum Casting. 209-216B
Computer Simulation of Convection in Moving Arc Weld Pools. 2271-2277A
- Concast**
See Continuous casting
- Conducting sheet analog**
See Heat transmission
- Conductivity**
See Superconductivity
- Conical mills**
See Ball mills
- Constitutional diagrams**
See Phase diagrams
- Construction**
See Honeycomb construction
- Continuous cast shapes, Crystal growth**
High Temperature Grain Growth During Slab Reheating of Oriented 3% Si—Fe Made Using Continuous Casting. 1335-1346A
- Continuous casting**
Rotational Electromagnetic Stirring in Continuous Casting of Round Strands. 119-131B
- Control**
See Dust control
Process control
- Convection**
The Effect of Convection on the Dendrite to Eutectic Transition. 991-1000A
Three-Dimensional Convection in Laser Melted Pools. 2265-2270A
Computer Simulation of Convection in Moving Arc Weld Pools. 2271-2277A
- Converters**
See Basic converters
Bottom blown converters
Copper converters
Rotary converters
Top blown converters
- Cooling**
See Supercooling
- Cooling curves**
Microstructure—Mechanical Property Relationships in Isothermally Transformed Vanadium Steels. 1191-1202A
An Assessment of the Additivity Principle in Predicting Continuous-Cooling Austenite-to-Pearlite Transformation Kinetics Using Isothermal Transformation Data. 1493-1503A
- Cooling rate**
The Effect of Solidification Rate on Microsegregation. 2063-2073A
- Copes (molds)**
See Sand molds
- Copper, Alloying additive**
Superplastic Behavior of a Zn—22Al—0.5Cu Alloy. 1873-1875A
- Copper, Alloying elements**
Effect of Copper Precipitation on the Development of Recrystallization Textures Through Continuous Annealing of Low-Carbon Sheet Steel. 621-633A
Microstructure of a Quenched and Tempered Copper-Bearing High-Strength Low-Alloy Steel. 791-798A
Formation of Copper Pockets in Iron Grains During the Sintering of Fe—Cu Alloys. 1429-1431A
The Effect of Hot-Rolling on Chill Cast Al—Al₃Ni, Chill-Cast Al—Al₂Cu, and Unidirectionally Solidified Al—Al₃Ni Eutectic Alloys. 1985-1993A
The Effect of Solidification Rate on Microsegregation. 2063-2073A
Effects of Copper on Proeutectoid Cementite Precipitation. 2163-2173A
- Copper, Binary systems**
An Ambiguity in the Definition of the Activity Coefficient at Infinite Dilution. 1484-1485A
- Copper, Crystal lattices**
Reexamination of Grain-Boundary Sliding by Diffusion. 1949-1953A
- Copper, Diffusion**
Diffusional Breakdown of a Silver Diffusion Barrier in a Cu—Ag—Ni Diffusion Triple. 933-944A
- Copper, Extraction**
Measurements of Oxygen Pressure in a Copper Flash Smelting Furnace by an EMF Method. 111-117B
Dissolution of Solid Magnetite in Fe—S—O Melt. 639-645B
- Heat Flow in Copper Converters. 677-685B
Arsenic Activities in Molten Copper and Copper Sulfide Melts. 755-761B
Thermodynamics of Gaseous SbS. 913-914B
Discussion of "Lime-Enhanced Reduction of Sulfide Concentrates: a Thermodynamic Discussion" and Authors' Reply. 914-918B
- Copper, Mechanical properties**
Orientation and Strain Dependence of Stored Energy of Cold Work in Axisymmetric Copper. 513-517A
- Copper, Physical properties**
Interfacial Tension and Flotation Characteristics of Liquid Metal—Sodium Flux Systems. 339-346B
- Copper, Reactions (chemical)**
Rates of Dissolution of Solid Iron, Cobalt, Nickel, and Silicon in Liquid Copper and Diffusion Rate of Iron From Liquid Cu—Fe Alloy Into Liquid Copper. 291-305B
- Copper, Refining**
A Kinetic Model for the Vacuum Refining of Inductively Stirred Copper Melts. 87-103B
A Pressurized Screw Feeder for Powder Injection. 229-231B
- Copper, Solubility**
A Solid-State EMF Study of the Cu—Cu₂O—NiO Three-Phase Equilibrium. 1104-1106A
- Copper, Ternary systems**
Estimation of Diffusion Path Slopes at Zero-Flux Plane Compositions. 362-364A
- Copper base alloys**
See also Beryllium bronzes
Brasses
- Copper base alloys, Corrosion**
On the Failure Mechanism of Chemically Embrittled Cu₃Au Single Crystals. 703-710A
- Copper base alloys, Phase transformations**
Transformation Sequence in a Cu—Al—Ni Shape Memory Alloy at Elevated Temperatures. 65-72A
- Copper base alloys, Phases (state of matter)**
Nature of Large Ti₄Cu₂O Particles Formed During Annealing of Cu₆₅Ti₃₅ Metallic Glass Ribbons. 575-581A
- Copper base alloys, Reactions (chemical)**
Activity Coefficient of Oxygen in Copper—Tellurium Melts. 171-177B
- Copper base alloys, Structural hardening**
Discussion of "The Early Stages of the Decomposition of Alloys" and Author's Reply. 742A
Particle Size and Orientation Effects on Softening in a Copper Matrix Containing Rod-Shaped Iron Particles. 1751-1755A
- Copper compounds, Solubility**
A Solid-State EMF Study of the Cu—Cu₂O—NiO Three-Phase Equilibrium. 1104-1106A
- Copper converters**
Heat Flow in Copper Converters. 677-685B
- Copper mattes**
Measurements of Oxygen Pressure in a Copper Flash Smelting Furnace by an EMF Method. 111-117B
Dissolution of Solid Magnetite in Fe—S—O Melt. 639-645B
Arsenic Activities in Molten Copper and Copper Sulfide Melts. 755-761B
Thermodynamics of Gaseous SbS. 913-914B
- Copper mattes, Solubility**
Solubility of Oxygen and Sulfur in Copper—Iron Mattes. Correction to "Solubility of Oxygen and Sulfur in Copper—Iron Mattes". 147-157B
400B
- Copper ores**
See Chalcocite
Chalcopyrite
- Core hardness**
See Hardness
- Core loss, Composition effects**
The Effect of Manganese and Sulfur Contents on the Magnetic Properties of Cold Rolled Lamination Steels. 1259-1266A
- Core loss, Microstructural effects**
The Effect of Thermomechanical History Upon the Microstructure and Magnetic Properties of Nonoriented Silicon Steels. 1267-1275A
The Kinetics of Carbide Precipitation in Silicon—Aluminum Steels. 1287-1294A
Grain Growth Characteristics and Magnetic Properties of Rapidly Quenched Silicon Steel Ribbons. 1295-1299A
- Corrosion**
See Bacterial corrosion
Carburization (corrosion)
Corrosion fatigue
Hot gas corrosion
Preferential attack (corrosion)
- Corrosion cracking**
See Stress corrosion cracking
- Corrosion fatigue**
Fatigue Crack Growth Rates in a Pressure Vessel Steel Under Various Conditions of Loading and the Environment. 1837-1849A
Liquid Cesium Tellurium-Induced Fatigue Embrittlement of Cold-Worked 316 Stainless Steel. 2090-2093A
- Corrosion fatigue, Field effects**
The Effect of Cathodic Polarization on the Corrosion Fatigue Behavior of a Precipitation Hardened Aluminum Alloy. 339-347A

Corrosion mechanisms

Corrosion mechanisms

See Bacterial corrosion

Corrosion products

The Formation of Volatile Corrosion Products During the Mixed Oxidation—Chlorination of Cobalt at 650°C. 1223-1228A

Corrosion rate, High temperature effects

High Temperature Corrosion of Superalloys in an Environment Containing Both Oxygen and Chlorine. 1087-1094A

Corrosion resistance

Mechanical Properties and Microstructure of Al—Li—Cu—Mg—Zr Die Forgings. 2007-2016A

Cost savings

See Economics

CO₂ arc welding

See Gas metal arc welding

Crack closure

Further Observations of SCC in α - β Brass: Considerations Regarding the Appearance of Crack Arrest Markings During SCC. 1081-1086A

Crack growth

See Crack propagation

Crack initiation

Microcrack Initiation and Acoustic Emission During Fracture Toughness Tests of A533B Steel. 843-852A

Crack propagation

Fatigue Crack Growth and Fracture Toughness Behavior of an Al—Li—Cu Alloy. 1011-1026A

Hydrogen-Induced Subcritical Crack Growth of a 12Cr—1Mo Ferritic Stainless Steel. 1229-1240A

Fatigue Crack Propagation in Nickel-Base Superalloy Single Crystals Under Multiaxial Cyclic Loads. 1739-1750A

The Influence of Load Ratio on Fatigue Crack Growth in 7090-T6 and IN9021-T4 P/M Aluminum Alloys. 1787-1795A

Micromechanistic Expressions of Continuum Microscale Parameters for Stable Crack Growth. 2249-2253A

Crack propagation, Environmental effects

Effect of Environment on Fatigue Crack Propagation Behavior of Alloy 718 at Elevated Temperatures. 370-374A

Crack resistance

See Crack propagation

Cracking (fracturing)

See Crack initiation

Stress corrosion cracking

Cratering (welding)

See Weld defects

Creep (materials)

See also Creep rate

Creep rupture strength

Creep strength

Metallic Surface Layers Deposited by Diffusional Creep During Internal Oxidation. 746-749A

An Examination of Class A to Class M Transition in Pb—9Sn and Other Alloys. 1447-1453A

Cyclic Creep and Anelastic Relaxation Analysis of an ODS Superalloy. 1577-1583A

Reexamination of Grain-Boundary Sliding by Diffusion. 1949-1953A

Changes in the Subboundary Mesh Size With Creep Strain in 304 Stainless Steel. 2093-2097A

Creep limit

See Creep (materials)

Creep properties

See Creep (materials)

Creep rate

Constrained Cavity Growth Models of Longitudinal Creep Deformation of Oxide Dispersion Strengthened Alloys. 281-293A

Creep rate, Corrosion effects

Examination of the Titanium Environment in a René 41 Nickel Base Superalloy by X-Ray Absorption Spectroscopy. 739-741A

Creep resistance

See Creep strength

Creep rupture strength, Alloying effects

The Effects of Replacing the Refractory Elements Tungsten, Niobium, and Tantalum With Molybdenum in Nickel-Base Superalloys on Microstructural, Microchemistry, and Mechanical Properties. 651-661A

The Microstructure and Mechanical Properties of a Modified 2.25Cr—1Mo Steel. 1027-1034A

Creep strength

Constrained Cavity Growth Models of Longitudinal Creep Deformation of Oxide Dispersion Strengthened Alloys. 281-293A

Creep strength, Alloying effects

Microstructure and Creep Behavior of a Niobium Alloyed Cast Heat-Resistant 26% Chromium Steel. 691-696A

Creep strength, Stress effects

Correlation Between Creep Stress Exponent and Ductility in Al—10 At.% Zn. 365-366A

Creeping

See Creep (materials)

Critical temperature

See also Eutectic temperature

Critical temperature, Size effects

The α \rightleftharpoons γ Transformation in Iron Powders. 37-44A

Cross slip

Deformation of a Burgers Oriented Bimetallic Bicrystal of α - β (Ti—13Mn). 451-460A

Cross tension test

See Tension tests

Crushing strength

See Compressive strength

Cryogenic properties, Alloying effects

Effect of Aluminum Content on Low Temperature Tensile Properties in Cryogenic Fe/Mn/Al/Nb/C Steels. 2097-2098A

Crystal defects

See also Dislocations

Interstitial defects

Lattice vacancies

Fault Structures in Rapidly Quenched Ni—Mo Binary Alloys. 2291-2294A

Crystal orientation

See Crystal structure

Crystal structure

See also Equiaxed structure

Description of the Intercrystalline Structure Distribution in Polycrystalline Materials. 2199-2207A

Crystal structure, Alloying effects

L₁-Type Ni—Al—Cr Alloys Processed by Rapid Solidification. 1685-1692A

Crystal structure, Deformation effects

Modification of α Morphology in Ti—6Al—4V by Thermomechanical Processing. 1935-1947A

Crystallinity

See Crystal structure

Crystallization

See also Recrystallization

Secondary recrystallization

A Straightforward New Procedure for Determining Crystallization Kinetics by Heating Rate DSC. 561-566A

Nonlinear Regression Analysis of Superimposed DSC Crystallization Peaks. 1479-1481A

Crystals

See Single crystals

Current density

Electrocapillarity in the Aluminum Reduction Cell. 547-552B

Heat Transfer and Fluid Flow in the Welding Arc. 1139-1148A

Currents

See Electric arcs

Curves

See Cooling curves

Stress strain curves

Cyanides, Sorption

Potentiometric Studies on the Adsorption of Au(CN)₂⁻ and Ag(CN)₂⁻ Onto Activated Carbon. 523-528B

Studies on Role of Oxygen in the Adsorption of Au(CN)₂⁻ and Ag(CN)₂⁻ Onto Activated Carbon. 529-533B

Decarburizing

The Kinetics of the Nitrogen Reaction With Liquid Iron—Chromium Alloys. 317-322B

Effects of Decarburization and Normalizing Heat Treatment in Boron-Silicon Iron Alloys. 1353-1359A

Dechromizing

Void Formation in INCONEL MA-754 by High Temperature Oxidation. 151-162A

Decomposition

See Eutectoid decomposition

Phase decomposition

Deep carburizing

See Carburizing

Deep drawability

See Drawability

Defects

See Blowholes

Casting defects

Crystal defects

Dislocations

Interstitial defects

Lattice vacancies

Weld defects

Deformability

See Formability

Deformation

See Plastic deformation

Prestraining

Demetalization

See Dechromizing

Dendrite

See Dendritic structure

Dendritic powder, Microstructure

Dendritic Microstructure in Argon Atomized Superalloy Powders. 2099-2102A

Dendritic structure

Microstructure and Stability of Melt Spun Inconel 713LC. 173-180A

The Effect of Quenching on Mushy-Zone Microstructures. 360-362A

Dendrite Characteristics in Directionally Solidified Pb—8Au and Pb—3Pd Alloys. 2279-2290A

- Dendritic structure, Alloying effects**
Microstructural Characterization of Rapidly Solidified Al—Li—Co Powders. 73-91A
- Dendritic structure, Composition effects**
Dendritic Microstructure in Argon Atomized Superalloy Powders. 2099-2102A
- Dendritic structure, Crystal growth**
The Effect of Convection on the Dendrite to Eutectic Transition.
Microstructural Variations Induced by Gravity Level During Directional Solidification of Near-Eutectic Iron—Carbon Type Alloys. 991-1000A
1121-1130A
- Dendritic structure, Impurity effects**
The Influence of Iron and Chromium on the Microstructure of Cast Al—Si—Mg Alloys. 45-52A
- Dendritic structure, Pressure effects**
The Effect of Gravity Level on the Average Primary Dendritic Spacing of a Directionally Solidified Superalloy. 2301-2303A
- Densification**
An Empirical Model for Hot Isostatic Pressing of Metal Powders. 1977-1984A
- Deoxidation**
See Deoxidizing
- Deoxidizers**
Solubility and Activity of Oxygen in Liquid Nickel in Equilibrium With α -Al₂O₃ and NiO x (1 + x)Al₂O₃. 763-770B
- Deoxidizing**
Solubility and Activity of Oxygen in Liquid Nickel in Equilibrium With α -Al₂O₃ and NiO x (1 + x)Al₂O₃.
A Model for the Silicon—Manganese Deoxidation of Steel Weld Metals. 763-770B
1797-1807A
- Dephosphorizing**
A Pressurized Screw Feeder for Powder Injection.
Soda Slag System for Hot Metal Dephosphorization. 229-231B
797-804B
- Depletion**
Lithium Depletion During Heat Treatment of Aluminum—Lithium Alloys. 635-643A
- Deposition**
See Aluminizing
Vapor deposition coating
- Depth profiling, Automation**
Announcement of a Computer Program for the Analysis of Compositionally Broadened X-Ray Diffraction Peaks. 899-901A
- Desulfurizing**
A Pressurized Screw Feeder for Powder Injection.
The Sulfur Partition Ratio and the Sulfide Capacity of Na₂O—SiO₂ Slags at 1200°C.
The Study of Desulfurization Kinetics in Grain Oriented 3% Silicon Iron. 229-231B
491-496B
1347-1351A
- Deuterium, Diffusion**
Hydrogen and Deuterium Diffusion in Vanadium—Niobium Alloys. 645-650A
- Diagrams**
See Phase diagrams
- Die forgings, Mechanical properties**
Mechanical Properties and Microstructure of Al—Li—Cu—Mg—Zr Die Forgings. 2007-2016A
- Differential thermal analysis**
A Straightforward New Procedure for Determining Crystallization Kinetics by Heating Rate DSC.
Nonlinear Regression Analysis of Superimposed DSC Crystallization Peaks. 561-566A
1479-1481A
- Diffraction**
See Electron diffraction
- Diffusion**
Diffusional Breakdown of a Silver Diffusion Barrier in a Cu—Ag—Ni Diffusion Triple. 933-944A
Discussion of "The Bainite Reaction in Fe—Si—C Alloys: the Primary Stage" and "The Bainite Reaction in Fe—Si—C Alloys: the Secondary Stage".
Determination of the Interdiffusion Coefficients in the Fe—Ni and Fe—Ni—P Systems Below 900°C. 1095-1100A
1131-1138A
- Diffusion, Composition effects**
Estimation of Diffusion Path Slopes at Zero-Flux Plane Compositions. 362-364A
- Diffusion, High temperature effects**
Interdiffusion in the Ni—Cr—Co—Mo System at 1300°C. 983-990A
- Diffusion bonding**
See Diffusion welding
- Diffusion coefficient**
See Diffusion
- Diffusion couples**
See Diffusion
- Diffusion rate**
Determination of Diffusion Coefficient of Oxygen in γ -Iron From Measurements of Internal Oxidation in Fe—Al Alloys. 221-229A
- Diffusion welding**
The Diffusion Bonding of Zr—2.5Nb to Steel. 429-434A
- Diffusivity**
The Trapping and Transport Phenomena of Hydrogen in Nickel. 181-187A
- Measurement of Tracer Diffusivities of Ca⁴⁵ and Fe⁵⁹ in Silica Saturated FeO—CaO—SiO₂ Melts With the Porous Frit Technique. 497-501B
1523-1527A
- Anomalous Fast Diffusion in the Fe—Zn System.
A Simplified Treatment of Carbon Diffusion in Compound Welds Having an Intermediate Layer. 2083-2084A
- On the Effective Hydrogen Permeability in Metastable β Titanium Alloy, Niobium and 2.25Cr—1Mo Ferritic Steel. 2086-2090A
- Diffusivity, Deformation effects**
Hydrogen Transport During Deformation in Nickel. I. Polycrystalline Nickel. 861-867A
Hydrogen Transport During Deformation in Nickel. II. Single Crystal Nickel. 869-875A
- Dilatometry**
Analysis of Transformation Kinetics by Nonisothermal Dilatometry. 1441-1445A
- Dimensions**
See Particle size
- Dioxides**
See Carbon dioxide
Silicon dioxide
- Direct reduction**
Mechanism of Growth of Metallic Phase in Direct Reduction of Iron Bearing Oxides.
Development of an Analytical Equation for Calculation of the Blast Furnace Fuel Rate. 433-442B
705-724B
- Direct reduction, Impurity effects**
The Gaseous Reduction of Solid Calciumwustites in CO/CO₂ and H₂/H₂O Gas Mixtures.
The Effect of Sulfur on the Gaseous Reduction of Solid Calciumwustites. 375-381B
383-393B
- Directional solidification**
Effect of Fluid Flow and Hafnium Content on Macrosegregation in the Directional Solidification of Nickel Base Superalloys.
The Effect of Convection on the Dendrite to Eutectic Transition.
Microstructural Variations Induced by Gravity Level During Directional Solidification of Near-Eutectic Iron—Carbon Type Alloys.
Directional Solidification and Characterization of Near Eutectic Sn₂Co₁₇/Co Alloys.
The Processing and Properties of Heavily Cold Worked Directionally Solidified Ni—W Eutectic Alloys.
Directional Solidification and Annealing of Mn₅₅Al₄₅ Alloys. 347-356B
991-1000A
1121-1130A
1149-1155A
1165-1171A
1247-1249A
- Directionally solidified eutectics, Crystal growth**
Dendrite Characteristics in Directionally Solidified Pb—8Au and Pb—3Pd Alloys. 2279-2290A
- Directionally solidified eutectics, Mechanical properties**
Tensile Properties of Directionally Solidified Al—4Cu Alloys With Columnar and Equiaxed Grains.
The Effect of Hot-Rolling on Chill-Cast Al—Al₃Ni, Chill-Cast Al—Al₃Cu, and Unidirectionally Solidified Al—Al₃Ni Eutectic Alloys. 823-832A
1985-1993A
- Dislocations**
An In Situ HVEM Study of Dislocation Generation at Al/SiC Interfaces in Metal Matrix Composites. 379-389A
- Dislocations, Heating effects**
On the Kinetics of the Spreading of Extrinsic Grain Boundary Dislocations. 1967-1975A
- Dispersion hardening alloys, Mechanical properties**
Constrained Cavity Growth Models of Longitudinal Creep Deformation of Oxide Dispersion Strengthened Alloys. 281-293A
- Dispersion hardening alloys, Oxidation**
Void Formation in INCONEL MA-754 by High Temperature Oxidation. 151-162A
- Displacements (lattice)**
See Interstitial defects
- Dissimilar metals, Welding**
The Diffusion Bonding of Zr—2.5Nb to Steel.
A Simplified Treatment of Carbon Diffusion in Compound Welds Having an Intermediate Layer. 429-434A
2083-2084A
- Dissociation energy**
See Free energy of formation
- Dissolution**
Dissolution Behavior of 304 Stainless Steel in HNO₃/HF Mixtures.
Rate of Dissolution of Solid Nickel in Liquid Tin Under Static Conditions.
Rates of Dissolution of Solid Iron, Cobalt, Nickel, and Silicon in Liquid Copper and Diffusion Rate of Iron From Liquid Cu—Fe Alloy Into Liquid Copper.
Dissolution of Solid Magnetite in Fe—S—O Melt. 137-149A
281-289B
291-305B
639-645B
- Dissolving**
See Dissolution
- Drags (molds)**
See Sand molds
- Drawability**
On the Directionality of Strain Localization When Stretching Aluminum Alloy Sheets in Biaxial Tension. 367-370A
- Drawing (heat treatment)**
See Tempering
- Drill steels**
See Tool steels.

Dual phase steels

Dual phase steels, Alloy development

Effect of Copper Precipitation on the Development of Recrystallization Textures Through Continuous Annealing of Low-Carbon Sheet Steel.

621-633A

Dual phase steels, Mechanical properties

The Ductility of a HSLA Steel at Temperatures Below 300K.

697-702A

Ductile brittle transition

A Study of the Effect of Precipitated Austenite on the Fracture of a Ferritic Cryogenic Steel.

243-252A

The Influence of Precipitated Austenite on Hydrogen Embrittlement in 5.5Ni Steel.

1157-1164A

The Effects of Interstitials and Hydrogen-Interstitial Interactions on Low Temperature Hardening and Embrittlement in Vanadium, Niobium, and Tantalum.

1179-1189A

Effect of Microstructure on Strength and Toughness of Heat-Treated Low Alloy Structural Steels.

1203-1209A

Ductile iron

See Nodular iron

Ductility

The Ductility of a HSLA Steel at Temperatures Below 300K.

697-702A

Ductility, Diffusion effects

Effects of Nitrogen on the Mechanical Behavior of Hydrogenated Vanadium, Niobium, and Tantalum.

527-535A

Absence of Hydrogen Influence on the Mechanical Stability of Retained Austenite in a 0.2C/12Cr/1Mo Steel.

1876-1877A

Ductility, Heating effects

Influence of Soaking Treatments on Hot Ductility of Al—4.85Mg Alloys Containing Manganese.

833-841A

Ductility, Impurity effects

Effects of Oxygen on the Mechanical Behavior of Hydrogenated Vanadium, Niobium, and Tantalum.

853-859A

Ductility, Microstructural effects

Effects of the Prior Austenite Grain Size on the Ductility of Fully Pearlitic Eutectoid Steel.

461-472A

Microstructural Dependence of Iron—High Manganese Tensile Behavior.

537-547A

High Temperature Ductility Loss in Carbon—Manganese and Niobium-Treated Steels.

1995-2006A

Ductility, Stress effects

Correlation Between Creep Stress Exponent and Ductility in Al—10 At.% Zn.

365-366A

Duomelt process

See Vacuum arc melting

Duplex stainless steels, Mechanical properties

Flow Localization During Plane Strain Punch-Stretching of a Ferrite—Austenite Steel.

1537-1546A

Dust collection

See Dust control

Dust control

Theoretical and Experimental Study of the Removal of Dust Particles From Flue Gases Using Two-Phase Steam—Water Droplet Mixtures.

665-676B

Dynamics

See Fluid dynamics
Hydrodynamics
Kinetics

Economics

Materials and Electricity.

755-775A

Elastic constants

See Modulus of elasticity

Elastic modulus

See Modulus of elasticity

Elasticity

See Pseudoelasticity

Electric arc furnaces

See Vacuum arc furnaces

Electric arc melting

See Vacuum arc melting

Electric arc welding

See Arc welding

Electric arcs

Pressures Produced by Gas Tungsten Arcs.

601-607B

Electric circuits

See Integrated circuits

Electric conductors (materials)

See Electrolytes

Electric current

See Electric arcs

Electric discharges

See Electric arcs

Electric furnaces

See also Electric induction furnaces

Vacuum arc furnaces

Thermodynamics of the Si—C—O System for the Production of Silicon Carbide and Metallic Silicon.

503-514B

Electric induction furnaces

Turbulent Recirculating Flow in Induction Furnaces: a Comparison of Measurements With Predictions Over a Range of Operating Conditions.

687-693B

Electric power generation

Materials and Electricity.

755-775A

Electric power plants

See Electric power generation

Electric power stations

See Electric power generation

Electric welding

See Arc welding

Gas metal arc welding

Gas tungsten arc welding

Plasma arc welding

Resistance spot welding

Spot welding

Submerged arc welding

Electrical phenomena

See Electric arcs

Electrode potentials

Electrical properties

See Carrier density

Superconductivity

Electrical steels, Crystal growth

Grain Growth Characteristics and Magnetic Properties of Rapidly Quenched Silicon Steel Ribbons.

1295-1299A

High Temperature Grain Growth During Slab Reheating of Oriented 3% Si—Fe Made Using Continuous Casting.

1335-1346A

Effects of Decarburization and Normalizing Heat Treatment in Boron-Silicon Iron Alloys.

1353-1359A

Electrical steels, Heat treatment

The Study of Desulfurization Kinetics in Grain Oriented 3% Silicon Iron.

1347-1351A

Electrical steels, Magnetic properties

The Effect of Manganese and Sulfur Contents on the Magnetic Properties of Cold Rolled Lamination Steels.

1259-1266A

The Effect of Thermomechanical History Upon the Microstructure and Magnetic Properties of Nonoriented Silicon Steels.

1267-1275A

Electrical steels, Microstructure

Factors Affecting the Final Grain Size of Decarburized Lamination Steels.

1277-1285A

New Information on Texture Development in Regular and High-Permeability Grain-Oriented Silicon Steels.

1301-1312A

Origin and Development of Through-the-Thickness Variations of Texture in the Processing of Grain-Oriented Silicon Steel.

1313-1322A

Formation of the Goss Orientation Near the Surface of 3% Silicon Steel During Hot Rolling.

1323-1334A

Electrical steels, Structural hardening

The Kinetics of Carbide Precipitation in Silicon—Aluminum Steels.

1287-1294A

Electrode potentials

A Solid-State EMF Study of the Cu—Cu₂O—NiO Three-Phase Equilibrium.

1104-1106A

Electrode potentials

See Gas metal arc welding

Electrohydrodynamics

See Magnetohydrodynamics

Electrolysis

See also Electrowinning

Reduction (electrolytic)

The Vapor—Liquid Equilibria of the Aluminum Chloride—Titanium Tetrachloride System.

609-610B

Electrolytes, Phases (state of matter)

Phase Diagram Studies of the Systems KCl—K₃MoCl₆ and LiCl—K₃MoCl₆.

231-232B

Electrolytic cells

Electrocapillarity in the Aluminum Reduction Cell.

547-552B

Electrolytic pickling

See Pickling

Electrolytic reduction

See Reduction (electrolytic)

Electromagnetic stirring

Rotational Electromagnetic Stirring in Continuous Casting of Round Strands.

119-131B

Turbulent Recirculating Flow in Induction Furnaces: a Comparison of Measurements With Predictions Over a Range of Operating Conditions.

687-693B

Electromotive force series

See Electrode potentials

Electromotive series

See Electrode potentials

Electron diffraction

Modulated Microstructures in β Cu—Zn—Al.

2153-2161A

Electron microscopy

See Transmission electron microscopy

Electroplating

See Fused salt plating

Electroreduction

See Electrowinning

Electrorefining

A Study on Purification of Metallurgical Grade Silicon by Molten Salt Electrorefining.

395-397B

Electrowinning

Laboratory Reduction Rate and Current Efficiency Studies of Batch Type Electrolytic Reduction of Uranium(VI) in a Sulfate System.

69-76B

- Elongation, Alloying effects**
Effect of Aluminum Content on Low Temperature Tensile Properties in Cryogenic Fe/Mn/Al/Nb/C Steels. 2097-2098A
- Embrittlement**
See also Hydrogen embrittlement
Liquid metal embrittlement
- Embrittlement, Composition effects**
A Comparative Study of the Heat Affected Zone (HAZ) Properties of Boron Containing Low Carbon Steels. 1529-1536A
- Embrittlement, Microstructural effects**
High Temperature Ductility Loss in Carbon—Manganese and Niobium-Treated Steels. 1995-2006A
- Endurance limit**
See Fatigue limit
- Energy**
See Free energy
Free energy of formation
Heat of formation
Heat of mixing
Heat of solution
Internal energy
- Energy of dissociation**
See Free energy of formation
- Energy of formation**
See Free energy of formation
- Enthalpy**
Legendre Polynomial Expansions of Thermodynamic Properties of Binary Solutions. 1057-1083A
Standard Enthalpies of Formation of TiSi_2 and VSi_2 by High-Temperature Calorimetry. 1217-1221A
- Entropy**
Legendre Polynomial Expansions of Thermodynamic Properties of Binary Solutions. 1057-1083A
- Equiaxed structure, Alloying effects**
Microstructural Characterization of Rapidly Solidified Al—Li—Co Powders. 73-91A
- Equilibrium diagrams**
See Phase diagrams
- Eutectic reactions**
The Effect of Convection on the Dendrite to Eutectic Transition. 991-1000A
Microstructural Variations Induced by Gravity Level During Directional Solidification of Near-Eutectic Iron—Carbon Type Alloys. 1121-1130A
- Eutectic temperature, Alloying effects**
Effect of Small Additions of Silver on the Eutectic Temperature in the Lead—Tin System. 829-832B
- Eutectics**
See also Directionally solidified eutectics
- Eutectics, Deformation effects**
The Effect of Hot-Rolling on Chill-Cast Al— Al_3Ni , Chill-Cast Al— Al_2Cu , and Unidirectionally Solidified Al— Al_3Ni Eutectic Alloys. 1985-1993A
- Eutectoid decomposition, Alloying effects**
Effects of Copper on Proeutectoid Cementite Precipitation. 2163-2173A
- Eutectoid reactions**
See also Eutectoid decomposition
Nucleation Kinetics of Proeutectoid Ferrite at Austenite Grain Boundaries in Fe—C—X Alloys. 1385-1397A
The Kinetics of Ferrite Nucleation at Austenite Grain Edges in Fe—C and Fe—C—X Alloys. 1399-1407A
- Explosive bonding**
Discussion of "Fundamental Aspects of Formation and Stability of Explosive Welds" and Reply. 374A
- Extraction**
See Solvent extraction
- Extractive metallurgy**
See Hydrometallurgy
- Extrusion compacting**
See Compacting
- Extrusions, Mechanical properties**
The Influence of Load Ratio on Fatigue Crack Growth in 7090-T6 and IN9021-T4 P/M Aluminum Alloys. 1787-1795A
- Failure analysis**
See Fractography
- Fatigue (materials)**
See also Corrosion fatigue
Fatigue life
Fatigue limit
Fatigue strength
Low cycle fatigue
Serrated Grain Boundary Formation During High Temperature Fatigue. 1100-1102A
Rolling Contact Deformation of 1100 Aluminum Disks. 1561-1572A
Fatigue Crack Propagation in Nickel-Base Superalloy Single Crystals Under Multiaxial Cyclic Loads. 1739-1750A
The Influence of Load Ratio on Fatigue Crack Growth in 7090-T6 and IN9021-T4 P/M Aluminum Alloys. 1787-1795A
Grain Boundary Contribution to the Bauschinger Effect in β -Brass Bicrystals. 2017-2029A
- Fatigue (materials), Environmental effects**
Effect of Environment on Fatigue Crack Propagation Behavior of Alloy 718 at Elevated Temperatures. 370-374A
- Fatigue cracking**
See Fatigue (materials)
- Fatigue life, Impurity effects**
Influence of Foreign Particles on Fatigue Behavior of Ti—6Al—4V Prealloyed Powder Compacts. 271-280A
- Fatigue limit**
Fatigue Crack Growth and Fracture Toughness Behavior of an Al—Li—Cu Alloy. 1011-1026A
- Fatigue properties**
See Fatigue (materials)
- Fatigue strength, Deformation effects**
Effect of Isothermal Forging on Microstructure and Fatigue Behavior of Blended Elemental Ti—6Al—4V Powder Compacts. 549-559A
- Feeders, Design**
A Pressurized Screw Feeder for Powder Injection. 229-231B
- Ferric compounds**
See Iron compounds
- Ferrite, Crystal growth**
Discussion of "The Bainite Reaction in Fe—Si—C Alloys: the Primary Stage" and "The Bainite Reaction in Fe—Si—C Alloys: the Secondary Stage". 1095-1100A
On the Critical Nucleus Composition of Ferrite in an Fe—C—Mn Alloy. 1381-1384A
Nucleation Kinetics of Proeutectoid Ferrite at Austenite Grain Boundaries in Fe—C—X Alloys. 1385-1397A
The Kinetics of Ferrite Nucleation at Austenite Grain Edges in Fe—C and Fe—C—X Alloys. 1399-1407A
Application of Microstructure Modeling to the Kinetics of Proeutectoid Ferrite Transformation in Hot-Rolled Microalloyed Steels. 1625-1629A
- Ferrites, Synthesis**
Electrochemical Determination of Thermodynamic Properties and X-Ray Diffraction Investigation of the Fe_3O_4 — ZnFe_2O_4 System. 515-521B
- Ferritic stainless steels, Mechanical properties**
Microstructures and Mechanical Properties of Melt-Quenched Ferritic Stainless Steels. 261-269A
Microstructure and Creep Behavior of a Niobium Alloyed Cast Heat-Resistant 26% Chromium Steel. 691-696A
Hydrogen-Induced Subcritical Crack Growth of a 12Cr—1Mo Ferritic Stainless Steel. 1229-1240A
Absence of Hydrogen Influence on the Mechanical Stability of Retained Austenite in a 0.2C/12Cr/1Mo Steel. 1876-1877A
- Ferromagnetic materials**
See Magnetite
- Ferrous alloys**
See also Alloy steels
Cast iron
Steels
- Ferrous alloys, Diffusion**
Determination of the Interdiffusion Coefficients in the Fe—Ni and Fe—Ni—P Systems Below 900°C. 1131-1138A
- Ferrous alloys, Microstructure**
On the Microstructure and Mechanical Behavior of Melt-Spun Fe—24Ni—0.5C Ribbons: Effect of Austenite Grain Size. 127-136A
- Ferrous alloys, Oxidation**
Surface Oxide on Ice Iron—Nickel Alloys. 163-167A
Determination of Diffusion Coefficient of Oxygen in γ -Iron From Measurements of Internal Oxidation in Fe—Al Alloys. 221-229A
Reactions of Fe—Cr and Ni—Cr Alloys in CO/CO_2 Gases at 850 and 950°C. 1065-1074A
- Ferrous alloys, Phase transformations**
Roles of Dislocations and Grain Boundaries in Martensite Nucleation. 1693-1702A
- Ferrous alloys, Phases (state of matter)**
Discussion of "Miscibility Gap in Fe—Ni—Al and Fe—Ni—Al—Co Systems" and "Role of Alloying Elements in Phase Decomposition in Alnico Magnet Alloys". 1629-1632A
Analytical Scanning Transmission Electron Microscopic Study of Metastable Modulated Structure in a Rapidly Quenched Fe—22Ni—8Al—2.4C Alloy. 2077-2080A
- Ferrous alloys, Physical properties**
A Calculation of Viscosities for Iron—Metalloid Liquids. 901-903A
- Ferrous alloys, Powder technology**
Processing of Iron—Titanium Powder Mixtures by Transient Liquid Phase Sintering. 205-213A
Formation of Copper Pockets in Iron Grains During the Sintering of Fe—Cu Alloys. 1429-1431A
The Critical Grain Size for Liquid Flow Into Pores During Liquid Phase Sintering. 1915-1919A
Effect of Entrapped Inert Gas on Pore Filling During Liquid Phase Sintering. 2175-2182A
- Ferrous alloys, Solubility**
Nitrogen Solubility in Liquid Iron and Fe—Mn Alloys. 238-239B
Comparison of Solution Models for Nonmetallic Solutes in Binary Liquid Alloys: Nitrogen in Fe—Cr and Fe—Ni. 785-789B
- Ferrous alloys, Thermal properties**
A Modified Interaction Parameter Formalism for Non-Dilute Solutions. 1211-1215A
- Ferrous compounds**
See Iron compounds
- Ferrous metals**
See Ferrous alloys

Fiber composites

- Fiber composites, Magnetic properties**
Directional Solidification and Annealing of $Mn_{55}Al_{45}$ Alloys. 1247-1249A
- Fiber composites, Oxidation**
The Effect of Thermal Exposure on the Microstructure and Fiber/Matrix Interface of an Al_2O_3/Al Composite. 1075-1080A
- Fiber composites, Thermal properties**
Thermal Transient Stresses Due to Rapid Cooling in a Thermally and Elastically Orthotropic Medium. 1051-1055A
- Fiber metallurgy**
See Fiber composites
- Fields (physics)**
See Magnetic fields
- Finite element method**
Effect of Stress—Strain-Law Transients on Formability. Invariance of Neck Formation to Material Strength and Strain Rate for Power-Law Materials. 1001-1009A
1632-1633A
- Finsider process**
See Direct reduction
- Flame reduction process**
See Direct reduction
- Flash smelting**
Measurements of Oxygen Pressure in a Copper Flash Smelting Furnace by an EMF Method. 111-117B
Dissolution of Solid Magnetite in Fe—S—O Melt. 639-645B
- Flexural vibration**
See Fatigue (materials)
- Flow**
See Fluid flow
Plastic flow
Turbulent flow
- Flow stress**
See Yield strength
- Fluid bed roasting**
See Fluidized bed roasting
- Fluid dynamics**
See also Hydrodynamics
A Mathematical Model of the Planar Flow Melt Spinning Process. 695-703B
- Fluid flow**
See also Turbulent flow
Heat Transfer and Fluid Flow in the Welding Arc. 1139-1148A
- Fluid mechanics**
See Fluid dynamics
Hydrodynamics
- Fluidity**
See Viscosity
- Fluidized bed roasting**
Agglomeration of Particles During Roasting of Zinc Sulfide Concentrates. 647-656B
- Fluosolids roasting**
See Fluidized bed roasting
- Fluxes**
Interfacial Tension and Flotation Characteristics of Liquid Metal—Sodium Flux Systems. 339-346B
- Force**
See Coercive force
- Forging**
Effect of Isothermal Forging on Microstructure and Fatigue Behavior of Blended Elemental Ti—6Al—4V Powder Compacts. 549-559A
- Forgings**
See also Die forgings
- Forgings, Mechanical properties**
The Influence of Load Ratio on Fatigue Crack Growth in 7090-T6 and IN9021-T4 P/M Aluminum Alloys. 1787-1795A
- Formability**
Effect of Stress—Strain-Law Transients on Formability. Flow Localization During Plane Strain Punch Stretching of a Ferrite—Austenite Steel. 1001-1009A
1537-1546A
- Forming**
See Forging
Hot isostatic pressing
Hot rolling
Stretch forming
Thermomechanical treatment
- Fractography**
Characterization of Cryogenic Fe—6Ni Steel Fracture Modes: a Three Dimensional Quantitative Analysis. 815-822A
Fracture Behavior in Medium-Carbon Martensitic Silicon- and Nickel-Steels. 1173-1178A
- Fracture mechanics**
Micromechanistic Expressions of Continuum Microscale Parameters for Stable Crack Growth. 2249-2253A
- Fracture strength**
Size Effects on the Microscopic Cleavage Stress, σ_F , in Martensitic Microstructures. 231-241A
- Fracture strength, Cooling effects**
Microstructures and Mechanical Properties of Melt-Quenched Ferritic Stainless Steels. 261-269A
- Fracture strength, Microstructural effects**
Microstructural Effects on the Cleavage Fracture Stress of Fully Pearlitic Eutectoid Steel. 1769-1786A
- Fracture testing**
Nomenclature for Metallographic Sections. 1095A
- Fracture toughness**
Microcrack Initiation and Acoustic Emission During Fracture Toughness Tests of A533B Steel. 843-852A
Fatigue Crack Growth and Fracture Toughness Behavior of an Al—Li—Cu Alloy. 1011-1026A
The Processing and Properties of Heavily Cold Worked Directionally Solidified Ni—W Eutectic Alloys. 1165-1171A
Hydrogen-Induced Subcritical Crack Growth of a 12Cr—1Mo Ferritic Stainless Steel. 1229-1240A
Mechanical Properties and Microstructure of Al—Li—Cu—Mg—Zr Die Forgings. 2007-2016A
- Fracture toughness, Alloying effects**
The Effect of Silicon and Nickel Additions on the Sulfide Spacing and Fracture Toughness of a 0.4 Carbon Low Alloy Steel. 669-678A
Microstructure and Creep Behavior of a Niobium Alloyed Cast Heat-Resistant 26% Chromium Steel. 691-696A
- Fracture toughness, Stress effects**
Influence of Prestrain History on Fracture Toughness Properties of Steels. 473-489A
- Fracturing**
See Brittle fracture
Transgranular fracture
- Free energy**
See also Free energy of formation
On the Gibbs Energy of Formation of Wustite. 179-184B
Legendre Polynomial Expansions of Thermodynamic Properties of Binary Solutions. 1057-1063A
Thermodynamic Properties and Defect Structure of Semiconducting Compound Phases: Tin Telluride. 1241-1245A
- Free energy of dissociation**
See Free energy of formation
- Free energy of formation**
Gibbs Free Energies of Formation of Molybdenum Carbide and Tungsten Carbide From 1173-1573K. 2031-2034A
- Free machining steels**
See Resulfurized steels
- Fuel elements**
See Nuclear fuel elements
- Fuels**
See Coke
- Furnaces**
See Basic converters
Blast furnaces
Bottom blown converters
Copper converters
Electric furnaces
Electric induction furnaces
Kilns
Rotary converters
Top blown converters
Vacuum arc furnaces
- Fused salt plating**
Phase Diagram Studies of the Systems KCl—K₃MoCl₆ and LiCl—K₃MoCl₆. 231-232B
- Fused salts**
Interfacial Tension and Flotation Characteristics of Liquid Metal—Sodium Flux Systems. 339-346B
- Fused salts, Phases (state of matter)**
Phase Diagram Studies of the Systems KCl—K₃MoCl₆ and LiCl—K₃MoCl₆. 231-232B
- Fusion welding**
See Arc welding
Gas metal arc welding
Gas tungsten arc welding
Laser beam welding
Plasma arc welding
Submerged arc welding
- Gadolinium, Binary systems**
Study of the Enthalpies of Formation in the Gd—Ni System. 777-780A
- Galena, Reduction (chemical)**
The Dissolution of Galena in Ferric Chloride Media. 5-17B
An Investigation of the Thermodynamics and Kinetics of the Ferric Chloride Brine Leaching of Galena Concentrate. 29-39B
Kinetics of Galena Dissolution in Ferric Chloride Solutions. 415-423B
- Gallium, Recovering**
Extraction Equilibria in the System GaCl₃—AlCl₃—HCl—H₂O—Tributyl Phosphate. 259-265B
- Galvanic cells**
See Electrolytic cells
- Galvanized steels, Welding**
Resistance Spot Welding of Galvanized Steel. I. Material Variations and Process Modifications. 879-885B
Resistance Spot Welding of Galvanized Steel. II. Mechanisms of Spot Weld Nugget Formation. 887-901B
- Galvannealing**
See Annealing
- Gas holes**
See Blowholes

- Gas metal arc welding**
A Model for the Silicon—Manganese Deoxidation of Steel Weld Metals. 1797-1807A
- Gas permeability**
See Permeability
- Gas scrubbing**
Removal of SO₂ With Oxygen in the Presence of Fe(III). 745-753B
- Gas tungsten arc welding**
Pressures Produced by Gas Tungsten Arcs. Solidification and Solidification Cracking in Nitrogen-Strengthened Austenitic Stainless Steels. 601-607B
Metal Vapors in Gas Tungsten Arcs. I. Spectroscopy and Monochromatic Photography. 727-737A
Metal Vapors in Gas Tungsten Arcs. II. Theoretical Calculations of Transport Properties. 1851-1863A
The Use of New PHACOMP in Understanding the Solidification Microstructure of Nickel Base Alloy Weld Metal. 1865-1871A
2107-2116A
- Gas turbines**
Void Formation in INCONEL MA-754 by High Temperature Oxidation. 151-162A
- Germanium, Alloying elements**
Solidification of Nb—Ge Alloys in Long Drop Tubes. 973-981A
- Gibbs free energy**
See Free energy
- Glass**
See Metallic glasses
- Glass transition temperature**
A Theoretical Evaluation of Chemical Ordering and Glass Transition in Liquid Mg—Sn Alloys. 607-615A
- Gold, Extraction**
Potentiometric Studies on the Adsorption of Au(CN)₂⁻ and Ag(CN)₂⁻ Onto Activated Carbon. 523-528B
Studies on Role of Oxygen in the Adsorption of Au(CN)₂⁻ and Ag(CN)₂⁻ Onto Activated Carbon. 529-533B
- Grain boundaries**
See also Grain sub boundaries
Carbon Segregation to Grain Boundaries in Rapidly Solidified Ni₃Al. 2084-2086A
- Grain boundaries, Heating effects**
On the Kinetics of the Spreading of Extrinsic Grain Boundary Dislocations. 1967-1975A
- Grain boundary migration**
Serrated Grain Boundary Formation During High Temperature Fatigue. 1100-1102A
- Grain boundary sliding**
Reexamination of Grain-Boundary Sliding by Diffusion. 1949-1953A
- Grain growth**
Grain Growth Characteristics and Magnetic Properties of Rapidly Quenched Silicon Steel Ribbons. 1295-1299A
New Information on Texture Development in Regular and High-Permeability Grain-Oriented Silicon Steels. 1301-1312A
High Temperature Grain Growth During Slab Reheating of Oriented 3% Si—Fe Made Using Continuous Casting. 1335-1346A
Grain Growth in Capped Steel. 1907-1913A
- Grain orientation**
Orienting Grains With {110} Surface Traces. 961-966A
Description of the Intercrystalline Structure Distribution in Polycrystalline Materials. 2199-2207A
- Grain orientation, Deformation effects**
Formation of the Goss Orientation Near the Surface of 3% Silicon Steel During Hot Rolling. 1323-1334A
- Grain refinement**
Discussion of "The Grain Refining of Aluminum and Phase Relationships in the Al—Ti—B System" and Reply. 349-351A
Superplasticity in a Thermomechanically Processed High-Magnesium, Al—Mg Alloy. 1035-1041A
Development of Al—Ti—C Grain Refiners Containing TiC. 2127-2137A
- Grain refinement, Alloying effects**
The Influence of Iron and Chromium on the Microstructure of Cast Al—Si—Mg Alloys. 45-52A
- Grain size**
A Model for Yielding in Anisotropic Metals. 107-114A
On the Microstructure and Mechanical Behavior of Melt-Spun Fe—24Ni—0.5C Ribbons: Effect of Austenite Grain Size. 127-136A
Application of Microstructure Modeling to the Kinetics of Proeutectoid Ferrite Transformation in Hot-Rolled Microalloyed Steels. 1625-1629A
- Grain size, Cooling effects**
Microstructures and Mechanical Properties of Melt-Quenched Ferritic Stainless Steels. 261-269A
- Grain size, Heating effects**
Factors Affecting the Final Grain Size of Decarburized Lamination Steels. 1277-1285A
- Grain size, Impurity effects**
The Influence of Iron and Chromium on the Microstructure of Cast Al—Si—Mg Alloys. 45-52A
- Grain structure**
Origin and Development of Through-the-Thickness Variations of Texture in the Processing of Grain-Oriented Silicon Steel. 1313-1322A
Fault Structures in Rapidly Quenched Ni—Mo Binary Alloys. 2291-2294A
- Grain structure, Impurity effects**
Retained Carbide Distribution in Intercritically Austenitized 52100 Steel. 31-36A
- Grain sub boundaries, Stress effects**
Changes in the Subboundary Mesh Size With Creep Strain in 304 Stainless Steel. 2093-2097A
- Gravitation**
Microstructural Variations Induced by Gravity Level During Directional Solidification of Near-Eutectic Iron—Carbon Type Alloys. 1121-1130A
The Effect of Gravity Level on the Average Primary Dendritic Spacing of a Directionally Solidified Superalloy. 2301-2303A
- Gravity**
See Gravitation
- Gravity die casting**
See Permanent mold casting
- Gray iron**
See Nodular iron
- Grinding mills**
See Ball mills
- Growth**
See Grain growth
- Hafnium, Alloying elements**
Effect of Fluid Flow and Hafnium Content on Macrosegregation in the Directional Solidification of Nickel Base Superalloys. 347-356B
- Halides**
See Bromides
Chlorides
- Halogenation**
See Chlorination
- Halogens**
See Chlorine
- Hardenability, Composition effects**
A Comparative Study of the Heat Affected Zone (HAZ) Properties of Boron Containing Low Carbon Steels. 1529-1536A
- Hardening**
See Aging (artificial)
Carburizing
Precipitation hardening
Solution strengthening
Strain aging
Strain hardening
Structural hardening
- Harding mills**
See Ball mills
- Hardness, Cooling effects**
Microstructures and Mechanical Properties of Melt-Quenched Ferritic Stainless Steels. 261-269A
- Hazelett process**
See Continuous casting
- Heat affected zone, Mechanical properties**
A Comparative Study of the Heat Affected Zone (HAZ) Properties of Boron Containing Low Carbon Steels. 1529-1536A
- Heat flow**
See Heat transmission
- Heat flux**
See Heat transmission
- Heat measurement**
See Calorimetry
- Heat of decomposition**
See Heat of formation
- Heat of dissociation**
See Heat of formation
- Heat of dissolution**
See Heat of solution
- Heat of formation**
Study of the Enthalpies of Formation in the Gd—Ni System. 777-780A
Thermodynamics of Gaseous SbS. 913-914B
Standard Enthalpies of Formation of TiSi₂ and VS₂ by High-Temperature Calorimetry. 1217-1221A
- Heat of mixing**
Calorimetric and Emf Studies on Liquid Li—Sn Alloys. 791-796B
- Heat of solution**
Thermotransport of Carbon in Two-Phase V—C and Nb—C Alloys. 1955-1966A
- Heat resistant alloys**
See Superalloys
- Heat transfer**
Computer Modeling of Heat Flow in Welds. 587-600B
A Mathematical Model of the Planar Flow Melt Spinning Process. 695-703B
The Role of Transient Convection in the Melting and Solidification in Arc Weldpools. 735-744B
The Air-Gap Formation Process at the Casting/Mold Interface and the Heat Transfer Mechanism Through the Gap. 833-844B
Heat and Moisture Transfer in Sand Molds Containing Water. 903-911B
Heat Transfer and Fluid Flow in the Welding Arc. 1139-1148A
- Heat transmission**
Heat Flow in Copper Converters. 677-685B
Three-Dimensional Convection in Laser Melted Pools. 2265-2270A
Computer Simulation of Convection in Moving Arc Weld Pools. 2271-2277A

Heat treatment

Heat treatment

- See Aging (artificial)
- Annealing
- Austenitizing
- Carburizing
- Grain refinement
- Homogenizing
- Isothermal annealing
- Normalizing (heat treatment)
- Precipitation hardening
- Quenching and tempering
- Spheroidizing
- Tempering

Heats (energies)

- See Heat of formation
- Heat of mixing
- Heat of solution

Heavy metals

- See Antimony
- Bismuth
- Lead (metal)
- Mercury (metal)
- Tin

Heliarc welding

- See Gas tungsten arc welding

Helmholtz free energy

- See Free energy

High alloy steels

- See Austenitic stainless steels
- Duplex stainless steels
- Ferritic stainless steels
- Stainless steels

High strength low alloy steels, Mechanical properties

- The Ductility of a HSLA Steel at Temperatures Below 300K. 697-702A
- High Temperature Ductility Loss in Carbon—Manganese and Niobium-Treated Steels. 1995-2006A

High strength low alloy steels, Microstructure

- Microstructure of a Quenched and Tempered Copper-Bearing High-Strength Low-Alloy Steel. 791-798A

High strength low alloy steels, Phase transformations

- Application of Microstructure Modeling to the Kinetics of Proeutectoid Ferrite Transformation in Hot-Rolled Microalloyed Steels. 1625-1629A

High strength low alloy steels, Structural hardening

- Effect of Tempering Temperature on the Work-Hardening Rate of Five HSLA Steels. 307-313A

High strength low alloy steels, Welding

- Inclusion Phases and the Nucleation of Acicular Ferrite in Submerged Arc Welds in High Strength Low Alloy Steels. 1611-1623A

High strength steels, Alloy development

- Effect of Copper Precipitation on the Development of Recrystallization Textures Through Continuous Annealing of Low-Carbon Sheet Steel. 621-633A

High strength steels, Corrosion

- Stress Corrosion Cracking in High Strength Steel Under Mode III Loading. 711-716A
- Hydrogen-Induced Delayed Fracture Under Mode II Loading. 717-725A
- Fatigue Crack Growth Rates in a Pressure Vessel Steel Under Various Conditions of Loading and the Environment. 1837-1849A

High strength steels, Mechanical properties

- Size Effects on the Microscopic Cleavage Stress, σ_F , in Martensitic Microstructures. 231-241A
- The Effect of Silicon and Nickel Additions on the Sulfide Spacing and Fracture Toughness of a 0.4 Carbon Low Alloy Steel. 669-678A
- Microcrack Initiation and Acoustic Emission During Fracture Toughness Tests of A533B Steel. 843-852A

HIP

- See Hot isostatic pressing

Homogenizing

- Influence of Soaking Treatments on Hot Ductility of Al—4.85Mg Alloys Containing Manganese. 833-841A

Honeycomb construction, Mechanical properties

- Examination of the Titanium Environment in a René 41 Nickel Base Superalloy by X-Ray Absorption Spectroscopy. 739-741A

Hot brittleness

- See Brittleness

Hot compacting

- See Compacting

Hot cracking (welds)

- See Weld defects

Hot dip coating

- See Aluminizing

Hot ductility

- See Ductility

Hot gas corrosion

- Stability of the Chromia Layer on Steels in Flowing Nonequilibrium $H_2-H_2O-CH_4-CO$ Mixtures at 950°C. 915-921A

Hot hardness

- See Hardness

Hot isostatic pressing

- An Empirical Model for Hot Isostatic Pressing of Metal Powders. 1977-1984A

Hot pressing

- See Hot isostatic pressing

Hot rolling

- Formation of the Goss Orientation Near the Surface of 3% Silicon Steel During Hot Rolling. 1323-1334A

Hot roughing

- See Hot rolling

Hot shortness

- See Brittleness

Hot strength

- See Tensile strength

Hot stretch forming

- See Stretch forming

Hot tensile strength

- See Tensile strength

Hot working

- See Hot rolling

Hydrochloric acid leaching

- Leaching of Cinnabar With HCl-Thiourea Solutions as the Basis of a Process for Mercury Obtention. 443-448B

Hydrodynamics

- Mathematical Modeling of Flows in Large Tundish Systems in Steelmaking. 449-459B
- Model Study of Mixing and Mass Transfer Rates of Slag-Metal in Top and Bottom Blown Converters. 461-469B
- Some Fundamental Aspects of Mixing in Metallurgical Reaction Systems. 487-490B

Hydrogen

- See also Deuterium
- Stresses Induced in Iron-Ore Pellets by Hydrogen Reduction. 217-227B

Hydrogen, Diffusion

- The Trapping and Transport Phenomena of Hydrogen in Nickel. 181-187A
- Effects of Nitrogen on the Mechanical Behavior of Hydrogenated Vanadium, Niobium, and Tantalum. 527-535A
- Hydrogen and Deuterium Diffusion in Vanadium—Niobium Alloys. 645-650A
- Hydrogen Transport During Deformation in Nickel. I. Polycrystalline Nickel. 861-867A
- Hydrogen Transport During Deformation in Nickel. II. Single Crystal Nickel. 869-875A
- Phase Transformation of Austenitic Stainless Steels as a Result of Cathodic Hydrogen Charging. 1593-1600A
- On the Effective Hydrogen Permeability in Metastable β Titanium Alloy, Niobium and 2.25Cr—1Mo Ferritic Steel. 2086-2090A

Hydrogen, Impurities

- Effects of Oxygen on the Mechanical Behavior of Hydrogenated Vanadium, Niobium, and Tantalum. 853-859A

Hydrogen compounds

- See Phosphoric acid

Hydrogen embrittlement

- The Trapping and Transport Phenomena of Hydrogen in Nickel. 181-187A
- Stress Corrosion Cracking in High Strength Steel Under Mode III Loading. 711-716A
- Hydrogen-Induced Delayed Fracture Under Mode II Loading. 717-725A
- A Comparative Study of the Embrittlement of Monel 400 at Room Temperature by Hydrogen and by Mercury. 889-898A
- The Influence of Precipitated Austenite on Hydrogen Embrittlement in 5.5Ni Steel. 1157-1164A
- The Effects of Interstitials and Hydrogen-Interstitial Interactions on Low Temperature Hardening and Embrittlement in Vanadium, Niobium, and Tantalum. 1179-1189A
- Hydrogen-Induced Subcritical Crack Growth of a 12Cr—1Mo Ferritic Stainless Steel. 1229-1240A
- Hydrogen Degradation of Spheroidized AISI 1020 Steel. 1485-1487A
- Effect of Notch Root Radius on Stress Intensity in Mode I and Mode III Loading. 1633-1637A
- Absence of Hydrogen Influence on the Mechanical Stability of Retained Austenite in a 0.2C/12Cr/1Mo Steel. 1876-1877A
- The Interaction of Hydrogen With the Interface of Al_2O_3 Particles in Iron. 2183-2186A

Hydrogen embrittlement, Impurity effects

- The Influence of Minute Alloy Elements (Carbon, Nitrogen, Sulfur, Manganese) on the Hydrogen Embrittlement of α -Iron. 331-337A
- A Study of the Hydrogen-Induced Degradation of Two Steels Differing in Sulfur Content. 2255-2263A

Hydrogen potential

- See Electrode potentials

Hydromagnetic stability

- See Magnetohydrodynamics

Hydromechanics

- See Hydrodynamics

Hydrometallurgy

- The Dissolution of Galena in Ferric Chloride Media. 5-11A
- The Leaching of Chalcopyrite With Ferric Chloride. 19-28B
- An Investigation of the Thermodynamics and Kinetics of the Ferric Chloride Brine Leaching of Galena Concentrate. 29-39B
- Diffusivity of Cobalt and Nickel Compounds as a Function of Concentration and Temperature. 425-432B
- Potentiometric Studies on the Adsorption of $Au(CN)_2^-$ and $Ag(CN)_2^-$ Onto Activated Carbon. 523-528B
- Studies on Role of Oxygen in the Adsorption of $Au(CN)_2^-$ and $Ag(CN)_2^-$ Onto Activated Carbon. 529-533B
- Chemical Equilibrium Studies on the Iron(III)—Sulfuric Acid/ β -Alkenyl 8 Hydroxy—Quinoline—Xylene System. 615-620B

- Water and Solute Activities of $\text{H}_2\text{SO}_4\text{—Fe}_2(\text{SO}_4)_3\text{—H}_2\text{O}$ and $\text{HCl—FeCl}_3\text{—H}_2\text{O}$ Solution Systems. II. Activities of Solutes. 621-627B
- Leaching Kinetics of Natural Cobalt Triarsenide in Chlorine Solutions. 629-637B
- Hypereutectic structures, Heating effects**
Growth of Silicon Particles in an Aluminum Matrix. 2139-2152A
- Hypereutectoid structures**
Development of Ferrous Laminated Composites With Unique Microstructures by Control of Carbon Diffusion. 1517-1527A
Effects of Copper on Proeutectoid Cementite Precipitation. 2163-2173A
- Hypoeutectic structures, Heating effects**
Growth of Silicon Particles in an Aluminum Matrix. 2139-2152A
- Hysteresis, Microstructural effects**
Grain Growth Characteristics and Magnetic Properties of Rapidly Quenched Silicon Steel Ribbons. 1295-1299A
- Image analysis**
Surface Oxide on fcc Iron—Nickel Alloys. 163-167A
- Immersion coating**
See Aluminizing
- Impact strength**
Fracture Behavior in Medium-Carbon Martensitic Silicon- and Nickel-Steels. 1173-1178A
- Impact strength, Impurity effects**
Low Temperature Impact Properties of Phosphorus and Sulfur Doped and Sensitized Type 304 Stainless Steel. 663-668A
- Impact strength, Microstructural effects**
Microstructure—Mechanical Property Relationships in Isothermally Transformed Vanadium Steels. 1191-1202A
Effect of Microstructure on Strength and Toughness of Heat-Treated Low Alloy Structural Steels. 1203-1209A
- Impact toughness**
See Impact strength
- Impermeability**
See Permeability
- Inclusions**
See Nonmetallic inclusions
- Induction furnaces**
See Electric induction furnaces
- Inert gas welding**
See Gas tungsten arc welding
- Ingot casting**
An Ice-Water Model Study on Formation of Blowhole-Free Skin With Reference to Solidification of Steel. 553-564B
Processing-Structure Characterization of Rheocast IN-100 Superalloy. 2049-2062A
- Initiation**
See Crack initiation
- Injection**
A Multi-Phase Model for Plumes in Powder Injection Refining Processes. 77-85B
A Pressurized Screw Feeder for Powder Injection. 229-231B
- Inorganic acids**
See Phosphoric acid
- Integrated circuits**
Diffusional Breakdown of a Silver Diffusion Barrier in a Cu—Ag—Ni Diffusion Triple. 933-944A
- Interface reactions**
The Diffusion Bonding of Zr—2.5Nb to Steel. 429-434A
Diffusional Breakdown of a Silver Diffusion Barrier in a Cu—Ag—Ni Diffusion Triple. 933-944A
The Effect of Thermal Exposure on the Microstructure and Fiber/Matrix Interface of an $\text{Al}_2\text{O}_3/\text{Al}$ Composite. 1075-1080A
- Interfaces**
Interfacial Tension and Flotation Characteristics of Liquid Metal—Sodium Flux Systems. 339-346B
An *In Situ* HVEM Study of Dislocation Generation at Al/SiC Interfaces in Metal Matrix Composites. 379-389A
- Interfacial surface tension**
See Surface tension
- Intermetallic compounds**
See Intermetallics
- Intermetallic phases**
The Influence of Iron and Chromium on the Microstructure of Cast Al—Si—Mg Alloys. 45-52A
Deformation and Recrystallization Textures in Commercially Pure Aluminum. 253-259A
Nature of Large $\text{Ti}_6\text{Cu}_2\text{O}$ Particles Formed During Annealing of $\text{Cu}_{55}\text{Ti}_{45}$ Metallic Glass Ribbons. 575-581A
Study of the Enthalpies of Formation in the Gd—Ni System. 777-780A
- Intermetallic phases, Alloying effects**
The Effects of Tantalum on the Microstructure of Two Polycrystalline Nickel-Base Superalloys: B-1900 + Hafnium and MAR-M247. 1891-1905A
- Intermetallics**
See also A15 compounds
- Intermetallics, Crystal growth**
Rate of Dissolution of Solid Nickel in Liquid Tin Under Static Conditions. 281-289B
- Internal energy**
Orientation and Strain Dependence of Stored Energy of Cold Work in Axisymmetric Copper. 513-517A
- Internal friction**
Orientation and Strain Dependence of Stored Energy of Cold Work in Axisymmetric Copper. 513-517A
- Internal oxidation**
Determination of Diffusion Coefficient of Oxygen in γ -Iron From Measurements of Internal Oxidation in Fe—Al Alloys. 221-229A
Examination of the Titanium Environment in a René 41 Nickel Base Superalloy by X-Ray Absorption Spectroscopy. 739-741A
Metallic Surface Layers Deposited by Diffusional Creep During Internal Oxidation. 746-749A
The Effect of Thermal Exposure on the Microstructure and Fiber/Matrix Interface of an $\text{Al}_2\text{O}_3/\text{Al}$ Composite. 1075-1080A
- Internal stress**
See Residual stress
- Interstitial defects**
Complex Defects in the Oxidation of Uranium. 911-914A
- Iron**
See also Alloy steels
Cast iron
Chromium iron
Nodular iron
- Iron, Alloying elements**
Particle Size and Orientation Effects on Softening in a Copper Matrix Containing Rod-Shaped Iron Particles. 1751-1755A
- Iron, Binary systems**
Magnetic Contributions to the Thermodynamic Functions of Alloys and the Phase Equilibria of Fe—Ni System Below 1200K. 1361-1372A
A Thermodynamic Analysis of the Phase Equilibria of the Fe—Ni System Above 1200K. 1373-1380A
- Iron, Diffusion**
Measurement of Tracer Diffusivities of Ca^{45} and Fe^{59} in Silica Saturated FeO—CaO— SiO_2 Melts With the Porous Frit Technique. 497-501B
Anomalous Fast Diffusion in the Fe—Zn System. 1523-1527A
- Iron, Extraction**
Chemical Equilibrium Studies on the Iron(III)—Sulfuric Acid/ β -Alkenyl β -Hydroxy—Quinoline—Xylene System. 615-620B
Water and Solute Activities of $\text{H}_2\text{SO}_4\text{—Fe}_2(\text{SO}_4)_3\text{—H}_2\text{O}$ and $\text{HCl—FeCl}_3\text{—H}_2\text{O}$ Solution Systems. II. Activities of Solutes. 621-627B
- Iron, Impurities**
The Influence of Iron and Chromium on the Microstructure of Cast Al—Si—Mg Alloys. 45-52A
- Iron, Mechanical properties**
The Influence of Minute Alloy Elements (Carbon, Nitrogen, Sulfur, Manganese) on the Hydrogen Embrittlement of α -Iron. 331-337A
- Iron, Oxidation**
Determination of Diffusion Coefficient of Oxygen in γ -Iron From Measurements of Internal Oxidation in Fe—Al Alloys. 221-229A
- Iron, Phase transformations**
The Alpha \rightleftharpoons Gamma Transformation in Iron Powders. 37-44A
- Iron, Quaternary systems**
A Solid-State EMF Study of Ternary Ni—S—O, Fe—S—O, and Quaternary Fe—Ni—S—O. 133-146B
Phase Relationships in the Iron-Rich Fe—Cr—Ni—C System at Solidification Temperatures. 1461-1469A
- Iron, Quinary systems**
Phase Relationships in the Fe—Cr—Mn—Ni—C System at Solidification Temperatures. 1825-1835A
- Iron, Reactions (chemical)**
Rates of Dissolution of Solid Iron, Cobalt, Nickel, and Silicon in Liquid Copper and Diffusion Rate of Iron From Liquid Cu—Fe Alloy Into Liquid Copper. 291-305B
- Iron, Solubility**
Nitrogen Solubility in Liquid Iron and Fe—Mn Alloys. 238-239B
The Solubility of Boron in Iron. 1481-1483A
- Iron, Ternary systems**
Thermodynamics of the Fe—Mo—C System at 985K. 391-398A
Direct Use of the Chemical Potential Function in Thermodynamic Modeling of Alloy Phase Diagrams. 1471-1477A
Balance of Distribution of Some Transition Metals Between the (M' , M'')B and (M' , M'') $_2$ B Phases. 1665-1669A
Experimental and Theoretical Study of the Phase Equilibria in the Fe—Ni—W System. 1809-1823A
- Iron and steel making**
See also Ironmaking
LD process
Oxygen steel making
Quelle-Basic oxygen process
Steel making
On the Gibbs Energy of Formation of Wustite. 179-184B
Stresses Induced in Iron-Ore Pellets by Hydrogen Reduction. 217-227B
The Composition and Temperature Dependence of the Sulfide Capacity of Metallurgical Slags. 331-337B
- Iron base alloys**
See Ferrous alloys
- Iron compounds**
See also Iron oxides
Magnetite
Pyrrhotite
Taconite
Wustite
- Iron compounds, Mechanical properties**
Fracture of Fe_3Al . 2298-2300A

Iron compounds

Iron compounds, Ternary systems

Electrochemical Determination of Thermodynamic Properties and X-Ray Diffraction Investigation of the Fe_3O_4 — ZnFe_2O_4 System.

515-521B

Iron ores

See also Magnetite
Pyrrhotite
Taconite

Modeling the Development of Strength in Pellets.

479-485B

Iron ores, Reduction (chemical)

Mechanism of Growth of Metallic Phase in Direct Reduction of Iron Bearing Oolites.

433-442B

Iron oxides

See also Magnetite
Wustite

Iron oxides, Reduction (chemical)

Application of Thermodynamic and Kinetic Principles in the Reduction of Metal Oxides by Carbon in a Plasma Environment.

197-207B

Iron powder

See Iron

Ironmaking

An Investigation of the Critical Influence of Potassium on the Reduction of Wustite.
Development of an Analytical Equation for Calculation of the Blast Furnace Fuel Rate.

657-663B

705-724B

Isomer shift

See Mossbauer spectroscopy

Isostatic pressing

See Hot isostatic pressing

Isothermal annealing

Lower Bainite With Midrib in Hypereutectoid Steels.

1113-1120A

Isothermal treatment

See Isothermal annealing

Joints

See Transition joints
Welded joints

Junghans Rossi casting

See Continuous casting

Kaldo process

See Oxygen steel making

Killed steels

See Aluminum killed steels

Kilns

Reduction of Phosphate Ores by Carbon. I. Process Variables for Design of Rotary Kiln System.

861-868B

Kinetics

See also Reaction kinetics

Rate of Dissolution of Solid Nickel in Liquid Tin Under Static Conditions.

281-289B

Acidic Rate- and Flow-Controlled Dissolution of Uraninite Ores.

405-413B

Leaching of Cinnabar With HCl-Thiourea Solutions as the Basis of a Process for Mercury Obtention.

443-448B

Some Fundamental Aspects of Mixing in Metallurgical Reaction Systems.

487-490B

Measurement of Tracer Diffusivities of Ca^{45} and Fe^{59} in Silica Saturated FeO — CaO — SiO_2 Melts With the Porous Frit Technique.

497-501B

The Nitrogen Reaction Between Carbon Saturated Iron and Na_2O — SiO_2 Slag. II. Kinetics.

541-545B

The Study of Desulfurization Kinetics in Grain Oriented 3% Silicon Iron.

1347-1351A

Analysis of Transformation Kinetics by Nonisothermal Dilatometry.

1441-1445A

Nucleation, Growth, and Overall Transformation Kinetics of Grain Boundary Allotriomorphs of Proeutectoid α in Ti—3.2 at.% Co and Ti—6.6 at.% Cr Alloys.

1703-1715A

Kryptol electric furnaces

See Electric furnaces

Ladle metallurgy

Some Fundamental Aspects of Mixing in Metallurgical Reaction Systems.

487-490B

Mixing Models for Gas Stirred Metallurgical Reactors.

725-733B

Soda Slag System for Hot Metal Dephosphorization.

797-804B

Lamina

See Laminates

Laminates, Development

Development of Ferrous Laminated Composites With Unique Microstructures by Control of Carbon Diffusion.

1517-1527A

Laminates, Mechanical properties

Structure-Performance Maps of Polymeric, Metal, and Ceramic Matrix Composites.

1547-1559A

Lanthanide metal compounds

See Samarium compounds

Lanthanide metals

See Cerium
Gadolinium

Laser beam welding

Three-Dimensional Convection in Laser Melted Pools.

2265-2270A

Laser welding

See Laser beam welding

Lattice defects

See Crystal defects

Lattice vacancies

Complex Defects in the Oxidation of Uranium.

911-914A

LD process

Model Study of Mixing and Mass Transfer Rates of Slag-Metal in Top and Bottom Blown Converters.

461-469B

Leaching

See also Acid leaching

Bacterial leaching

Hydrochloric acid leaching

The Dissolution of Galena in Ferric Chloride Media.

5-17B

The Leaching of Chalcopyrite With Ferric Chloride.

19-28B

An Investigation of the Thermodynamics and Kinetics of the Ferric Chloride Brine Leaching of Galena Concentrate.

29-39B

Kinetics of Galena Dissolution in Ferric Chloride Solutions.

415-423B

Diffusivity of Cobalt and Nickel Compounds as a Function of Concentration and Temperature.

425-432B

Leaching Kinetics of Natural Cobalt Triarsenide in Chlorine Solutions.

629-637B

Lead (metal), Binary systems

Activity of Arsenic in Molten Lead.

235-238B

Effect of Small Additions of Silver on the Eutectic Temperature in the Lead—Tin System.

829-832B

Lead (metal), Extraction

The Dissolution of Galena in Ferric Chloride Media.

5-17B

An Investigation of the Thermodynamics and Kinetics of the Ferric Chloride Brine Leaching of Galena Concentrate.

29-39B

The Settling of Metallic Lead From Lead Blast Furnace Slag.

267-270B

Kinetics of Galena Dissolution in Ferric Chloride Solutions.

415-423B

Reduction of Lead Minerals by CO/CO_2 Gas Mixtures: Application of the Grain Model.

575-586B

PbO Solubility in Lead-Blast Furnace Slags.

817-827B

Lead (metal), Impurities

A Kinetic Model for the Vacuum Refining of Inductively Stirred Copper Melts.

87-103B

Lead (metal), Physical properties

Interfacial Tension and Flotation Characteristics of Liquid Metal—Sodium Flux Systems.

339-346B

Lead (metal), Powder technology

An Empirical Model for Hot Isostatic Pressing of Metal Powders.

1977-1984A

Lead base alloys, Crystal growth

The Effect of Convection on the Dendrite to Eutectic Transition.

991-1000A

Dendrite Characteristics in Directionally Solidified Pb—8Au and Pb—3Pd Alloys.

2279-2290A

Lead base alloys, Mechanical properties

An Examination of Class A to Class M Transition in Pb—9Sn and Other Alloys.

1447-1453A

Lead compounds, Reduction (chemical)

Kinetics of Reduction of Lead Oxide in Liquid Slag by Carbon in Iron.

271-279B

Reduction of Lead Minerals by CO/CO_2 Gas Mixtures: Application of the Grain Model.

575-586B

Lead compounds, Solubility

PbO Solubility in Lead-Blast Furnace Slags.

817-827B

Lead ores

See Galena

Life

See Fatigue life

Light metals

See Aluminum

Aluminum base alloys

Magnesium

Magnesium base alloys

Titanium

Titanium base alloys

Light water reactors

See Boiling water reactors

Pressurized water reactors

Lime

Discussion of "Lime-Enhanced Reduction of Sulfide Concentrates: a Thermodynamic Discussion" and Authors' Reply.

914-918B

Lime, Reactions (chemical)

Lime-Enhanced Reduction of Sulfide Concentrates: a Thermodynamic Discussion.

185-196B

Line defects

See Dislocations

Linz Donawitz process

See LD process

Liquid metal embrittlement

A Comparative Study of the Embrittlement of Monel 400 at Room Temperature by Hydrogen and by Mercury.

889-898A

Liquid Cesium Tellurium-Induced Fatigue Embrittlement of Cold-Worked 316 Stainless Steel.

2090-2093A

Liquid metals, Physical properties

Interfacial Tension and Flotation Characteristics of Liquid Metal—Sodium Flux Systems.

339-346B

A Calculation of Viscosities for Iron—Metalloid Liquids.

901-903A

Liquid metals, Reactions (chemical)

Activity Coefficient of Oxygen in Copper—Tellurium Melts.

171-177B

Rate of Dissolution of Solid Nickel in Liquid Tin Under Static Conditions.

261-269B

- Rates of Dissolution of Solid Iron, Cobalt, Nickel, and Silicon in Liquid Copper and Diffusion Rate of Iron From Liquid Cu—Fe Alloy Into Liquid Copper. 291-305B
- Liquid phase diffusion**
See Diffusion
- Liquid phase sintering**
Processing of Iron—Titanium Powder Mixtures by Transient Liquid Phase Sintering. 205-213A
An Analysis of the Surface Menisci in a Mixture of Liquid and Deformable Grains. 325-330A
The Effect of the Binder Phase Melting Temperature on Enhanced Sintering. 903-906A
Formation of Copper Pockets in Iron Grains During the Sintering of Fe—Cu Alloys. 1429-1431A
The Critical Grain Size for Liquid Flow Into Pores During Liquid Phase Sintering. 1915-1919A
Effect of Entrapped Inert Gas on Pore Filling During Liquid Phase Sintering. 2175-2182A
- Lithium, Alloying elements**
Microstructural Characterization of Rapidly Solidified Al—Li—Co Powders. 73-91A
Fatigue Crack Growth and Fracture Toughness Behavior of an Al—Li—Cu Alloy. 1011-1026A
The Effect of Thermal Exposure on the Microstructure and Fiber Matrix Interface of an Al_2O_3 /Al Composite. 1075-1080A
Mechanical Properties and Microstructure of Al—Li—Cu—Mg—Zr Die Forgings. 2007-2016A
- Lithium, Binary systems**
Calorimetric and Emf Studies on Liquid Li—Sn Alloys. 791-796B
- Lithium, Diffusion**
Lithium Depletion During Heat Treatment of Aluminum—Lithium Alloys. 635-643A
- Lithium base alloys, Thermal properties**
Calorimetric and Emf Studies on Liquid Li—Sn Alloys. 791-796B
- Lixivation**
See Leaching
- Low alloy steels**
See also Boron steels
Carbon manganese steels
Electrical steels
Resulturized steels
Silicon manganese steels
Silicon steels
- Low alloy steels, Phase transformations**
Nucleation Kinetics of Proeutectoid Ferrite at Austenite Grain Boundaries in Fe—C—X Alloys. 1385-1397A
The Kinetics of Ferrite Nucleation at Austenite Grain Edges in Fe—C and Fe—C—X Alloys. 1399-1407A
- Low cycle fatigue, Microstructural effects**
Orientation and Temperature Dependence of Some Mechanical Properties of the Single-Crystal Nickel-Base Superalloy René N4. II. Low Cycle Fatigue Behavior. 497-505A
- Macrofractography**
See Fractography
- Magnesium, Binary systems**
A Theoretical Evaluation of Chemical Ordering and Glass Transition in Liquid Mg—Sn Alloys. 607-615A
- Magnesium base alloys, Composite materials**
Structure-Performance Maps of Polymeric, Metal, and Ceramic Matrix Composites. 1547-1559A
- Magnesium base alloys, Mechanical properties**
Dependence of Total Elongations of Superplastic Materials on m. 685-690A
- Magnetic alloys, Phases (state of matter)**
Discussion of "Miscibility Gap in Fe—Ni—Al and Fe—Ni—Al—Co Systems" and "Role of Alloying Elements in Phase Decomposition in Alnico Magnet Alloys". 1629-1632A
- Magnetic fields**
Magnetic Contributions to the Thermodynamic Functions of Alloys and the Phase Equilibria of Fe—Ni System Below 1200K. 1361-1372A
- Magnetic flux welding**
See Gas metal arc welding
- Magnetic force**
See Magnetic fields
- Magnetic hysteresis**
See Hysteresis
- Magnetic materials**
See Magnetic alloys
Magnetite
- Magnetic permeability, Composition effects**
The Effect of Manganese and Sulfur Contents on the Magnetic Properties of Cold Rolled Lamination Steels. 1259-1266A
- Magnetic permeability, Microstructural effects**
The Effect of Thermomechanical History Upon the Microstructure and Magnetic Properties of Nonoriented Silicon Steels. 1267-1275A
- Magnetic properties**
See Coercive force
Magnetic permeability
- Magnetic susceptibility**
See Magnetic permeability
- Magnetite, Reduction (chemical)**
Dissolution of Solid Magnetite in Fe—S—O Melts. 639-645B
- Magnetization**
Directional Solidification and Annealing of $Mn_{55}Al_{45}$ Alloys. 1247-1249A
- Magnetohydrodynamic waves**
See Magnetohydrodynamics
- Magnetohydrodynamics**
Turbulent Recirculating Flow in Induction Furnaces: a Comparison of Measurements With Predictions Over a Range of Operating Conditions. 687-693B
- Magnets**
See Permanent magnets
- Manganese, Alloying elements**
Nitrogen Solubility in Liquid Iron and Fe—Mn Alloys. 238-239B
Decomposition Characteristics of Al—Mn—Zr Alloys Rapidly-Quenched From the Melt. 799-806A
The Effect of Manganese and Sulfur Contents on the Magnetic Properties of Cold Rolled Lamination Steels. 1259-1266A
Compositional Analysis of the Icosahedral Phase in Rapidly Quenched Al—Mn and Al—V Alloys. 1657-1664A
On the Microstructure of Rapidly Solidified Al—15Mn Ribbons: Effect of Annealing in the Temperature Range 300-600°C. 1671-1683A
- Manganese, Binary systems**
Thermodynamics of the Mn—P System. 777-783B
- Manganese, Diffusion**
Analysis of Solute Distribution in Dendrites of Carbon Steel With δ/γ Transformation During Solidification. 845-859B
- Manganese, Quinary systems**
Phase Relationships in the Fe—Cr—Mn—Ni—C System at Solidification Temperatures. 1825-1835A
- Manganese, Ternary systems**
Balance of Distribution of Some Transition Metals Between the $(M', M'')B$ and $(M', M'')_2B$ Phases. 1665-1669A
- Manganese base alloys, Magnetic properties**
Directional Solidification and Annealing of $Mn_{55}Al_{45}$ Alloys. 1247-1249A
- Manganese steels**
See also Silicon manganese steels
- Manganese steels, Mechanical properties**
Microstructural Dependence of Iron—High Manganese Tensile Behavior. 537-547A
Effect of Aluminum Content on Low Temperature Tensile Properties in Cryogenic Fe/Mn/Al/Nb/C Steels. 2097-2098A
- Manganese steels, Phase transformations**
Nucleation Kinetics of Proeutectoid Ferrite at Austenite Grain Boundaries in Fe—C—X Alloys. 1385-1397A
The Kinetics of Ferrite Nucleation at Austenite Grain Edges in Fe—C and Fe—C—X Alloys. 1399-1407A
- Manganese steels, Phases (state of matter)**
On the Critical Nucleus Composition of Ferrite in an Fe—C—Mn Alloy. 1381-1384A
- Manganese steels, Structural hardening**
Strain Hardening of Hadfield Manganese Steel. 1725-1737A
- Martensite, Crystal growth**
Lower Bainite With Midrib in Hypereutectoid Steels. 1113-1120A
- Martensitic transformations**
Microstructural Effects of Martensitic Transformation Cycling of a Cu—Zn—Al Alloy: Vestigial Structures in the Parent Phase. 195-203A
Deformation of Martensite in a Polycrystalline Cu—Zn—Al Alloy. 945-959A
The Chemical Composition of Precipitated Austenite in 9Ni Steel. 967-972A
The Influence of Precipitated Austenite on Hydrogen Embrittlement in 5.5Ni Steel. 1157-1164A
Phase Transformation of Austenitic Stainless Steels as a Result of Cathodic Hydrogen Charging. 1593-1600A
Roles of Dislocations and Grain Boundaries in Martensite Nucleation. 1693-1702A
Martensitic Transformation of Cu—2Be Alloys Induced by Explosive Cladding. 1685-1690A
- Martensitic transformations, Composition effects**
Deformation and Transition Behavior Associated With the R-Phase in Ti—Ni Alloys. 53-63A
- Mass transfer**
Model Study of Mixing and Mass Transfer Rates of Slag-Metal in Top and Bottom Blown Converters. 461-469B
Heat Transfer and Fluid Flow in the Welding Arc. 1139-1148A
- Master alloys, Phases (state of matter)**
The Aluminum—Strontium Phase Diagram. 1250-1253A
- Materials testing**
See Depth profiling
- Mathematical analysis**
See also Numerical analysis
An Analysis of Radial Segregation for Different Sized Spherical Solids in Rotary Cylinders. 247-257B
Estimation of Diffusion Path Slopes at Zero-Flux Plane Compositions. 362-364A
The C.L. m— δ Equation of Superplasticity. 679-684A
Development of an Analytical Equation for Calculation of the Blast Furnace Fuel Rate. 705-724B
Legendre Polynomial Expansions of Thermodynamic Properties of Binary Solutions. 1057-1063A
Computation of Thermodynamic Properties of Multi-Component Solutions: Extension of Toop Model. 1102-1104A
- Mathematical models**
A Model for Yielding in Anisotropic Metals. 107-114A

Mathematical models

- Short Range Order Hardening With Second Neighbor Interactions in fcc Solid Solutions. 189-194A
 Acidic Rate- and Flow-Controlled Dissolution of Uraninite Ores. 405-413B
 Mathematical Modeling of Flows in Large Tundish Systems in Steelmaking. 449-459B
 Modeling the Development of Strength in Pellets. 479-485B
 Heat Flow in Copper Converters. 677-685B
 Dependence of Total Elongations of Superplastic Materials on m. 685-690A
 Mixing Models for Gas Stirred Metallurgical Reactors. 725-733B
 The Role of Transient Convection in the Melting and Solidification in Arc Weldpools. 735-744B
 A Modified Interaction Parameter Formalism for Non-Dilute Solutions. 1211-1215A
 Reexamination of Grain-Boundary Sliding by Diffusion. 1949-1953A
 An Empirical Model for Hot Isostatic Pressing of Metal Powders. 1977-1984A
 A Simplified Treatment of Carbon Diffusion in Compound Welds Having an Intermediate Layer. 2083-2084A
 The Interaction of Hydrogen With the Interface of Al_2O_3 Particles in Iron. 2183-2186A

Mathematics

- See also Finite element method
 Mathematical analysis
 Mathematical models
 Numerical analysis
 A Mathematical Model of the Planar Flow Melt Spinning Process. 695-703B

Mattes

- See Copper mattes

Measurement

- See Calorimetry

Measuring instruments

- See Calorimeters

Mechanical hysteresis

- See Hysteresis

Mechanical properties

- See also Abrasion resistance
 Bonding strength
 Brittleness
 Compressive strength
 Creep (materials)
 Creep rate
 Creep rupture strength
 Creep strength
 Ductile brittle transition
 Ductility
 Elongation
 Fatigue (materials)
 Fatigue life
 Fatigue limit
 Fatigue strength
 Fracture strength
 Fracture toughness
 Hardness
 Hydrogen embrittlement
 Impact strength
 Internal friction
 Modulus of elasticity
 Plastic flow
 Pseudoelasticity
 Reduction of area
 Residual stress
 Shear strength
 Shear stress
 Stress relaxation
 Superplasticity
 Temper brittleness
 Tensile properties
 Tensile strength
 Wear resistance
 Yield strength

Mechanical properties, Alloying effects

- L_{12} -Type Ni—Al—Cr Alloys Processed by Rapid Solidification. 1685-1692A

Mechanical properties, Deformation effects

- Processing-Structure Characterization of Rheocast IN-100 Superalloy. 2049-2062A

Mechanical tests

- See Fracture testing
 Tension tests

Mechanical twinning

- Transmission Electron Microscopic Observations of Mechanical Twinning in Metastable β Titanium Alloys. 1409-1420A

Mechanics

- See Fluid dynamics
 Fracture mechanics
 Hydrodynamics
 Kinetics

Melt spinning

- On the Microstructure and Mechanical Behavior of Melt-Spun Fe—24Ni—0.5C Ribbons: Effect of Austenite Grain Size. 127-136A
 Microstructure of a Rapidly-Solidified Nickel-Base Eutectic Superalloy. 407-417A
 A Mathematical Model of the Planar Flow Melt Spinning Process. 695-703B

Melting

- See Vacuum arc melting

Melting furnaces

- See Basic converters
 Bottom blown converters
 Copper converters
 Rotary converters
 Top blown converters
 Vacuum arc furnaces

Memory (shape)

- See Shape memory

Mercury (metal), Diffusion

- Tracer Diffusion in Mercury: a Predictive Equation. 355-358A

Mercury (metal), Environment

- A Comparative Study of the Embrittlement of Monel 400 at Room Temperature by Hydrogen and by Mercury. 889-898A

Mercury (metal), Extraction

- Leaching of Cinnabar With HCl-Thiourea Solutions as the Basis of a Process for Mercury Obtention. 443-448B

Metal carbides

- See Tungsten carbide

Metal powders

- See also Alloy powders

Metal powders, Phase transformations

- The Alpha \rightleftharpoons Gamma Transformation in Iron Powders. 37-44A

Metal vapors

- Metal Vapors in Gas Tungsten Arcs. I. Spectroscopy and Monochromatic Photography. 1851-1863A
 Metal Vapors in Gas Tungsten Arcs. II. Theoretical Calculations of Transport Properties. 1865-1871A

Metal working

- See Cold working
 Forging
 Hot rolling
 Stretch forming
 Thermomechanical treatment
 Warm working

Metallic glasses, Crystal growth

- Nonlinear Regression Analysis of Superimposed DSC Crystallization Peaks. 1479-1481A

Metallic glasses, Phases (state of matter)

- Nature of Large $Ti_{40}Cu_{20}O$ Particles Formed During Annealing of $Cu_{50}Ti_{45}$ Metallic Glass Ribbons. 575-581A

Metallographic structures

- See Microstructure

Metallography

- See also Image analysis
 Specimen preparation
 Estimation of Average Size of Convex Particles. 742-745A
 Orienting Grains With [110] Surface Traces. 961-966A
 Nomenclature for Metallographic Sections. 1095A

Metalloid compounds

- See Silicon carbide
 Silicon dioxide

Metalloids

- See Arsenic
 Boron
 Silicon
 Tellurium

Metallurgical constituents

- See Sigma phase

Metastable phases

- Transformation Sequence in a Cu—Al—Ni Shape Memory Alloy at Elevated Temperatures. 65-72A
 Microstructures of Niobium—Germanium Alloys Processed in Inert Gas in the 100 Meter Drop Tube. 1421-1428A
 On the Microstructure of Rapidly Solidified Al—15Mn Ribbons: Effect of Annealing in the Temperature Range 300-600°C. 1671-1683A
 Icosahedral and Decagonal Phase Formation in Al—Mn Alloys. 2117-2125A

MHD

- See Magnetohydrodynamics

Microalloyed steels

- See High strength low alloy steels

Microbial leaching

- See Bacterial leaching

Microcracking

- See Crack initiation

Microfractography

- See Fractography

Microscopy

- See Stereomicroscopy
 Transmission electron microscopy

Microstructure

- See also Spheroidal structure
 Solidification of Nb—Ge Alloys in Long Drop Tubes. 973-981A
 Lower Bainite With Midrib in Hypereutectoid Steels. 1113-1120A

Microstructure, Alloying effects

- Microstructure of a Quenched and Tempered Copper-Bearing High-Strength Low-Alloy Steel. 791-798A

Microstructure, Cooling effects

- Microstructure of a Rapidly-Solidified Nickel-Base Eutectic Superalloy. 407-417A

Microstructure, Deformation effects

- Microstructural Analysis of Residual Projectiles—a New Method to Explain Penetration Mechanisms. 435-442A
- Effect of Isothermal Forging on Microstructure and Fatigue Behavior of Blended Elemental Ti—6Al—4V Powder Compacts. 549-559A
- The Effect of Thermomechanical History Upon the Microstructure and Magnetic Properties of Nonoriented Silicon Steels. 1267-1275A
- The Effect of Hot-Rolling on Chill-Cast Al—Al₃Ni, Chill-Cast Al—Al₂Cu, and Unidirectionally Solidified Al—Al₃Ni Eutectic Alloys. 1985-1993A
- Processing-Structure Characterization of Rheocast IN-100 Superalloy. 2049-2062A
- Characterization and Modeling of the High Temperature Flow Behavior of Aluminum Alloy 2024. 2227-2237A

Microstructure, Field effects

- Microstructural Variations Induced by Gravity Level During Directional Solidification of Near-Eutectic Iron—Carbon Type Alloys. 1121-1130A

Mig arc welding

See Gas metal arc welding

Mills

See Ball mills

Miscibility

- Discussion of "Miscibility Gap in Fe—Ni—Al and Fe—Ni—Al—Co Systems" and "Role of Alloying Elements in Phase Decomposition in Alnico Magnet Alloys" 1629-1632A

Mixing

- Some Fundamental Aspects of Mixing in Metallurgical Reaction Systems. 487-490B
- Mixing Models for Gas Stirred Metallurgical Reactors. 725-733B

Modification

- Misra Technique Applied to Solidification of Cast Iron. 358-360A

Modulus of elasticity

- The Effect of Thermal Exposure on the Microstructure and Fiber/Matrix Interface of an Al₂O₃/Al Composite. 1075-1080A

Molds

See Sand molds

Molten metals

See Liquid metals

Molten salts

See Fused salts

Molybdenum, Alloying additive

- The Effects of Replacing the Refractory Elements Tungsten, Niobium, and Tantalum With Molybdenum in Nickel-Base Superalloys on Microstructural, Microchemistry, and Mechanical Properties. 651-661A

Molybdenum, Coatings

- Phase Diagram Studies of the Systems KCl—K₃MoCl₆ and LiCl—K₃MoCl₆. 231-232B

Molybdenum, Diffusion

- Interdiffusion in the Ni—Cr—Co—Mo System at 1300°C. 983-990A

Molybdenum, Ternary systems

- Thermodynamics of the Fe—Mo—C System at 985K. 391-398A

Molybdenum chromium nickel steels

See Nickel chromium molybdenum steels

Molybdenum chromium steels

See Chromium molybdenum steels

Molybdenum compounds, Thermal properties

- Gibbs Free Energies of Formation of Molybdenum Carbide and Tungsten Carbide From 1173-1573K. 2031-2034A

Molybdenum nickel chromium steels

See Nickel chromium molybdenum steels

Molybdenum steels

See also Chromium molybdenum steels
Chromium molybdenum vanadium steels
Nickel chromium molybdenum steels

Molybdenum steels, Phase transformations

- Nucleation Kinetics of Proeutectoid Ferrite at Austenite Grain Boundaries in Fe—C—X Alloys. 1385-1397A

Monocrystals

See Single crystals

Mossbauer spectroscopy

- The Chemical Composition of Precipitated Austenite in 9Ni Steel. 967-972A

Necking

- Instabilities During Tension of Thin Voids Viscoplastic Sheets. 1637-1640A

New technology

- The Structure and Properties of a Nickel-Base Superalloy Produced by Osprey Atomization—Deposition. 583-591A

Nickel, Alloying additive

- The Effect of Alloying Additions on the Superplastic Properties of Ti—6Al—4V. 93-106A

Nickel, Alloying elements

- The Effect of Silicon and Nickel Additions on the Sulfide Spacing and Fracture Toughness of a 0.4 Carbon Low Alloy Steel. 669-678A
- Comparison of Solution Models for Nonmetallic Solutes in Binary Liquid Alloys: Nitrogen in Fe—Cr and Fe—Ni. 785-789B
- Sulfide Stress Cracking Susceptibility of Nickel Containing Steels. 1601-1610A

- Roles of Dislocations and Grain Boundaries in Martensite Nucleation. 1693-1702A
- The Effect of Hot-Rolling on Chill-Cast Al—Al₃Ni, Chill-Cast Al—Al₂Cu, and Unidirectionally Solidified Al—Al₃Ni Eutectic Alloys. 1985-1993A

Nickel, Binary systems

- Study of the Enthalpies of Formation in the Gd—Ni System. 777-780A
- Magnetic Contributions to the Thermodynamic Functions of Alloys and the Phase Equilibria of Fe—Ni System Below 1200K. 1361-1372A
- A Thermodynamic Analysis of the Phase Equilibria of the Fe—Ni System Above 1200K. 1373-1380A

Nickel, Diffusion

- The Trapping and Transport Phenomena of Hydrogen in Nickel. 181-187A
- Hydrogen Transport During Deformation in Nickel. I. Polycrystalline Nickel. 861-867A
- Hydrogen Transport During Deformation in Nickel. II. Single Crystal Nickel. 869-875A
- Diffusional Breakdown of a Silver Diffusion Barrier in a Cu—Ag—Ni Diffusion Triple. 933-944A
- Determination of the Interdiffusion Coefficients in the Fe—Ni and Fe—Ni—P Systems Below 900°C. 1131-1138A

Nickel, Mechanical properties

- A Model for Yielding in Anisotropic Metals. 107-114A

Nickel, Quaternary systems

- A Solid-State EMF Study of Ternary Ni—S—O, Fe—S—O, and Quaternary Fe—Ni—S—O. 133-146B
- Phase Relationships in the Iron-Rich Fe—Cr—Ni—C System at Solidification Temperatures. 1461-1469A

Nickel, Quinary systems

- Phase Relationships in the Fe—Cr—Mn—Ni—C System at Solidification Temperatures. 1825-1835A

Nickel, Reactions (chemical)

- Rate of Dissolution of Solid Nickel in Liquid Tin Under Static Conditions. 261-289B
- Rates of Dissolution of Solid Iron, Cobalt, Nickel, and Silicon in Liquid Copper and Diffusion Rate of Iron From Liquid Cu—Fe Alloy Into Liquid Copper. 291-305B

Nickel, Recovering

- Diffusivity of Cobalt and Nickel Compounds as a Function of Concentration and Temperature. 425-432B

Nickel, Refining

- Solubility and Activity of Oxygen in Liquid Nickel in Equilibrium With α -Al₂O₃ and NiO x (1 + x)Al₂O₃. 763-770B

Nickel, Solubility

- A Solid-State EMF Study of the Cu—Cu₂O—NiO Three-Phase Equilibrium. 1104-1106A

Nickel, Ternary systems

- Estimation of Diffusion Path Slopes at Zero-Flux Plane Compositions. 362-364A
- Balance of Distribution of Some Transition Metals Between the (M', M'')B and (M', M'')₂B Phases. 1665-1669A
- Experimental and Theoretical Study of the Phase Equilibria in the Fe—Ni—W System. 1809-1823A

Nickel base alloys, Brazing

- Examination of the Titanium Environment in a René 41 Nickel Base Superalloy by X-Ray Absorption Spectroscopy. 739-741A

Nickel base alloys, Casting

- Processing-Structure Characterization of Rheocast IN-100 Superalloy. 2049-2062A

Nickel base alloys, Coating

- CVD Aluminide Nickel. 215-220A

Nickel base alloys, Composite materials

- Structure-Performance Maps of Polymeric, Metal, and Ceramic Matrix Composites. 1547-1559A

Nickel base alloys, Corrosion

- Relative Stress Corrosion Susceptibilities of Alloys 690 and 600 in Simulated Boiling Water Reactor Environments. 877-887A
- A Comparative Study of the Embrittlement of Monel 400 at Room Temperature by Hydrogen and by Mercury. 889-898A
- High Temperature Corrosion of Superalloys in an Environment Containing Both Oxygen and Chlorine. 1087-1094A

Nickel base alloys, Crystal growth

- Effect of Fluid Flow and Hafnium Content on Macroseggregation in the Directional Solidification of Nickel Base Superalloys. 347-356B
- The Effect of Gravity Level on the Average Primary Dendritic Spacing of a Directionally Solidified Superalloy. 2301-2303A

Nickel base alloys, Crystal lattices

- Fault Structures in Rapidly Quenched Ni—Mo Binary Alloys. 2291-2294A

Nickel base alloys, Diffusion

- Measurement of Segregation and Distribution Coefficients in MAR-M200 and Hafnium-Modified MAR-M200 Superalloys. 419-428A
- Interdiffusion in the Ni—Cr—Co—Mo System at 1300°C. 983-990A

Nickel base alloys, Mechanical properties

- Effect of Cyclic Deformation on the Pseudoelasticity Characteristics of Ti—Ni Alloys. 115-120A
- Constrained Cavity Growth Models of Longitudinal Creep Deformation of Oxide Dispersion Strengthened Alloys. 281-293A
- Effect of Environment on Fatigue Crack Propagation Behavior of Alloy 718 at Elevated Temperatures. 370-374A
- Orientation and Temperature Dependence of Some Mechanical Properties of the Single-Crystal Nickel-Base Superalloy René N4. I. Tensile Behavior. 491-496A

Nickel base alloys

- Orientation and Temperature Dependence of Some Mechanical Properties of the Single-Crystal Nickel-Base Superalloy René N4, II. Low Cycle Fatigue Behavior. 497-505A
- Orientation and Temperature Dependence of Some Mechanical Properties of the Single-Crystal Nickel-Base Superalloy René N4: III. Tension—Compression Anisotropy. 507-512A
- The Effects of Replacing the Refractory Elements Tungsten, Niobium, and Tantalum With Molybdenum in Nickel-Base Superalloys on Microstructural, Microchemistry, and Mechanical Properties. 651-661A
- The Processing and Properties of Heavily Cold Worked Directionally Solidified Ni—W Eutectic Alloys. 1165-1171A
- Cyclic Creep and Anelastic Relaxation Analysis of an ODS Superalloy. 1577-1583A
- Fatigue Crack Propagation in Nickel-Base Superalloy Single Crystals Under Multiaxial Cyclic Loads. 1739-1750A
- Nickel base alloys, Microstructure**
Microstructure of a Rapidly-Solidified Nickel-Base Eutectic Superalloy. 407-417A
- Nickel base alloys, Oxidation**
Void Formation in INCONEL MA-754 by High Temperature Oxidation. 151-162A
Surface Oxide on fcc Iron—Nickel Alloys. 163-167A
Ni₃Nb Alloy Species in Oxide Surfaces of Inconel 718. 351-355A
A Relationship Between Indigenous Impurity Elements and Protective Oxide Scale Adherence Characteristics. 923-932A
Reactions of Fe—Cr and Ni—Cr Alloys in CO/CO₂ Gases at 850 and 950°C. 1085-1074A
- Nickel base alloys, Phase transformations**
Deformation and Transition Behavior Associated With the R-Phase in Ti—Ni Alloys. 53-63A
Precipitation Processes in Near-Equiatomic TiNi Shape Memory Alloys. 1505-1515A
- Nickel base alloys, Phases (state of matter)**
L₁₂-Type Ni—Al—Cr Alloys Processed by Rapid Solidification. 1685-1692A
Influence of Alloy Chemistry on Carbide Precipitation in a Nickel Base Superalloy. 2075-2077A
- Nickel base alloys, Powder technology**
Microstructure and Stability of Melt Spun Inconel 713LC. 173-180A
The Structure and Properties of a Nickel-Base Superalloy Produced by Osprey Atomization—Deposition. 583-591A
Dendritic Microstructure in Argon Atomized Superalloy Powders. 2099-2102A
- Nickel base alloys, Refining**
Relationship Between Furnace Voltage Signatures and the Operational Parameters Arc Power, Arc Current, CO Pressure, and Electrode Gap During Vacuum Arc Melting Inconel 718. 357-365B
- Nickel base alloys, Structural hardening**
The Effects of Tantalum on the Microstructure of Two Polycrystalline Nickel-Base Superalloys: B-1900 + Hafnium and MAR-M247. 1891-1905A
Dislocation/Precipitate Interactions During Coarsening of a Plastically Strained High-Misfit Nickel-Base Superalloy. 2239-2247A
- Nickel base alloys, Thermal properties**
A Modified Interaction Parameter Formalism for Non-Dilute Solutions. 1211-1215A
- Nickel base alloys, Welding**
The Welding Metallurgy of Hastelloy Alloys C-4, C-22, and C-276. 2035-2047A
The Use of New PHACOMP in Understanding the Solidification Microstructure of Nickel Base Alloy Weld Metal. 2107-2116A
- Nickel chromium molybdenum steels, Corrosion**
Hydrogen-Induced Delayed Fracture Under Mode II Loading. Sulfide Stress Cracking Susceptibility of Nickel Containing Steels. 717-725A
1601-1610A
- Nickel chromium molybdenum steels, Mechanical properties**
Influence of Prestrain History on Fracture Toughness Properties of Steels. 473-489A
The Influence of Precipitated Austenite on Hydrogen Embrittlement in 5.5Ni Steel. 1157-1164A
Effect of Microstructure on Strength and Toughness of Heat-Treated Low Alloy Structural Steels. 1203-1209A
- Nickel chromium steels**
See also Nickel chromium molybdenum steels
- Nickel chromium steels, Mechanical properties**
The Effect of Silicon and Nickel Additions on the Sulfide Spacing and Fracture Toughness of a 0.4 Carbon Low Alloy Steel. 669-678A
Effect of Microstructure on Strength and Toughness of Heat-Treated Low Alloy Structural Steels. 1203-1209A
- Nickel compounds, Chemical analysis**
Ni₃Nb Alloy Species in Oxide Surfaces of Inconel 718. 351-355A
- Nickel compounds, Crystal lattices**
L₁₂-Type Ni—Al—Cr Alloys Processed by Rapid Solidification. 1685-1692A
- Nickel compounds, Diffusion**
Carbon Segregation to Grain Boundaries in Rapidly Solidified Ni₃Al. 2084-2086A
- Nickel compounds, Phase transformations**
Precipitation Processes in Near-Equiatomic TiNi Shape Memory Alloys. 1505-1515A
- Nickel molybdenum chromium steels**
See Nickel chromium molybdenum steels
- Nickel molybdenum steels**
See Nickel chromium molybdenum steels
- Nickel steels**
See also Nickel chromium molybdenum steels
Nickel chromium steels
- Nickel steels, Chemical analysis**
The Chemical Composition of Precipitated Austenite in 9Ni Steel. 967-972A
- Nickel steels, Mechanical properties**
A Study of the Effect of Precipitated Austenite on the Fracture of a Ferritic Cryogenic Steel. 243-252A
Fracture Behavior in Medium-Carbon Martensitic Silicon- and Nickel-Steels. 1173-1178A
- Nickel steels, Metallography**
Characterization of Cryogenic Fe—6Ni Steel Fracture Modes: a Three Dimensional Quantitative Analysis. 815-822A
- Nickel steels, Phase transformations**
Nucleation Kinetics of Proeutectoid Ferrite at Austenite Grain Boundaries in Fe—C—X Alloys. 1385-1397A
The Kinetics of Ferrite Nucleation at Austenite Grain Edges in Fe—C and Fe—C—X Alloys. 1399-1407A
- Niobium, Alloying additive**
Microstructure and Creep Behavior of a Niobium Alloyed Cast Heat-Resistant 26% Chromium Steel. 691-696A
- Niobium, Diffusion**
Hydrogen and Deuterium Diffusion in Vanadium—Niobium Alloys. 645-650A
On the Effective Hydrogen Permeability in Metastable β Titanium Alloy, Niobium and 2.25Cr—1Mo Ferritic Steel. 2086-2090A
- Niobium, Mechanical properties**
Effects of Nitrogen on the Mechanical Behavior of Hydrogenated Vanadium, Niobium, and Tantalum. 527-535A
Effects of Oxygen on the Mechanical Behavior of Hydrogenated Vanadium, Niobium, and Tantalum. 853-859A
The Effects of Interstitials and Hydrogen-Interstitial Interactions on Low Temperature Hardening and Embrittlement in Vanadium, Niobium, and Tantalum. 1179-1189A
- Niobium, Solubility**
Thermotransport of Carbon in Two-Phase V—C and Nb—C Alloys. 1955-1966A
- Niobium base alloys, Crystal growth**
Solidification of Nb—Ge Alloys in Long Drop Tubes. 973-981A
- Niobium base alloys, Diffusion**
Hydrogen and Deuterium Diffusion in Vanadium—Niobium Alloys. 645-650A
- Niobium base alloys, Phases (state of matter)**
Microstructures of Niobium—Germanium Alloys Processed in Inert Gas in the 100 Meter Drop Tube. 1421-1428A
- Niobium compounds, Chemical analysis**
Ni₃Nb Alloy Species in Oxide Surfaces of Inconel 718. 351-355A
- Niobium compounds, Superconductivity**
The Effect of High Temperature Plastic Flow on the Superconducting Transition in A15 Compounds. 399-405A
- Nitrogen, Binary systems**
The Vanadium—Nitrogen System: a Review. 1647-1656A
- Nitrogen, Diffusion**
Effects of Nitrogen on the Mechanical Behavior of Hydrogenated Vanadium, Niobium, and Tantalum. 527-535A
- Nitrogen, Impurities**
The Effects of Interstitials and Hydrogen-Interstitial Interactions on Low Temperature Hardening and Embrittlement in Vanadium, Niobium, and Tantalum. 1179-1189A
- Nitrogen, Reactions (chemical)**
The Kinetics of the Nitrogen Reaction With Liquid Iron—Chromium Alloys. 317-322B
- Nitrogen, Solubility**
Nitrogen Solubility in Liquid Iron and Fe—Mn Alloys. 238-239B
The Nitrogen Reaction Between Carbon Saturated Iron and Na₂O—SiO₂ Slag. I. Thermodynamics. 535-540B
The Nitrogen Reaction Between Carbon Saturated Iron and Na₂O—SiO₂ Slag. II. Kinetics. 541-545B
Comparison of Solution Models for Nonmetallic Solute in Binary Liquid Alloys: Nitrogen in Fe—Cr and Fe—Ni. 785-789B
- Nodular iron, Microstructure**
On the Formation of Widmanstätten Austenite. 741A
- Nonferrous metals, Extraction**
Removal of SO₂ With Oxygen in the Presence of Fe(III). 745-753B
- Nonferrous smelting**
See Smelting
- Nonmetallic inclusions**
Inclusion Phases and the Nucleation of Acicular Ferrite in Submerged Arc Welds in High Strength Low Alloy Steels. 1611-1623A
A Model for the Silicon—Manganese Deoxidation of Steel Weld Metals. 1797-1807A
- Normalizing (heat treatment)**
Effects of Decarburization and Normalizing Heat Treatment in Boron-Silicon Iron Alloys. 1353-1359A
- Notch brittleness**
See Brittleness
- Notch ductility**
See Ductility

- Notch impact strength**
See Impact strength
- Notched bar tensile test**
See Tension tests
- Nuclear fuel claddings**
See Nuclear fuel elements
- Nuclear fuel elements, Corrosion**
Liquid Cesium Tellurium-Induced Fatigue Embrittlement of Cold-Worked 316 Stainless Steel. 2090-2093A
- Nuclear reactors**
See Boiling water reactors
Pressurized water reactors
- Nucleation**
On the Critical Nucleus Composition of Ferrite in an Fe—C—Mn Alloy. 1381-1384A
The Kinetics of Ferrite Nucleation at Austenite Grain Edges in Fe—C and Fe—C—X Alloys. 1399-1407A
Nucleation, Growth, and Overall Transformation Kinetics of Grain Boundary Allotriomorphs of Proeutectoid α in Ti—3.2 at.% Co and Ti—6.6 at.% Cr Alloys. 1703-1715A
- Nuclei (transformation)**
See Nucleation
- Numerical analysis**
Numerical Modeling of the Propagation of an Adiabatic Shear Band. 443-450A
Thermal Transient Stresses Due to Rapid Cooling in a Thermally and Elastically Orthotropic Medium. 1051-1055A
Instabilities During Tension of Thin Voided Viscoplastic Sheets. 1637-1640A
- OBM process**
See Quelle-Basic oxygen process
- Order disorder**
See Short range order
- Ores**
See Chalcocite
Chalcopyrite
Chromium ores
Galena
Iron ores
Magnetite
Pyrrhotite
Taconite
- Orientation**
See Grain orientation
Orientation relationships
- Orientation relationships**
Description of the Intercrystalline Structure Distribution in Polycrystalline Materials. 2199-2207A
- OSM process**
See Oxygen steel making
- Oxidation**
See also Internal oxidation
Intrinsic Kinetics of the Oxidation of Chalcopyrite Particles Under Isothermal and Nonisothermal Conditions. 51-60B
Reactions of Fe—Cr and Ni—Cr Alloys in CO/CO₂ Gases at 850 and 950°C. 1065-1074A
- Oxidation potential**
See Electrode potentials
- Oxidation rate**
The Formation of Volatile Corrosion Products During the Mixed Oxidation—Chlorination of Cobalt at 650°C. 1223-1228A
- Oxidation rate, Impurity effects**
Complex Defects in the Oxidation of Uranium. 911-914A
- Oxidation reduction potential**
See Electrode potentials
- Oxidation resistance**
Stability of the Chromia Layer on Steels in Flowing Nonequilibrium H₂—H₂O—CH₄—CO Mixtures at 950°C. 915-921A
- Oxide coatings**
Surface Oxide on fcc Iron—Nickel Alloys. 163-167A
Reactions of Fe—Cr and Ni—Cr Alloys in CO/CO₂ Gases at 850 and 950°C. 1065-1074A
- Oxide coatings, Chemical analysis**
Ni₃Nb Alloy Species in Oxide Surfaces of Inconel 718. 351-355A
- Oxide coatings, Mechanical properties**
A Relationship Between Indigenous Impurity Elements and Protective Oxide Scale Adherence Characteristics. 923-932A
- Oxide films**
See Oxide coatings
- Oxides**
See also Aluminum oxide
Carbon dioxide
Carbon monoxide
Iron oxides
Lime
Silicon dioxide
Wustite
- Oxides, Reduction (chemical)**
Kinetics of Reduction of Lead Oxide in Liquid Slag by Carbon in Iron. 271-279B
- Oxides, Solubility**
PbO Solubility in Lead-Blast Furnace Slags. 817-827B
- Oxides, Ternary systems**
Electrochemical Determination of Thermodynamic Properties and X-Ray Diffraction Investigation of the Fe₃O₄—ZnFe₂O₄ System. 515-521B
- Oxidizing**
See Oxidation
- Oxygen, Binary systems**
An Ambiguity in the Definition of the Activity Coefficient at Infinite Dilution. 1484-1485A
- Oxygen, Diffusion**
Determination of Diffusion Coefficient of Oxygen in γ -Iron From Measurements of Internal Oxidation in Fe—Al Alloys. 221-229A
- Oxygen, Impurities**
Effects of Oxygen on the Mechanical Behavior of Hydrogenated Vanadium, Niobium, and Tantalum. 853-859A
- Oxygen, Quaternary systems**
A Solid-State EMF Study of Ternary Ni—S—O, Fe—S—O, and Quaternary Fe—Ni—S—O. 133-146B
- Oxygen, Reactions (chemical)**
Measurements of Oxygen Pressure in a Copper Flash Smelting Furnace by an EMF Method. 111-117B
Activity Coefficient of Oxygen in Copper—Tellurium Melts. 171-177B
- Oxygen, Solubility**
Solubility of Oxygen and Sulfur in Copper—Iron Mattes. Correction to "Solubility of Oxygen and Sulfur in Copper—Iron Mattes". 147-157B
400B
- Oxygen, Ternary systems**
Thermodynamics of the Si—C—O System for the Production of Silicon Carbide and Metallic Silicon. 503-514B
- Oxygen conversion processes**
See Oxygen steel making
- Oxygen steel making**
See also LD process
Quelle-Basic oxygen process
Theoretical and Experimental Study of the Removal of Dust Particles From Flue Gases Using Two-Phase Steam—Water Droplet Mixtures. 665-676B
Soda Slag System for Hot Metal Dephosphorization. 797-804B
- Packing (crystal density)**
See Crystal structure
- Palladium base alloys, Mechanical properties**
Metallic Surface Layers Deposited by Diffusional Creep During Internal Oxidation. 746-749A
- Parameters**
See Welding parameters
- Particle size**
The Alpha \rightleftharpoons Gamma Transformation in Iron Powders. 37-44A
The Critical Grain Size for Liquid Flow Into Pores During Liquid Phase Sintering. 1915-1919A
- Particle size distribution**
Estimation of Average Size of Convex Particles. 742-745A
- Pelleting**
Modeling the Development of Strength in Pellets. 479-485B
- Pelletizing**
See Pelleting
- Pellets, Mechanical properties**
Modeling the Development of Strength in Pellets. 479-485B
- Pellets, Reduction (chemical)**
Stresses Induced in Iron-Ore Pellets by Hydrogen Reduction. 217-227B
- Penetration**
Microstructural Analysis of Residual Projectiles—a New Method to Explain Penetration Mechanisms. 435-442A
- Permanent magnets, Magnetic properties**
Directional Solidification and Characterization of Near Eutectic Sm₂Co₁₇/Co Alloys. 1149-1155A
- Permanent mold casting**
The Air-Gap Formation Process at the Casting/Mold Interface and the Heat Transfer Mechanism Through the Gap. 833-844B
- Permeability**
On the Effective Hydrogen Permeability in Metastable β Titanium Alloy, Niobium and 2.25Cr—1Mo Ferritic Steel. 2086-2090A
- Permeability (magnetic)**
See Magnetic permeability
- Permeation**
See Penetration
- Phase decomposition**
See also Eutectoid decomposition
The Dissolution of Cementite in a Low Carbon Steel During Isothermal Annealing at 700°C. 617-620A
Discussion of "The Early Stages of the Decomposition of Alloys" and Author's Reply. 742A
Precipitation Processes in Near-Equiatomic TiNi Shape Memory Alloys. 1505-1515A
Discussion of "Miscibility Gap in Fe—Ni—Al and Fe—Ni—Al—Co Systems" and "Role of Alloying Elements in Phase Decomposition in Alnico Magnet Alloys". 1629-1632A
On the Microstructure of Rapidly Solidified Al—15Mn Ribbons: Effect of Annealing in the Temperature Range 300-600°C. 1671-1683A
- Phase decomposition, Heating effects**
Transformation Sequence in a Cu—Al—Ni Shape Memory Alloy at Elevated Temperatures. 65-72A

Phase diagram reactions

Phase diagram reactions

See Austenitizing
Eutectic reactions
Eutectoid decomposition
Eutectoid reactions
Martensitic transformations
Phase decomposition

Phase diagrams

A Solid-State EMF Study of Ternary Ni—S—O, Fe—S—O, and Quaternary Fe—Ni—S—O. 133-146B
Phase Diagram Studies of the Systems KCl—K₃MoCl₆ and LiCl—K₃MoCl₆. 231-232B
A Theoretical Evaluation of Chemical Ordering and Glass Transition in Liquid Mg—Sn Alloys. 607-615A
Thermodynamics of the Mn—P System. 777-783B
The Aluminum—Strontium Phase Diagram. 1250-1253A
A Thermodynamic Analysis of the Phase Equilibria of the Fe—Ni System Above 1200K. 1373-1380A
Phase Relationships in the Iron-Rich Fe—Cr—Ni—C System at Solidification Temperatures. 1461-1469A
Direct Use of the Chemical Potential Function in Thermodynamic Modeling of Alloy Phase Diagrams. 1471-1477A
The Solubility of Boron in Iron. 1481-1483A
The Vanadium—Nitrogen System: a Review. 1647-1656A
Experimental and Theoretical Study of the Phase Equilibria in the Fe—Ni—W System. 1809-1823A
Phase Relationships in the Fe—Cr—Mn—Ni—C System at Solidification Temperatures. 1825-1835A
A Modified Regular-Solution Model for Terminal Solutions. 1878-1879A

Phase stability

Deformation and Transition Behavior Associated With the R-Phase in Ti—Ni Alloys. 53-63A
Microstructure and Stability of Melt Spun Inconel 713LC. 173-180A

Phase stability, Diffusion effects

Phase Transformation of Austenitic Stainless Steels as a Result of Cathodic Hydrogen Charging. 1593-1600A
Absence of Hydrogen Influence on the Mechanical Stability of Retained Austenite in a 0.2C/12Cr/1Mo Steel. 1876-1877A

Phase transformations

See also Allotropic transformation
Austenitizing
Martensitic transformations
Surface Oxide on fcc Iron—Nickel Alloys. 163-167A
A Straightforward New Procedure for Determining Crystallization Kinetics by Heating Rate DSC. 561-566A
Analysis of Transformation Kinetics by Nonisothermal Dilatometry. 1441-1445A

Phases (state of matter)

See also Intermetallic phases
Metastable phases
Sigma phase
Solidification of Nb—Ge Alloys in Long Drop Tubes. 973-981A

Phases (state of matter), Alloying effects

L₁-Type Ni—Al—Cr Alloys Processed by Rapid Solidification. 1685-1692A

Phases (state of matter), Cooling effects

Analytical Scanning Transmission Electron Microscopic Study of Metastable Modulated Structure in a Rapidly Quenched Fe—22Ni—8Al—2.4C Alloy. 2077-2080A

Phases (state of matter), Deformation effects

Modification of α Morphology in Ti—6Al—4V by Thermomechanical Processing. 1935-1947A

Phases (state of matter), Field effects

Magnetic Contributions to the Thermodynamic Functions of Alloys and the Phase Equilibria of Fe—Ni System Below 1200K. 1361-1372A

Phosphates

See also Phosphoric acid

Phosphates, Reduction (chemical)

Reduction of Phosphate Ores by Carbon. I. Process Variables for Design of Rotary Kiln System. 861-868B
Reduction of Phosphate Ore by Carbon. II. Rate Limiting Steps. 869-877B

Phosphoric acid, Synthesis

Reduction of Phosphate Ores by Carbon. I. Process Variables for Design of Rotary Kiln System. 861-868B
Reduction of Phosphate Ore by Carbon. II. Rate Limiting Steps. 869-877B

Phosphorus, Binary systems

Thermodynamics of the Mn—P System. 777-783B

Phosphorus, Diffusion

Analysis of Solute Distribution in Dendrites of Carbon Steel With δ/γ Transformation During Solidification. 845-859B
Determination of the Interdiffusion Coefficients in the Fe—Ni and Fe—Ni—P Systems Below 900°C. 1131-1138A

Phosphorus, Impurities

Retained Carbide Distribution in Intercritically Austenitized 52100 Steel. 31-36A
Low Temperature Impact Properties of Phosphorus and Sulfur Doped and Sensitized Type 304 Stainless Steel. 663-668A

Photo oxidation

See Oxidation

Physical chemistry

Thermodynamic Study of Fe₂O₃—Fe₂(SO₄)₃ Equilibrium Using an Oxidation Electrolyte (Na₂SO₄—I). 323-329B
Comparison of Solution Models for Nonmetallic Solutes in Binary Liquid Alloys: Nitrogen in Fe—Cr and Fe—Ni. 785-789B

Reduction of Phosphate Ore by Carbon. II. Rate Limiting Steps. 869-877B

Physical metallurgy

Discussion of "Line-Enhanced Reduction of Sulfide Concentrates: a Thermodynamic Discussion" and Authors' Reply. The Welding Metallurgy of Hastelloy Alloys C-4, C-22, and C-276. 914-918B
2035-2047A

Physical properties

See Anisotropy
Capillarity
Carrier density
Coercive force
Cryogenic properties
Diffusivity
Heat of formation
Heat of mixing
Heat of solution
Magnetic permeability
Miscibility
Permeability
Porosity
Solid solubility
Solubility
Superconductivity
Surface tension
Texture
Thermal stability
Viscosity
Volatility

Pickling

Dissolution Behavior of 304 Stainless Steel in HNO₃/HF Mixtures. 137-149A

Plasma arc welding

Heat Transfer and Fluid Flow in the Welding Arc. 1139-1148A

Plastic deformation

Deformation of a Burgers Oriented Bimetallic Bicrystal of α - β (Ti—13Mn). 451-460A
High-Temperature Plastic Deformation of Two V—Ga Alloys With A15 Structure. 519-525A
Rolling Contact Deformation of 1100 Aluminum Disks. 1561-1572A
Invariance of Neck Formation to Material Strength and Strain Rate for Power-Law Materials. 1632-1633A

Plastic flow

Flow Localization During Plane Strain Punch Stretching of a Ferrite—Austenite Steel. 1537-1546A
Characterization and Modeling of the High Temperature Flow Behavior of Aluminum Alloy 2024. 2227-2237A

Plastic flow, Anisotropy

On the Directionality of Strain Localization When Stretching Aluminum Alloy Sheets in Biaxial Tension. 367-370A

Plastic strain

See Plastic deformation

Plasticity

See Superplasticity

Plate metal, Mechanical properties

Size Effects on the Microscopic Cleavage Stress, σ_c , in Martensitic Microstructures. 231-241A

Platinum, Binary systems

An HVEM Study of an Unusual Ordering Reaction in Platinum—Carbon. 807-814A

Platinum metal alloys

See Palladium base alloys

Platinum metals

See Platinum

Point defects

See Interstitial defects
Lattice vacancies

Polarization (electrodes)

See Cathodic polarization

Poling

See Deoxidizing

Pollution

See Air pollution

Pollution abatement

Line-Enhanced Reduction of Sulfide Concentrates: a Thermodynamic Discussion. 185-196B
Removal of SO₂ With Oxygen in the Presence of Fe(III). 745-753B

Pores

See Porosity

Porosity

Effect of Entrapped Inert Gas on Pore Filling During Liquid Phase Sintering. 2175-2182A

Porosity, Corrosion effects

Void Formation in INCONEL MA-754 by High Temperature Oxidation. 151-162A

Porosity, Size effects

The Critical Grain Size for Liquid Flow Into Pores During Liquid Phase Sintering. 1915-1919A

Portevin-Le Chatelier effect

See Serrated yielding

Potassium, Alloying additive

A Model for the Formation of the Non-Sag Structure of Potassium-Doped Tungsten Wire. 1455-1459A

- Potassium, Impurities**
An Investigation of the Critical Influence of Potassium on the Reduction of Wustite. 657-663B
- Pots (electrolytic)**
See Electrolytic cells
- Powder compacts**
See also Sintered compacts
- Powder compacts, Fabrication**
The Structure and Properties of a Nickel-Base Superalloy Produced by Osprey Atomization—Deposition. 583-591A
- Powder compacts, Mechanical properties**
Influence of Foreign Particles on Fatigue Behavior of Ti—6Al—4V Prealloyed Powder Compacts. 271-280A
Effect of Isothermal Forging on Microstructure and Fatigue Behavior of Blended Elemental Ti—6Al—4V Powder Compacts. 549-559A
The Influence of Load Ratio on Fatigue Crack Growth in 7090-T6 and IN9021-T4 P/M Aluminum Alloys. 1787-1795A
- Powders**
See also Alloy powders
Dendritic powder
Metal powders
A Multi-Phase Model for Plumes in Powder Injection Refining Processes. 77-85B
- Power generation**
See Electric power generation
- Power plants**
See Electric power generation
- Powerhouses**
See Electric power generation
- Precious metal alloys**
See Palladium base alloys
- Precious metals**
See Gold
Platinum
Silver
- Precipitates**
High Temperature Ductility Loss in Carbon—Manganese and Niobium-Treated Steels. 1995-2006A
- Precipitates, Chemical analysis**
The Chemical Composition of Precipitated Austenite in 9Ni Steel. 967-972A
- Precipitates, Composition effects**
Influence of Alloy Chemistry on Carbide Precipitation in a Nickel Base Superalloy. 2075-2077A
- Precipitates, Crystal growth**
Precipitation and Ostwald Ripening in Dilute Aluminum Base—Zr—V Alloys. 2187-2198A
Dislocation/Precipitate Interactions During Coarsening of a Plastically Strained High-Misfit Nickel-Base Superalloy. 2239-2247A
- Precipitation**
Transformation Sequence in a Cu—Al—Ni Shape Memory Alloy at Elevated Temperatures. 65-72A
Precipitation Processes in Near-Equiatomic TiNi Shape Memory Alloys. 1505-1515A
- Precipitation hardening**
See also Aging (artificial)
Strain aging
Metallographic and Differential Scanning Calorimetry Analyses of Precipitation and Recrystallization in an Al—Mn Alloy. 593-605A
Discussion of "The Early Stages of the Decomposition of Alloys" and Author's Reply. 742A
Fatigue Crack Growth and Fracture Toughness Behavior of an Al—Li—Cu Alloy. 1011-1026A
Superplasticity in a Thermomechanically Processed High-Magnesium, Al—Mg Alloy. 1035-1041A
The Influence of Thermomechanical Processing Variables on Superplasticity in a High-Magnesium, Al—Mg Alloy. 1043-1050A
Microstructure—Mechanical Property Relationships in Isothermally Transformed Vanadium Steels. 1191-1202A
Matrix and Interfacial Precipitation in the W—Ni—Fe System. 1921-1934A
- Precipitation hardening, Alloying effects**
Decomposition Characteristics of Al—Mn—Zr Alloys Rapidly-Quenched From the Melt. 799-806A
The Effects of Tantalum on the Microstructure of Two Polycrystalline Nickel-Base Superalloys: B-1900 + Hafnium and MAR-M247. 1891-1905A
Precipitation and Ostwald Ripening in Dilute Aluminum Base—Zr—V Alloys. 2187-2198A
- Precipitation hardening, Stress effects**
Dislocation/Precipitate Interactions During Coarsening of a Plastically Strained High-Misfit Nickel-Base Superalloy. 2239-2247A
- Precipitation hardening alloys, Corrosion**
The Effect of Cathodic Polarization on the Corrosion Fatigue Behavior of a Precipitation Hardened Aluminum Alloy. 339-347A
- Precipitation heat treatment**
See Aging (artificial)
Precipitation hardening
- Preferential attack (corrosion)**
Dissolution Behavior of 304 Stainless Steel in HNO₃/HF Mixtures. 137-149A
- Pregnant liquors**
Extraction Equilibria in the System GaCl₃—AlCl₃—HCl—H₂O—Tributyl Phosphate. 259-265B
- Pressing**
See Hot isostatic pressing
- Pressure**
Pressures Produced by Gas Tungsten Arcs. 601-607B
- Pressure welding**
See Diffusion welding
Resistance spot welding
- Pressurized water reactors**
Fatigue Crack Growth Rates in a Pressure Vessel Steel Under Various Conditions of Loading and the Environment. 1837-1849A
- Prestraining**
Influence of Prestrain History on Fracture Toughness Properties of Steels. 473-489A
- Prestraining**
Flow Behavior of an Aluminum-Killed Steel After Tensile Prestraining and Strain-Aging. 1573-1575A
- Process control**
Development of an Analytical Equation for Calculation of the Blast Furnace Fuel Rate. 705-724B
- Projectiles, Microstructure**
Microstructural Analysis of Residual Projectiles—a New Method to Explain Penetration Mechanisms. 435-442A
- Propagation**
See Crack propagation
- Properzi process**
See Continuous casting
- Protective coatings**
Stability of the Chromia Layer on Steels in Flowing Nonequilibrium H₂—H₂O—CH₄—CO Mixtures at 950°C. 915-921A
- Protective coatings, Oxidation**
A Relationship Between Indigenous Impurity Elements and Protective Oxide Scale Adherence Characteristics. 923-932A
- Pseudoelasticity, Deformation effects**
Effect of Cyclic Deformation on the Pseudoelasticity Characteristics of Ti—Ni Alloys. 115-120A
- Pyrometallurgy**
Kinetics of Reduction of Lead Oxide in Liquid Slag by Carbon in Iron. 271-279B
Oxidation of Cobalt Sulfide. 367-373B
Dissolution of Solid Magnetite in Fe—S—O Melt. 639-645B
Agglomeration of Particles During Roasting of Zinc Sulfide Concentrates. 647-656B
An Investigation of the Critical Influence of Potassium on the Reduction of Wustite. 657-663B
Removal of SO₂ With Oxygen in the Presence of Fe(III). 745-753B
- Pyrrhotite, Reduction (chemical)**
Lime-Enhanced Reduction of Sulfide Concentrates: a Thermodynamic Discussion. 185-196B
- Quaternary systems, Phases (state of matter)**
A Solid-State EMF Study of Ternary Ni—S—O, Fe—S—O, and Quaternary Fe—Ni—S—O. 133-146B
Phase Relationships in the Iron-Rich Fe—Cr—Ni—C System at Solidification Temperatures. 1461-1469A
- Quelle-Basic oxygen process**
Model Study of Mixing and Mass Transfer Rates of Slag—Metal in Top and Bottom Blown Converters. 461-469B
- Quenching (cooling)**
See Quenching and tempering
Rapid solidification
- Quenching and tempering**
Retained Carbide Distribution in Intercritically Austenitized 52100 Steel. 31-36A
- Quenching stresses**
See Residual stress
- Quinary systems, Phases (state of matter)**
Phase Relationships in the Fe—Cr—Mn—Ni—C System at Solidification Temperatures. 1825-1835A
- Q-BOP**
See Quelle-Basic oxygen process
- Rapid solidification**
Microstructural Characterization of Rapidly Solidified Al—Li—Co Powders. 73-91A
Microstructures and Mechanical Properties of Melt-Quenched Ferritic Stainless Steels. 261-269A
Solidification of Nb—Ge Alloys in Long Drop Tubes. 973-981A
Microstructures of Niobium—Germanium Alloys Processed in Inert Gas in the 100 Meter Drop Tube. 1421-1428A
Compositional Analysis of the Icosahedral Phase in Rapidly Quenched Al—Mn and Al—V Alloys. 1657-1664A
Analytical Scanning Transmission Electron Microscopic Study of Metastable Modulated Structure in a Rapidly Quenched Fe—22Ni—8Al—2.4C Alloy. 2077-2080A
- Rare earth compounds**
See Samarium compounds
- Rare earth metals**
See also Cerium
Gadolinium
- Rare earth metals, Chemical analysis**
Research on Determination of the Rare-Earth Content in Metal Phases of Steel. 315-323A
- Reaction kinetics**
The Leaching of Chalcopyrite With Ferric Chloride. 19-28B

Reaction kinetics

- An Investigation of the Thermodynamics and Kinetics of the Ferric Chloride Brine Leaching of Galena Concentrate. Intrinsic Kinetics of the Oxidation of Chalcopyrite Particles Under Isothermal and Nonisothermal Conditions. Interfacial Rates of Reaction of CO₂ With Liquid Iron Silicates, Silica-Saturated Manganese Silicates, and Some Calcium Iron Silicates. 307-316B
The Reaction of SiO₂ With Liquid Slags. Kinetics of Galena Dissolution in Ferric Chloride Solutions. Leaching Kinetics of Natural Cobalt Triarsenide in Chlorine Solutions. 397-399B
Reduction of Phosphate Ore by Carbon. II. Rate Limiting Steps. 415-423B
629-637B
869-877B
- Reaction sintering**
See Activated sintering
- Reactions (chemical)**
See Carbothermic reactions
Chlorination
Deoxidizing
Desulfurizing
Electrolysis
Interface reactions
Internal oxidation
Oxidation
- Reactivity (chemical)**
See Activity (chemical)
- Reactors**
See Boiling water reactors
Pressurized water reactors
- Recrystallization**
See also Grain refinement
Secondary recrystallization
The Influence of Thermomechanical Processing Variables on Superplasticity in a High-Magnesium, Al—Mg Alloy. 1043-1050A
- Recrystallization, Alloying effects**
Effect of Copper Precipitation on the Development of Recrystallization Textures Through Continuous Annealing of Low-Carbon Sheet Steel. 621-633A
A Model for the Formation of the Non-Sag Structure of Potassium-Doped Tungsten Wire. 1455-1459A
- Recrystallization, Microstructural effects**
Deformation and Recrystallization Textures in Commercially Pure Aluminum. 253-259A
Metallographic and Differential Scanning Calorimetry Analyses of Precipitation and Recrystallization in an Al—Mn Alloy. 593-605A
- Red hardness**
See Hardness
- Red shortness**
See Brittleness
- Redox potential**
See Electrode potentials
- Reduction (chemical)**
See Direct reduction
Flash smelting
- Reduction (electrolytic)**
See also Electrowinning
Electrolytic Reduction of Uranium(VI) to Uranium(IV) in Acidic Chloride and Acidic Sulfate Solutions. 41-50B
- Reduction (metal working)**
See Hot rolling
- Reduction of area, impurity effects**
The Effects of Interstitials and Hydrogen-Interstitial Interactions on Low Temperature Hardening and Embrittlement in Vanadium, Niobium, and Tantalum. 1179-1189A
- Reduction potential**
See Electrode potentials
- Refining**
See Electrorefining
Vacuum refining
- Refractory alloys**
See Niobium base alloys
Tungsten base alloys
Vanadium base alloys
- Refractory metal compounds**
See Chromium compounds
Molybdenum compounds
Niobium compounds
Tungsten carbide
Tungsten compounds
Vanadium compounds
- Refractory metals**
See Chromium
Molybdenum
Niobium
Tantalum
Tungsten
Vanadium
- Reinforcement**
See Fiber composites
- Relaxation**
See also Stress relaxation
Cyclic Creep and Anelastic Relaxation Analysis of an ODS Superalloy. 1577-1583A
- Residual stress**
Orientation and Strain Dependence of Stored Energy of Cold Work in Axisymmetric Copper. 513-517A
- Resistance spot welding**
Resistance Spot Welding of Galvanized Steel. I. Material Variations and Process Modifications. 879-885B
Resistance Spot Welding of Galvanized Steel. II. Mechanisms of Spot Weld Nugget Formation. 887-901B
- Resistance welding**
See Resistance spot welding
- Resistance welds**
See Welded joints
- Resistivity**
See Superconductivity
- Resulfurized steels, Phases (state of matter)**
Manganese Sulfide Precipitation in Low-Carbon Resulfurized Free-Machining Steel. 2080-2083A
- Retained austenite**
The Influence of Precipitated Austenite on Hydrogen Embrittlement in 5.5Ni Steel. 1157-1164A
- Retained austenite, Alloying effects**
On the Microstructure and Mechanical Behavior of Melt-Spun Fe—24Ni—0.5C Ribbons: Effect of Austenite Grain Size. 127-136A
- Revaporization**
See Vaporizing
- Reviews**
Biotechnology/Materials: the Growing Interface. 5-30A
- Rheocasting**
Processing-Structure Characterization of Rheocast IN-100 Superalloy. 2049-2062A
- Rheological properties**
See Viscosity
- Ribbons (metallic)**
See Tapes (metallic)
- Roasting**
See also Fluidized bed roasting
Intrinsic Kinetics of the Oxidation of Chalcopyrite Particles Under Isothermal and Nonisothermal Conditions. 51-60B
Thermodynamic Study of Fe₂O₃—Fe₂(SO₄)₃ Equilibrium Using an Oxanionic Electrolyte (Na₂SO₄—I). 323-329B
Electrochemical Determination of Thermodynamic Properties and X-Ray Diffraction Investigation of the Fe₂O₄—ZnFe₂O₄ System. 515-521B
- Rods, Melting**
Experimental Studies on Drop Formation at the Tip of Melting Rods. 471-477B
- Roll spot welding**
See Resistance spot welding
- Rolling**
See Hot rolling
- Rolling contact**
Rolling Contact Deformation of 1100 Aluminum Disks. 1561-1572A
- Rolling texture**
Deformation and Recrystallization Textures in Commercially Pure Aluminum. 253-259A
- Rotary converters**
An Analysis of Radial Segregation for Different Sized Spherical Solids in Rotary Cylinders. 247-257B
- Rotary furnaces**
See Rotary converters
- Rotary induction furnaces**
See Electric induction furnaces
- Rotary kilns**
See Kilns
- Rotary tilting furnaces**
See Rotary converters
- Rotating machines**
An Analysis of Radial Segregation for Different Sized Spherical Solids in Rotary Cylinders. 247-257B
- Rotor furnaces**
See Rotary converters
- Rotor process**
See Rotary converters
- Roughing (rolling)**
See Hot rolling
- Rounds, Casting**
Rotational Electromagnetic Stirring in Continuous Casting of Round Strands. 119-131B
- Rupture strength**
See Creep rupture strength
- Samarium compounds, Magnetic properties**
Directional Solidification and Characterization of Near Eutectic Sm₂Co₁₇/Co Alloys. 1149-1155A
- Sand casting**
Heat and Moisture Transfer in Sand Molds Containing Water. 903-911B
- Sand molds, Thermal properties**
Heat and Moisture Transfer in Sand Molds Containing Water. 903-911B

- Scandium compounds, Thermal properties**
Standard Enthalpies of Formation of $TiSi_2$ and VS_i_2 by High-Temperature Calorimetry. 1217-1221A
- Schottky defect**
See Lattice vacancies
- Scrubbers**
Theoretical and Experimental Study of the Removal of Dust Particles From Flue Gases Using Two-Phase Steam-Water Droplet Mixtures. 665-676B
- Scrubbing**
See Gas scrubbing
- Season cracking**
See Stress corrosion cracking
- Secondary recrystallization**
Factors Affecting the Final Grain Size of Decarburized Lamination Steels. 1277-1285A
Origin and Development of Through-the-Thickness Variations of Texture in the Processing of Grain-Oriented Silicon Steel. 1313-1322A
- Secondary recrystallization, Heating effects**
Effects of Decarburization and Normalizing Heat Treatment in Boron-Silicon Iron Alloys. 1353-1359A
- Seeding**
See Nucleation
- Segregations**
An Analysis of Radial Segregation for Different Sized Spherical Solids in Rotary Cylinders. 247-257B
Measurement of Segregation and Distribution Coefficients in MAR-M200 and Hafnium-Modified MAR-M200 Superalloys. 419-428A
Low Temperature Impact Properties of Phosphorus and Sulfur Doped and Sensitized Type 304 Stainless Steel. 663-668A
Analysis of Solute Distribution in Dendrites of Carbon Steel With δ/γ Transformation During Solidification. 845-859B
High Temperature Ductility Loss in Carbon-Manganese and Niobium-Treated Steels. 1995-2006A
Carbon Segregation to Grain Boundaries in Rapidly Solidified $NiAl$. 2084-2086A
- Segregations, Alloying effects**
Effect of Fluid Flow and Hafnium Content on Macrosegregation in the Directional Solidification of Nickel Base Superalloys. 347-356B
The Effect of Silicon and Nickel Additions on the Sulfide Spacing and Fracture Toughness of a 0.4 Carbon Low Alloy Steel. 669-678A
- Segregations, Cooling effects**
The Effect of Solidification Rate on Microsegregation. 2063-2073A
- Self diffusion**
See Diffusion
- Semicontinuous casting**
See Continuous casting
- Semikilling**
See Deoxidizing
- Sensitizing**
Low Temperature Impact Properties of Phosphorus and Sulfur Doped and Sensitized Type 304 Stainless Steel. 663-668A
- Serrated yielding**
Numerical Modeling of the Propagation of an Adiabatic Shear Band. 443-450A
Serrated Grain Boundary Formation During High Temperature Fatigue. 1100-1102A
Instabilities During Tension of Thin Voided Viscoplastic Sheets. 1637-1640A
- Shaft kilns**
See Kilns
- Shape memory**
Transformation Sequence in a Cu-Al-Ni Shape Memory Alloy at Elevated Temperatures. 65-72A
Microstructural Effects of Martensitic Transformation Cycling of a Cu-Zn-Al Alloy: Vestigial Structures in the Parent Phase. 195-203A
Deformation of Martensite in a Polycrystalline Cu-Zn-Al Alloy. 945-959A
- Shape memory, Deformation effects**
Deformation and Transition Behavior Associated With the R-Phase in Ti-Ni Alloys. 53-63A
Effect of Cyclic Deformation on the Pseudoelasticity Characteristics of Ti-Ni Alloys. 115-120A
- Shear properties**
See Shear strength
Shear stress
- Shear strength, Corrosion effects**
Examination of the Titanium Environment in a René 41 Nickel Base Superalloy by X-Ray Absorption Spectroscopy. 739-741A
- Shear stress**
Discussion of "The Bainite Reaction in Fe-Si-C Alloys: the Primary Stage" and "The Bainite Reaction in Fe-Si-C Alloys: the Secondary Stage". 1095-1100A
- Sheet metal, Crystal growth**
Effect of Copper Precipitation on the Development of Recrystallization Textures Through Continuous Annealing of Low-Carbon Sheet Steel. 621-633A
Grain Growth in Capped Steel. 1907-1913A
- Shielded arc welding**
See Gas metal arc welding
Gas tungsten arc welding
Plasma arc welding
Submerged arc welding
- Short arc welding**
See Gas metal arc welding
- Short range order**
Short Range Order Hardening With Second Neighbor Interactions in fcc Solid Solutions. 189-194A
An HVEM Study of an Unusual Ordering Reaction in Platinum-Carbon. 807-814A
- Sigma hard facing**
See Gas metal arc welding
- Sigma phase**
The Use of New PHACOMP in Understanding the Solidification Microstructure of Nickel Base Alloy Weld Metal. 2107-2116A
- Sigma welding**
See Gas metal arc welding
- Silica**
See Silicon dioxide
- Silicides, Thermal properties**
Standard Enthalpies of Formation of $TiSi_2$ and VS_i_2 by High-Temperature Calorimetry. 1217-1221A
- Silicon, Alloying elements**
The Effect of Silicon and Nickel Additions on the Sulfide Spacing and Fracture Toughness of a 0.4 Carbon Low Alloy Steel. 669-678A
The Effect of Solidification Rate on Microsegregation. 2063-2073A
- Silicon, Reactions (chemical)**
Rates of Dissolution of Solid Iron, Cobalt, Nickel, and Silicon in Liquid Copper and Diffusion Rate of Iron From Liquid Cu-Fe Alloy Into Liquid Copper. 291-305B
- Silicon, Refining**
A Study on Purification of Metallurgical Grade Silicon by Molten Salt Electrorefining. 395-397B
- Silicon, Synthesis**
Thermodynamics of the Si-C-O System for the Production of Silicon Carbide and Metallic Silicon. 503-514B
- Silicon, Ternary systems**
Thermodynamics of the Si-C-O System for the Production of Silicon Carbide and Metallic Silicon. 503-514B
- Silicon carbide, Composite materials**
An In Situ HVEM Study of Dislocation Generation at Al/SiC Interfaces in Metal Matrix Composites. 379-389A
- Silicon carbide, Synthesis**
Thermodynamics of the Si-C-O System for the Production of Silicon Carbide and Metallic Silicon. 503-514B
- Silicon compounds**
See Silicon carbide
Silicon dioxide
- Silicon dioxide, Diffusion**
The Reaction of $SiO(g)$ With Liquid Slags. 397-399B
- Silicon iron**
See Silicon steels
- Silicon manganese steels, Corrosion**
Stress Corrosion Cracking in High Strength Steel Under Mode III Loading. 711-716A
- Silicon steels**
See also Electrical steels
Silicon manganese steels
- Silicon steels, Composite materials**
Superplasticity of a Stainless Steel Clad Ultrahigh Carbon Steel. 2295-2298A
- Silicon steels, Crystal growth**
Discussion of "The Bainite Reaction in Fe-Si-C Alloys: the Primary Stage" and "The Bainite Reaction in Fe-Si-C Alloys: the Secondary Stage". 1095-1100A
Grain Growth Characteristics and Magnetic Properties of Rapidly Quenched Silicon Steel Ribbons. 1295-1299A
- Silicon steels, Mechanical properties**
Fracture Behavior in Medium-Carbon Martensitic Silicon and Nickel-Steels. 1173-1178A
- Silicon steels, Phase transformations**
Nucleation Kinetics of Proeutectoid Ferrite at Austenite Grain Boundaries in Fe-C-X Alloys. 1385-1397A
The Kinetics of Ferrite Nucleation at Austenite Grain Edges in Fe-C and Fe-C-X Alloys. 1399-1407A
- Silicon steels, Phases (state of matter)**
Development of Ferrous Laminated Composites With Unique Microstructures by Control of Carbon Diffusion. 1517-1527A
- Silver, Alloying additive**
Effect of Small Additions of Silver on the Eutectic Temperature in the Lead-Tin System. 829-832B
- Silver, Diffusion**
Diffusional Breakdown of a Silver Diffusion Barrier in a Cu-Ag-Ni Diffusion Triple. 933-944A
- Silver, Extraction**
Potentiometric Studies on the Adsorption of $Au(CN)_2^-$ and $Ag(CN)_2^-$ Onto Activated Carbon. 523-526B
Studies on Role of Oxygen in the Adsorption of $Au(CN)_2^-$ and $Ag(CN)_2^-$ Onto Activated Carbon. 529-533B

Silver, Physical properties

The Temperature Coefficient of the Surface Tension of Pure Liquid Metals.
Interfacial Tension and Flotation Characteristics of Liquid Metal—Sodium Flux Systems.

163-170B

339-346B

Simulation

See Computer simulation

Single crystals, Diffusion

Hydrogen Transport During Deformation in Nickel. II. Single Crystal Nickel.

869-875A

Single crystals, Mechanical properties

Orientation and Temperature Dependence of Some Mechanical Properties of the Single-Crystal Nickel-Base Superalloy René N4: III. Tension—Compression Anisotropy.

507-512A

Sintered compacts, Microstructure

Formation of Copper Pockets in Iron Grains During the Sintering of Fe—Cu Alloys.

1429-1431A

Sintering (powder metallurgy)

See Activated sintering
Liquid phase sintering

Size distribution (particle)

See Particle size distribution

Slags

See also Blast furnace slags

The Slag—Metal Equilibrium in Tin Smelting.

61-68B

"Central Atoms" Models for Ternary Silicate and Aluminosilicate Melts.

105-110B

The Settling of Metallic Lead From Lead Blast Furnace Slag. Kinetics of Reduction of Lead Oxide in Liquid Slag by Carbon in Iron.

267-270B

Interfacial Rates of Reaction of CO₂ With Liquid Iron Silicates, Silica-Saturated Manganese Silicates, and Some Calcium Iron Silicates.

307-316B

The Composition and Temperature Dependence of the Sulfide Capacity of Metallurgical Slags.

331-337B

Model Study of Mixing and Mass Transfer Rates of Slag-Metal in Top and Bottom Blown Converters.

461-469B

The Sulfur Partition Ratio and the Sulfide Capacity of Na₂O—SiO₂ Slags at 1200°C.

491-496B

Soda Slag System for Hot Metal Dephosphorization.

797-804B

Slags, Diffusion

Measurement of Tracer Diffusivities of Ca⁴⁵ and Fe⁵⁹ in Silica Saturated FeO—CaO—SiO₂ Melts With the Porous Frit Technique.

497-501B

Slags, Physical properties

Measurement of the Surface Tensions of Iron-Saturated Iron Silicate and Iron-Saturated Calcium Ferrite Melts by Pad-day's Cone Technique.

771-776B

Slags, Solubility

The Nitrogen Reaction Between Carbon Saturated Iron and Na₂O—SiO₂ Slag. I. Thermodynamics.

535-540B

The Nitrogen Reaction Between Carbon Saturated Iron and Na₂O—SiO₂ Slag. II. Kinetics.

541-545B

Slags, Thermal properties

Thermodynamic Analysis of Ordered Liquid Solutions by a Modified Quasichemical Approach—Application to Silicate Slags.

805-815B

Slip

See also Cross slip

Orientation and Temperature Dependence of Some Mechanical Properties of the Single-Crystal Nickel-Base Superalloy René N4. I. Tensile Behavior.

491-496A

Deformation of Martensite in a Polycrystalline Cu—Zn—Al Alloy.

945-959A

Smelting

See also Flash smelting

The Slag—Metal Equilibrium in Tin Smelting.

61-68B

Soaking

Influence of Soaking Treatments on Hot Ductility of Al—4.85Mg Alloys Containing Manganese.

833-841A

Soft annealing

See Annealing

Softening

See Strain softening

Solid solubility

A Solid-State EMF Study of the Cu—Cu₂O—NiO Three-Phase Equilibrium.

1104-1106A

Alloying Behavior of Co₃Ti.

1433-1439A

Thermotransport of Carbon in Two-Phase V—C and Nb—C Alloys.

1955-1966A

Solidification

See also Directional solidification

Rapid solidification

Numerical Simulation of Solidification in an Aluminum Casting.

209-216B

The Role of Transient Convection in the Melting and Solidification in Arc Weldpools.

735-744B

Analysis of Solute Distribution in Dendrites of Carbon Steel With δ/γ Transformation During Solidification.

845-859B

Icosahedral and Decagonal Phase Formation in Al—Mn Alloys.

2117-2125A

Three-Dimensional Convection in Laser Melted Pools.

2265-2270A

Computer Simulation of Convection in Moving Arc Weld Pools.

2271-2277A

Dendrite Characteristics in Directionally Solidified Pb—8Au and Pb—3Pd Alloys.

2279-2290A

The Effect of Gravity Level on the Average Primary Dendritic Spacing of a Directionally Solidified Superalloy.

2301-2303A

Solidification, Field effects

Misra Technique Applied to Solidification of Cast Iron.

358-360A

Solids flow

An Analysis of Radial Segregation for Different Sized Spherical Solids in Rotary Cylinders.

247-257B

Solubility

See also Solid solubility

The Trapping and Transport Phenomena of Hydrogen in Nickel.

181-187A

Solubility, Alloying effects

Nitrogen Solubility in Liquid Iron and Fe—Mn Alloys.

238-239B

Solution hardening

See Solution strengthening

Solution strengthening, Alloying effects

Decomposition Characteristics of Al—Mn—Zr Alloys Rapidly-Quenched From the Melt.

799-806A

Solvent action

Comparison of Solution Models for Nonmetallic Solutes in Binary Liquid Alloys: Nitrogen in Fe—Cr and Fe—Ni.

785-789B

Solvent extraction

Chemical Equilibrium Studies on the Iron(III)—Sulfuric Acid/ β -Alkenyl δ -Hydroxy—Quinoline—Xylene System.

615-620B

Water and Solute Activities of H₂SO₄—Fe₂(SO₄)₃—H₂O and HCl—FeCl₃—H₂O Solution Systems. II. Activities of Solutes.

621-627B

Solvus (metallurgical)

See Solid solubility

Sorption

See Adsorption

Specimen preparation

Surface Oxide on fcc Iron—Nickel Alloys.

163-167A

Spectroscopy

See Mossbauer spectroscopy

Speller

See Zinc

Spheroidal iron

See Nodular iron

Spheroidal structure, Impurity effects

Retained Carbide Distribution in Intercritically Austenitized 52100 Steel.

31-36A

Spheroidizing

Growth of Silicon Particles in an Aluminum Matrix.

2139-2152A

Sponginess

See Porosity

Spot welding

See also Resistance spot welding

The Role of Transient Convection in the Melting and Solidification in Arc Weldpools.

735-744B

Stability

See Phase stability

Thermal stability

Stainless steels

See also Austenitic stainless steels

Duplex stainless steels

Ferritic stainless steels

Stainless steels, Composite materials

Superplasticity of a Stainless Steel Clad Ultrahigh Carbon Steel.

2295-2298A

Stainless steels, Physical properties

Comparison of Surface Tension Measurements Using the Levitated Droplet Method.

159-162B

Static fatigue

See Creep rupture strength

Steel alloys

See Alloy steels

Steel constituents

See Austenite

Bainite

Cementite

Ferrite

Martensite

Retained austenite

Steel converters

See Basic converters

Bottom blown converters

Rotary converters

Top blown converters

Steel making

See also LD process

Oxygen steel making

Quelle-Basic oxygen process

The Kinetics of the Nitrogen Reaction With Liquid Iron—Chromium Alloys.

317-322B

Mathematical Modeling of Flows in Large Tundish Systems in Steelmaking.

449-459B

Measurement of Tracer Diffusivities of Ca⁴⁵ and Fe⁵⁹ in Silica Saturated FeO—CaO—SiO₂ Melts With the Porous Frit Technique.

497-501B

The Nitrogen Reaction Between Carbon Saturated Iron and Na₂O—SiO₂ Slag. I. Thermodynamics.

535-540B

- The Nitrogen Reaction Between Carbon Saturated Iron and $\text{Na}_2\text{O}-\text{SiO}_2$ Slag. II. Kinetics. 541-545B
 Mixing Models for Gas Stirred Metallurgical Reactors. 725-733B
 Thermodynamic Analysis of Ordered Liquid Solutions by a Modified Quasichemical Approach—Application to Silicate Slags. 805-815B
- Steels**
 See also Alloy steels
 Aluminum killed steels
 Austenitic stainless steels
 Bearing steels
 Boron steels
 Carbon manganese steels
 Carbon steels
 Chromium molybdenum steels
 Chromium molybdenum vanadium steels
 Chromium steels
 Dual phase steels
 Duplex stainless steels
 Electrical steels
 Ferritic stainless steels
 Galvanized steels
 High strength low alloy steels
 High strength steels
 Low alloy steels
 Manganese steels
 Molybdenum steels
 Nickel chromium molybdenum steels
 Nickel chromium steels
 Nickel steels
 Resulfurized steels
 Silicon manganese steels
 Silicon steels
 Stainless steels
 Tool steels
 Vanadium steels
- Steels, Casting**
 Rotational Electromagnetic Stirring in Continuous Casting of Round Strands. 119-131B
 An Ice-Water Model Study on Formation of Blowhole-Free Skin With Reference to Solidification of Steel. 553-564B
 Heat and Moisture Transfer in Sand Molds Containing Water. 903-911B
- Steels, Chemical analysis**
 Research on Determination of the Rare-Earth Content in Metal Phases of Steel. 315-323A
- Steels, Mechanical properties**
 The Interaction of Hydrogen With the Interface of Al_2O_3 Particles in Iron. 2183-2186A
- Steels, Phase transformations**
 An Assessment of the Additivity Principle in Predicting Continuous-Cooling Austenite-to-Pearlite Transformation Kinetics Using Isothermal Transformation Data. 1493-1503A
 Effects of Copper on Proeutectoid Cementite Precipitation. 2163-2173A
- Steels, Refining**
 The Nitrogen Reaction Between Carbon Saturated Iron and $\text{Na}_2\text{O}-\text{SiO}_2$ Slag. I. Thermodynamics. 535-540B
 The Nitrogen Reaction Between Carbon Saturated Iron and $\text{Na}_2\text{O}-\text{SiO}_2$ Slag. II. Kinetics. 541-545B
- Steels, Welding**
 A Simplified Treatment of Carbon Diffusion in Compound Welds Having an Intermediate Layer. 2083-2084A
- Stereomicroscopy**
 Estimation of Average Size of Convex Particles. 742-745A
 Application of Microstructure Modeling to the Kinetics of Proeutectoid Ferrite Transformation in Hot-Rolled Microalloyed Steels. 1625-1629A
 Modulated Microstructures in β Cu—Zn—Al. 2153-2161A
- Stirring**
 See Electromagnetic stirring
- Stitch welding**
 See Spot welding
- Stora Kaldo process**
 See Oxygen steel making
- Stored energy**
 See Internal energy
- Strain aging**
 Flow Behavior of an Aluminum-Killed Steel After Tensile Prestraining and Strain-Aging. 1573-1575A
 Strain Aging and Load Relaxation Behavior of Type 316 Stainless Steel at Room Temperature. 1757-1767A
- Strain hardening**
 Metallographic and Differential Scanning Calorimetry Analyses of Precipitation and Recrystallization in an Al—Mn Alloy. 593-605A
 Effect of Stress—Strain-Law Transients on Formability. 1001-1009A
 The Processing and Properties of Heavily Cold Worked Directionally Solidified Ni—W Eutectic Alloys. 1165-1171A
 Strain Hardening of Hadfield Manganese Steel. 1725-1737A
- Strain hardening, Heating effects**
 Effect of Tempering Temperature on the Work-Hardening Rate of Five HSLA Steels. 307-313A
- Strain rate**
 Effect of Stress—Strain-Law Transients on Formability. 1001-1009A
 Superplasticity in a Thermomechanically Processed High-Magnesium, Al—Mg Alloy. 1035-1041A
- Strain softening**
 Particle Size and Orientation Effects on Softening in a Copper Matrix Containing Rod-Shaped Iron Particles. 1751-1755A
- Strength of materials**
 See Mechanical properties
- Strengthening (solution)**
 See Solution strengthening
- Stress aging**
 See Strain aging
- Stress analysis**
 Invariance of Neck Formation to Material Strength and Strain Rate for Power-Law Materials. 1632-1633A
- Stress corrosion cracking**
 On the Failure Mechanism of Chemically Embrittled Cu_3Au Single Crystals. 703-710A
 Stress Corrosion Cracking in High Strength Steel Under Mode III Loading. 711-716A
 Hydrogen-Induced Delayed Fracture Under Mode II Loading. 717-725A
 Relative Stress Corrosion Susceptibilities of Alloys 690 and 600 in Simulated Boiling Water Reactor Environments. 877-887A
 Further Observations of SCC in α — β Brass: Considerations Regarding the Appearance of Crack Arrest Markings During SCC. 1081-1086A
 Effect of Notch Root Radius on Stress Intensity in Mode I and Mode III Loading. 1633-1637A
 Mechanical Properties and Microstructure of Al—Li—Cu—Mg—Zr Die Forgings. 2007-2016A
- Stress corrosion cracking, Alloying effects**
 Sulfide Stress Cracking Susceptibility of Nickel Containing Steels. 1601-1610A
- Stress corrosion resistance**
 See Corrosion resistance
- Stress relaxation**
 Strain Aging and Load Relaxation Behavior of Type 316 Stainless Steel at Room Temperature. 1757-1767A
- Stress relieving**
 See Grain refinement
- Stress rupture strength**
 See Creep rupture strength
- Stress strain curves**
 Effect of Cyclic Deformation on the Pseudoelectricity Characteristics of Ti—Ni Alloys. 115-120A
 Unloading Yield Effects in Aluminum Alloys. 121-126A
 Numerical Modeling of the Propagation of an Adiabatic Shear Band. 443-450A
 High-Temperature Plastic Deformation of Two V—Ga Alloys With A15 Structure. 519-525A
 Effect of Stress—Strain-Law Transients on Formability. 1001-1009A
 Rolling Contact Deformation of 1100 Aluminum Disks. 1561-1572A
 Instabilities During Tension of Thin Voids Viscoplastic Sheets. 1637-1640A
 Strain Hardening of Hadfield Manganese Steel. 1725-1737A
 Strain Aging and Load Relaxation Behavior of Type 316 Stainless Steel at Room Temperature. 1757-1767A
 Grain Boundary Contribution to the Bauschinger Effect in β -Brass Bicrystals. 2017-2029A
 Characterization and Modeling of the High Temperature Flow Behavior of Aluminum Alloy 2024. 2227-2237A
- Stress strain curves, Deformation effects**
 Effect of Isothermal Forging on Microstructure and Fatigue Behavior of Blended Elemental Ti—6Al—4V Powder Compacts. 549-559A
- Stress strain curves, Microstructural effects**
 Microstructural Dependence of Iron—High Manganese Tensile Behavior. 537-547A
 A Rationalization of Stress—Strain Behavior of Two-Ductile Phase Alloys. 2209-2226A
- Stresses**
 See Residual stress
 Shear stress
 Thermal stresses
- Stressing**
 See Prestressing
- Stretch forming**
 Flow Localization During Plane Strain Punch Stretching of a Ferrite—Austenite Steel. 1537-1546A
- Stretching**
 See Stretch forming
- Strip**
 See Coils (strip)
- Strong liquor**
 See Pregnant liquors
- Strontium, Binary systems**
 The Aluminum—Strontium Phase Diagram. 1250-1253A
- Structural hardening**
 See also Aging (artificial)
 Precipitation hardening
 Solution strengthening
 Strain aging
 Strain hardening
 Short Range Order Hardening With Second Neighbor Interactions in fcc Solid Solutions. 189-194A
- Structures (crystalline)**
 See Columnar structure
 Crystal structure
 Dendritic structure
 Equiaxed structure
 Grain structure

Structures (crystalline)

- Hypereutectic structures
Hypereutectoid structures
Hypoeutectic structures
Microstructure
Spheroidal structure
Widmanstätten structure
- Subgrain boundaries**
See Grain sub boundaries
- Submerged arc welding**
Inclusion Phases and the Nucleation of Acicular Ferrite in Submerged Arc Welds in High Strength Low Alloy Steels. 1611-1623A
- Submerged arc welds**
See Welded joints
- Sulfates, Environment**
Further Observations of SCC in α - β Brass: Considerations Regarding the Appearance of Crack Arrest Markings During SCC. 1081-1086A
- Sulfides, Crystal growth**
Manganese Sulfide Precipitation in Low-Carbon Resulfurized Free-Machining Steel. 2080-2083A
- Sulfides, Environment**
Sulfide Stress Cracking Susceptibility of Nickel Containing Steels. 1601-1610A
- Sulfides, Oxidation**
Oxidation of Cobalt Sulfide. 367-373B
- Sulfides, Reduction (chemical)**
Lime-Enhanced Reduction of Sulfide Concentrates: a Thermodynamic Discussion. 185-196B
- Sulfides, Solubility**
The Composition and Temperature Dependence of the Sulfide Capacity of Metallurgical Slags.
The Sulfur Partition Ratio and the Sulfide Capacity of $\text{Na}_2\text{O}-\text{SiO}_2$ Slags at 1200°C. 331-337B
491-496B
- Sulfur, Diffusion**
The Composition and Temperature Dependence of the Sulfide Capacity of Metallurgical Slags.
The Study of Desulfurization Kinetics in Grain Oriented 3% Silicon Iron. 331-337B
1347-1351A
- Sulfur, Impurities**
The Effect of Sulfur on the Gaseous Reduction of Solid Calcium silicates.
Low Temperature Impact Properties of Phosphorus and Sulfur Doped and Sensitized Type 304 Stainless Steel.
A Relationship Between Indigenous Impurity Elements and Protective Oxide Scale Adherence Characteristics.
The Effect of Manganese and Sulfur Contents on the Magnetic Properties of Cold Rolled Lamination Steels.
A Study of the Hydrogen-Induced Degradation of Two Steels Differing in Sulfur Content. 383-393B
663-668A
923-932A
1259-1266A
2255-2263A
- Sulfur, Quaternary systems**
A Solid-State EMF Study of Ternary Ni-S-O, Fe-S-O, and Quaternary Fe-Ni-S-O. 133-146B
- Sulfur, Solubility**
Solubility of Oxygen and Sulfur in Copper-Iron Mattes.
Correction to "Solubility of Oxygen and Sulfur in Copper-Iron Mattes". 147-157B
400B
- Sulphur**
See Sulfur
- Superalloys, Brazing**
Examination of the Titanium Environment in a René 41 Nickel Base Superalloy by X-Ray Absorption Spectroscopy. 739-741A
- Superalloys, Casting**
Processing-Structure Characterization of Rheocast IN-100 Superalloy. 2049-2062A
- Superalloys, Coating**
CVD Aluminide Nickel. 215-220A
- Superalloys, Composite materials**
Structure-Performance Maps of Polymeric, Metal, and Ceramic Matrix Composites. 1547-1559A
- Superalloys, Corrosion**
Relative Stress Corrosion Susceptibilities of Alloys 690 and 600 in Simulated Boiling Water Reactor Environments.
High Temperature Corrosion of Superalloys in an Environment Containing Both Oxygen and Chlorine. 877-887A
1087-1094A
- Superalloys, Crystal growth**
Effect of Fluid Flow and Hafnium Content on Macrosegregation in the Directional Solidification of Nickel Base Superalloys.
The Effect of Gravity Level on the Average Primary Dendritic Spacing of a Directionally Solidified Superalloy. 347-356B
2301-2303A
- Superalloys, Diffusion**
Measurement of Segregation and Distribution Coefficients in MAR-M200 and Hafnium-Modified MAR-M200 Superalloys. 419-428A
- Superalloys, Mechanical properties**
Constrained Cavity Growth Models of Longitudinal Creep Deformation of Oxide Dispersion Strengthened Alloys.
Effect of Environment on Fatigue Crack Propagation Behavior of Alloy 718 at Elevated Temperatures.
Orientation and Temperature Dependence of Some Mechanical Properties of the Single-Crystal Nickel-Base Superalloy René N4. I. Tensile Behavior.
Orientation and Temperature Dependence of Some Mechanical Properties of the Single-Crystal Nickel-Base Superalloy René N4. II. Low Cycle Fatigue Behavior. 281-293A
370-374A
491-496A
497-505A
- Orientation and Temperature Dependence of Some Mechanical Properties of the Single-Crystal Nickel-Base Superalloy René N4. III. Tension-Compression Anisotropy.
The Effects of Replacing the Refractory Elements Tungsten, Niobium, and Tantalum With Molybdenum in Nickel-Base Superalloys on Microstructural, Microchemistry, and Mechanical Properties.
Cyclic Creep and Anelastic Relaxation Analysis of an ODS Superalloy.
Fatigue Crack Propagation in Nickel-Base Superalloy Single Crystals Under Multiaxial Cyclic Loads. 507-512A
651-661A
1577-1583A
1739-1750A
- Superalloys, Microstructure**
Microstructure of a Rapidly-Solidified Nickel-Base Eutectic Superalloy. 407-417A
- Superalloys, Oxidation**
Void Formation in INCONEL MA-754 by High Temperature Oxidation.
 Ni_3Nb Alloy Species in Oxide Surfaces of Inconel 718. 151-162A
351-355A
- Superalloys, Phases (state of matter)**
Influence of Alloy Chemistry on Carbide Precipitation in a Nickel Base Superalloy. 2075-2077A
- Superalloys, Powder technology**
Microstructure and Stability of Melt Spun Inconel 713LC.
The Structure and Properties of a Nickel-Base Superalloy Produced by Osprey Atomization-Deposition.
Dendritic Microstructure in Argon Atomized Superalloy Powders. 173-180A
583-591A
2099-2102A
- Superalloys, Refining**
Relationship Between Furnace Voltage Signatures and the Operational Parameters Arc Power, Arc Current, CO Pressure, and Electrode Gap During Vacuum Arc Melting Inconel 718. 357-365B
- Superalloys, Structural hardening**
The Effects of Tantalum on the Microstructure of Two Polycrystalline Nickel-Base Superalloys: B-1900 + Hafnium and MAR-M247.
Dislocation/Precipitate Interactions During Coarsening of a Plastically Strained High-Misfit Nickel-Base Superalloy. 1891-1905A
2239-2247A
- Superalloys, Welding**
The Welding Metallurgy of Hastelloy Alloys C-4, C-22, and C-276.
The Use of New PHACOMP in Understanding the Solidification Microstructure of Nickel Base Alloy Weld Metal. 2035-2047A
2107-2116A
- Superconductivity**
Solidification of Nb-Ge Alloys in Long Drop Tubes. 973-981A
- Supercooling**
Solidification of Nb-Ge Alloys in Long Drop Tubes. 973-981A
- Superplasticity**
The C.L. m- δ Equation of Superplasticity.
Dependence of Total Elongations of Superplastic Materials on m.
Superplasticity in a Thermomechanically Processed High-Magnesium, Al-Mg Alloy.
The Influence of Thermomechanical Processing Variables on Superplasticity in a High-Magnesium, Al-Mg Alloy.
Superplasticity of a Stainless Steel Clad Ultrahigh Carbon Steel. 679-684A
685-690A
1035-1041A
1043-1050A
2295-2298A
- Superplasticity, Alloying effects**
The Effect of Alloying Additions on the Superplastic Properties of Ti-6Al-4V.
Superplastic Behavior of a Zn-22Al-0.5Cu Alloy. 93-106A
1873-1875A
- Surface chemistry, Heating effects**
Lithium Depletion During Heat Treatment of Aluminum-Lithium Alloys. 635-643A
- Surface cleaning**
See Cleaning
- Surface diffusion**
See Diffusion
- Surface hardening**
See Carburizing
- Surface properties**
See Surface structure
Surface tension
- Surface structure**
Modulated Microstructures in β Cu-Zn-Al. 2153-2161A
- Surface structure, Diffusion effects**
Phase Transformation of Austenitic Stainless Steels as a Result of Cathodic Hydrogen Charging. 1593-1600A
- Surface structure, Stress effects**
Metallic Surface Layers Deposited by Diffusional Creep During Internal Oxidation. 746-749A
- Surface tension**
Comparison of Surface Tension Measurements Using the Levitated Droplet Method.
The Temperature Coefficient of the Surface Tension of Pure Liquid Metals.
Interfacial Tension and Flotation Characteristics of Liquid Metal-Sodium Flux Systems.
Measurement of the Surface Tensions of Iron-Saturated Iron Silicate and Iron-Saturated Calcium Ferrite Melts by Paday's Cone Technique. 159-162B
163-170B
339-346B
771-776B
- Surface tension, Field effects**
Electrocapillarity in the Aluminum Reduction Cell. 547-552B
- Susceptibility (magnetic)**
See Magnetic permeability

- Synthetic coke**
See Coke
- Systems (metallurgical)**
See Binary systems
Quaternary systems
Quinary systems
Ternary systems
- Taconite, Reduction (chemical)**
Application of Thermodynamic and Kinetic Principles in the Reduction of Metal Oxides by Carbon in a Plasma Environment. 197-207B
- Tanks (electrolytic)**
See Electrolytic cells
- Tantalum, Alloying additive**
The Effects of Tantalum on the Microstructure of Two Polycrystalline Nickel-Base Superalloys: B-1900 + Hafnium and MAR-M247. 1891-1905A
- Tantalum, Mechanical properties**
Effects of Nitrogen on the Mechanical Behavior of Hydrogenated Vanadium, Niobium, and Tantalum. 527-535A
Effects of Oxygen on the Mechanical Behavior of Hydrogenated Vanadium, Niobium, and Tantalum. 853-859A
The Effects of Interstitials and Hydrogen-Interstitial Interactions on Low Temperature Hardening and Embrittlement in Vanadium, Niobium, and Tantalum. 1179-1189A
- Tantalum, Solubility**
Alloying Behavior of Co_2Ti . 1433-1439A
- Tapes (metallic), Crystal lattices**
Fault Structures in Rapidly Quenched Ni—Mo Binary Alloys. 2291-2294A
- Tellurides**
Thermodynamic Properties and Defect Structure of Semiconducting Compound Phases: Tin Telluride. 1241-1245A
- Tellurium, Alloying elements**
Activity Coefficient of Oxygen in Copper—Tellurium Melts. 171-177B
- Tellurium, Environment**
Liquid Cesium Tellurium-Induced Fatigue Embrittlement of Cold-Worked 316 Stainless Steel. 2090-2093A
- Temper brittleness**
New Considerations on Tempered Martensite Embrittlement. 745-746A
- Temperature**
See Critical temperature
Eutectic temperature
Glass transition temperature
Transition temperature (superconductivity)
- Tempering**
See also Quenching and tempering
The Influence of Precipitated Austenite on Hydrogen Embrittlement in 5.5Ni Steel. 1157-1164A
Fracture Behavior in Medium-Carbon Martensitic Silicon- and Nickel-Steels. 1173-1178A
- Tenacity**
See Tensile strength
- Tensile modulus**
See Modulus of elasticity
- Tensile properties**
See also Elongation
Reduction of area
Tensile strength
Yield strength
Fatigue Crack Growth and Fracture Toughness Behavior of an Al—Li—Cu Alloy. 1011-1026A
The Influence of Precipitated Austenite on Hydrogen Embrittlement in 5.5Ni Steel. 1157-1164A
- Tensile properties, Alloying effects**
The Microstructure and Mechanical Properties of a Modified 2.25Cr—1Mo Steel. 1027-1034A
- Tensile properties, Deformation effects**
Effect of Isothermal Forging on Microstructure and Fatigue Behavior of Blended Elemental Ti—6Al—4V Powder Compacts. 549-559A
The Effect of Hot-Rolling on Chill-Cast Al— Al_3Ni , Chill-Cast Al— Al_2Cu , and Unidirectionally Solidified Al— Al_3Ni Eutectic Alloys. 1985-1993A
- Tensile properties, Microstructural effects**
Orientation and Temperature Dependence of Some Mechanical Properties of the Single-Crystal Nickel-Base Superalloy René N4. I. Tensile Behavior. 491-496A
Tensile Properties of Directionally Solidified Al—4Cu Alloys With Columnar and Equiaxed Grains. 823-832A
Microstructure—Mechanical Property Relationships in Isothermally Transformed Vanadium Steels. 1191-1202A
- Tensile properties, Stress effects**
Flow Behavior of an Aluminum-Killed Steel After Tensile Prestraining and Strain-Aging. 1573-1575A
- Tensile shear strength**
See Shear strength
- Tensile strength**
Superplasticity in a Thermomechanically Processed High-Magnesium, Al—Mg Alloy. 1035-1041A
The Influence of Thermomechanical Processing Variables on Superplasticity in a High-Magnesium, Al—Mg Alloy. 1043-1050A
The Effect of Thermal Exposure on the Microstructure and Fiber/Matrix Interface of an $\text{Al}_2\text{O}_3/\text{Al}$ Composite. 1075-1080A
The Processing and Properties of Heavily Cold Worked Directionally Solidified Ni—W Eutectic Alloys. 1165-1171A
- Mechanical Properties and Microstructure of Al—Li—Cu—Mg—Zr Die Forgings. 2007-2016A
- Tensile strength, Microstructural effects**
Orientation and Temperature Dependence of Some Mechanical Properties of the Single-Crystal Nickel-Base Superalloy René N4: III. Tension—Compression Anisotropy, Microstructural Dependence of Iron—High Manganese Tensile Behavior. 507-512A
537-547A
- Tensile strength, Stress effects**
Thermal Transient Stresses Due to Rapid Cooling in a Thermally and Elastically Orthotropic Medium. 1051-1055A
- Tensile tests**
See Tension tests
- Tensile yield strength**
See Yield strength
- Tension**
See Surface tension
- Tension tests**
Unloading Yield Effects in Aluminum Alloys. 121-126A
Instabilities During Tension of Thin Voided Viscoplastic Sheets. 1637-1640A
- Ternary systems, Diffusion**
Estimation of Diffusion Path Slopes at Zero-Flux Plane Compositions. 382-364A
- Ternary systems, Phases (state of matter)**
A Solid-State EMF Study of Ternary Ni—S—O, Fe—S—O, and Quaternary Fe—Ni—S—O. 133-146B
Discussion of "The Grain Refining of Aluminum and Phase Relationships in the Al—Ti—B System" and Reply. 349-351A
Thermodynamics of the Fe—Mo—C System at 985K. 391-398A
Direct Use of the Chemical Potential Function in Thermodynamic Modeling of Alloy Phase Diagrams. 1471-1477A
Balance of Distribution of Some Transition Metals Between the $(\text{M}', \text{M}'')\text{B}$ and $(\text{M}', \text{M}'')_2\text{B}$ Phases. 1665-1669A
Experimental and Theoretical Study of the Phase Equilibria in the Fe—Ni—W System. 1809-1823A
- Ternary systems, Thermal properties**
Computation of Thermodynamic Properties of Multi-Component Solutions: Extension of Toop Model. 1102-1104A
- Texture**
See also Rolling texture
The Effect of Thermomechanical History Upon the Microstructure and Magnetic Properties of Nonoriented Silicon Steels. 1267-1275A
New Information on Texture Development in Regular and High-Permeability Grain-Oriented Silicon Steels. 1301-1312A
Origin and Development of Through-the-Thickness Variations of Texture in the Processing of Grain-Oriented Silicon Steel. 1313-1322A
Description of the Intercrystalline Structure Distribution in Polycrystalline Materials. 2199-2207A
- Texture, Deformation effects**
Formation of the Goss Orientation Near the Surface of 3% Silicon Steel During Hot Rolling. 1323-1334A
- Thermal analysis**
See Differential thermal analysis
- Thermal flux**
See Heat transmission
- Thermal measurements**
See Calorimetry
- Thermal properties**
See Heat of formation
Heat of mixing
Heat of solution
Thermal stability
Volatility
- Thermal reduction**
See Flash smelting
- Thermal stability**
The Effect of Thermal Exposure on the Microstructure and Fiber/Matrix Interface of an $\text{Al}_2\text{O}_3/\text{Al}$ Composite. 1075-1080A
- Thermal stresses**
Thermal Transient Stresses Due to Rapid Cooling in a Thermally and Elastically Orthotropic Medium. 1051-1055A
- Thermochemistry**
Rates of Dissolution of Solid Iron, Cobalt, Nickel, and Silicon in Liquid Copper and Diffusion Rate of Iron From Liquid Cu—Fe Alloy Into Liquid Copper. 291-305B
- Thermodynamics**
An Investigation of the Thermodynamics and Kinetics of the Ferric Chloride Brine Leaching of Galena Concentrate. 29-39B
"Central Atoms" Models for Ternary Silicate and Alumino-Silicate Melts. 105-110B
Activity of Arsenic in Molten Lead. 235-238B
Thermodynamic Study of Fe_2O_3 — $\text{Fe}_2(\text{SO}_4)_3$ Equilibrium Using an Oxidation Electrolyte (Na_2SO_4 —I). 323-329B
Thermodynamics of the Fe—Mo—C System at 985K. 391-398A
Thermodynamics of the Si—C—O System for the Production of Silicon Carbide and Metallic Silicon. 503-514B
Electrochemical Determination of Thermodynamic Properties and X-Ray Diffraction Investigation of the Fe_2O_3 — ZnFe_2O_4 System. 515-521B
Thermodynamic Analysis of Ordered Liquid Solutions by a Modified Quasichemical Approach—Application to Silicate Slags. 805-815B

Thermodynamics

- Computation of Thermodynamic Properties of Multi-Component Solutions: Extension of Toop Model. 1102-1104A
- A Solid-State EMF Study of the Cu—Cu₂O—NiO Three-Phase Equilibrium. 1104-1106A
- A Modified Interaction Parameter Formalism for Non-Dilute Solutions. 1211-1215A
- Thermodynamic Properties and Defect Structure of Semiconducting Compound Phases: Tin Telluride. 1241-1245A
- Magnetic Contributions to the Thermodynamic Functions of Alloys and the Phase Equilibria of Fe—Ni System Below 1200K. 1361-1372A
- Direct Use of the Chemical Potential Function in Thermodynamic Modeling of Alloy Phase Diagrams. 1471-1477A
- An Ambiguity in the Definition of the Activity Coefficient at Infinite Dilution. 1484-1485A
- Thermodynamic Properties of Carbides in 2.25Cr—1Mo Steel at 985K. 1585-1592A
- A Modified Regular-Solution Model for Terminal Solutions. 1878-1879A
- Thermoelastic properties**
See Internal friction
Shape memory
- Thermomechanical treatment**
Deformation and Transition Behavior Associated With the R-Phase in Ti—Ni Alloys. 53-63A
- Superplasticity in a Thermomechanically Processed High-Magnesium, Al—Mg Alloy. 1035-1041A
- The Influence of Thermomechanical Processing Variables on Superplasticity in a High-Magnesium, Al—Mg Alloy. 1043-1050A
- Modification of α Morphology in Ti—6Al—4V by Thermomechanical Processing. 1935-1947A
- Thermostability**
See Thermal stability
- Tig arc welding**
See Gas tungsten arc welding
- Tilting furnaces**
See Basic converters
Bottom blown converters
Copper converters
Top blown converters
- Tilting rotary furnaces**
See Rotary converters
- Tin, Binary systems**
A Theoretical Evaluation of Chemical Ordering and Glass Transition in Liquid Mg—Sn Alloys. 607-615A
- Calorimetric and Emf Studies on Liquid Li—Sn Alloys. 791-796B
- Effect of Small Additions of Silver on the Eutectic Temperature in the Lead—Tin System. 829-832B
- Tin, Extraction**
The Slag—Metal Equilibrium in Tin Smelting. 61-68B
- Tin, Physical properties**
Interfacial Tension and Flotation Characteristics of Liquid Metal—Sodium Flux Systems. 339-346B
- Tin, Powder technology**
An Empirical Model for Hot Isostatic Pressing of Metal Powders. 1977-1984A
- Tin, Reactions (chemical)**
Rate of Dissolution of Solid Nickel in Liquid Tin Under Static Conditions. 281-289B
- Tin base alloys, Crystal growth**
The Effect of Convection on the Dendrite to Eutectic Transition. 991-1000A
- Tin compounds, Superconductivity**
The Effect of High Temperature Plastic Flow on the Superconducting Transition in A15 Compounds. 399-405A
- Tin compounds, Thermal properties**
Thermodynamic Properties and Defect Structure of Semiconducting Compound Phases: Tin Telluride. 1241-1245A
- Titanium, Alloying elements**
Processing of Iron—Titanium Powder Mixtures by Transient Liquid Phase Sintering. 205-213A
- Titanium, Ternary systems**
Discussion of "The Grain Refining of Aluminum and Phase Relationships in the Al—Ti—B System" and Reply. 349-351A
- Titanium base alloys, Composite materials**
Structure-Performance Maps of Polymeric, Metal, and Ceramic Matrix Composites. 1547-1559A
- Titanium base alloys, Diffusion**
On the Effective Hydrogen Permeability in Metastable β Titanium Alloy, Niobium and 2.25Cr—1Mo Ferritic Steel. 2086-2090A
- Titanium base alloys, Mechanical properties**
The Effect of Alloying Additions on the Superplastic Properties of Ti—6Al—4V. 93-106A
- Effect of Cyclic Deformation on the Pseudoelasticity Characteristics of Ti—Ni Alloys. 115-120A
- Influence of Foreign Particles on Fatigue Behavior of Ti—6Al—4V Prealloyed Powder Compacts. 271-280A
- Deformation of a Burgers Oriented Bimetallic Bicrystal of α — β (Ti—13Mn). 451-460A
- Effect of Isothermal Forging on Microstructure and Fatigue Behavior of Blended Elemental Ti—6Al—4V Powder Compacts. 549-559A
- Dependence of Total Elongations of Superplastic Materials on n. 685-690A
- A Rationalization of Stress—Strain Behavior of Two-Ductile Phase Alloys. 2209-2226A
- Titanium base alloys, Phase transformations**
Deformation and Transition Behavior Associated With the R-Phase in Ti—Ni Alloys. 53-63A
- Transmission Electron Microscopic Observations of Mechanical Twinning in Metastable β Titanium Alloys. 1409-1420A
- Precipitation Processes in Near-Equiatomic TiNi Shape Memory Alloys. 1505-1515A
- Nucleation, Growth, and Overall Transformation Kinetics of Grain Boundary Allotriomorphs of Proeutectoid α in Ti—3.2 at.% Co and Ti—6.6 at.% Cr Alloys. 1703-1715A
- Titanium base alloys, Phases (state of matter)**
Modification of α Morphology in Ti—6Al—4V by Thermomechanical Processing. 1935-1947A
- Titanium compounds, Impurities**
The Vapor—Liquid Equilibria of the Aluminum Chloride—Titanium Tetrachloride System. 609-610B
- Titanium compounds, Phase transformations**
Precipitation Processes in Near-Equiatomic TiNi Shape Memory Alloys. 1505-1515A
- Titanium compounds, Solubility**
Alloying Behavior of Co₃Ti. 1433-1439A
- Titanium compounds, Thermal properties**
Standard Enthalpies of Formation of TiSi₂ and VS₂ by High-Temperature Calorimetry. 1217-1221A
- Tool steels, Microstructure**
Microstructural Analysis of Residual Projectiles—a New Method to Explain Penetration Mechanisms. 435-442A
- Top blown converters**
Model Study of Mixing and Mass Transfer Rates of Slag-Metal in Top and Bottom Blown Converters. 461-469B
- Torsional strength**
See Shear strength
- Toughness**
See Fracture toughness
- Tracers, Diffusion**
Tracer Diffusion in Mercury: a Predictive Equation. 355-358A
- Transferring**
See Heat transfer
Mass transfer
- Transformations (materials)**
See Allotropic transformation
Martensitic transformations
Phase transformations
- Transformer steels**
See Electrical steels
- Transgranular fracture**
Fracture of Fe₃Al. 2298-2300A
- Transition joints, Diffusion**
A Simplified Treatment of Carbon Diffusion in Compound Welds Having an Intermediate Layer. 2083-2084A
- Transition metal alloys**
See Cadmium base alloys
Cobalt base alloys
Copper base alloys
Ferrous alloys
Manganese base alloys
Nickel base alloys
Niobium base alloys
Palladium base alloys
Titanium base alloys
Tungsten base alloys
Vanadium base alloys
Zinc base alloys
Zirconium base alloys
- Transition metal compounds**
See Chromium compounds
Cobalt compounds
Copper compounds
Iron compounds
Iron oxides
Molybdenum compounds
Nickel compounds
Niobium compounds
Scandium compounds
Titanium compounds
Tungsten carbide
Tungsten compounds
Vanadium compounds
Zinc compounds
- Transition metals**
See also Chromium
Cobalt
Copper
Gold
Hafnium
Iron
Manganese
Mercury (metal)
Molybdenum
Nickel
Niobium
Platinum
Silver
Tantalum
Titanium
Tungsten

- Vanadium
Yttrium
Zinc
Zirconium
- Transition metals, Physical properties**
Comparison of Surface Tension Measurements Using the Levitated Droplet Method. 159-162B
The Temperature Coefficient of the Surface Tension of Pure Liquid Metals. 163-170B
- Transition temperature (superconductivity), Deformation effects**
The Effect of High Temperature Plastic Flow on the Superconducting Transition in A15 Compounds. 399-405A
- Transmission**
See Heat transmission
- Transmission electron microscopy**
Surface Oxide on fcc Iron—Nickel Alloys. 163-167A
- Traps**
The Interaction of Hydrogen With the Interface of Al_2O_3 Particles in Iron. 2183-2186A
- Tubes**
See Capillary tubes
- Tundishes, Design**
Mathematical Modeling of Flows in Large Tundish Systems in Steelmaking. 449-459B
- Tungsten, Crystal growth**
A Model for the Formation of the Non-Sag Structure of Potassium-Doped Tungsten Wire. 1455-1459A
- Tungsten, Solubility**
Alloying Behavior of Co_3Ti . 1433-1439A
- Tungsten, Ternary systems**
Experimental and Theoretical Study of the Phase Equilibria in the Fe—Ni—W System. 1809-1823A
- Tungsten arc welding**
See Gas tungsten arc welding
- Tungsten base alloys, Mechanical properties**
The Processing and Properties of Heavily Cold Worked Directionally Solidified Ni—W Eutectic Alloys. 1165-1171A
- Tungsten base alloys, Microstructure**
Microstructural Analysis of Residual Projectiles—a New Method to Explain Penetration Mechanisms. 435-442A
- Tungsten base alloys, Powder technology**
An Analysis of the Surface Menisci in a Mixture of Liquid and Deformable Grains. 325-330A
The Effect of the Binder Phase Melting Temperature on Enhanced Sintering. 903-906A
The Critical Grain Size for Liquid Flow Into Pores During Liquid Phase Sintering. 1915-1919A
- Tungsten base alloys, Structural hardening**
Matrix and Interfacial Precipitation in the W—Ni—Fe System. 1921-1934A
- Tungsten carbide, Thermal properties**
Gibbs Free Energies of Formation of Molybdenum Carbide and Tungsten Carbide From 1173-1573K. 2031-2034A
- Tungsten compounds**
See also Tungsten carbide
- Tungsten compounds, Thermal properties**
Gibbs Free Energies of Formation of Molybdenum Carbide and Tungsten Carbide From 1173-1573K. 2031-2034A
- Turbine blades, Coating**
CVD Aluminide Nickel. 215-220A
- Turbines**
See Gas turbines
- Turbulent flow**
Turbulent Recirculating Flow in Induction Furnaces: a Comparison of Measurements With Predictions Over a Range of Operating Conditions. 687-693B
- Tuyeres**
Heat Flow in Copper Converters. 677-685B
- Twinning**
See also Mechanical twinning
Deformation of Martensite in a Polycrystalline Cu—Zn—Al Alloy. 945-959A
Strain Hardening of Hadfield Manganese Steel. 1725-1737A
- Ultimate shear strength**
See Shear strength
- Ultimate tensile strength**
See Tensile strength
- Undercooling**
See Supercooling
- Uranium, Extraction**
Electrolytic Reduction of Uranium(VI) to Uranium(IV) in Acidic Chloride and Acidic Sulfate Solutions. 41-50B
Laboratory Reduction Rate and Current Efficiency Studies of Batch Type Electrolytic Reduction of Uranium(VI) in a Sulfate System. 69-76B
Acid Rate- and Flow-Controlled Dissolution of Uraninite Ores. 405-413B
- Uranium, Oxidation**
Complex Defects in the Oxidation of Uranium. 911-914A
- Uranium, Phase transformations**
The β -to- α Phase Transformation in a Uranium Alloy. 1717-1723A
- Vacancies (crystal defects)**
See Lattice vacancies
- Vacancies (lattice)**
See Lattice vacancies
- Vacuum arc furnaces**
Relationship Between Furnace Voltage Signatures and the Operational Parameters Arc Power, Arc Current, CO Pressure, and Electrode Gap During Vacuum Arc Melting Inconel 718. 357-365B
- Vacuum arc melting**
Relationship Between Furnace Voltage Signatures and the Operational Parameters Arc Power, Arc Current, CO Pressure, and Electrode Gap During Vacuum Arc Melting Inconel 718. 357-365B
- Vacuum brazing**
Examination of the Titanium Environment in a René 41 Nickel Base Superalloy by X-Ray Absorption Spectroscopy. 739-741A
- Vacuum furnaces**
See Vacuum arc furnaces
- Vacuum melting**
See Vacuum arc melting
- Vacuum refining**
A Kinetic Model for the Vacuum Refining of Inductively Stirred Copper Melts. 87-103B
- Vanadium, Alloying additive**
The Microstructure and Mechanical Properties of a Modified 2.25Cr—1Mo Steel. 1027-1034A
- Vanadium, Alloying elements**
Precipitation and Ostwald Ripening in Dilute Aluminum Base—Zr—V Alloys. 2187-2198A
- Vanadium, Binary systems**
The Vanadium—Nitrogen System: a Review. 1647-1656A
- Vanadium, Diffusion**
Hydrogen and Deuterium Diffusion in Vanadium—Niobium Alloys. 645-650A
- Vanadium, Mechanical properties**
Effects of Nitrogen on the Mechanical Behavior of Hydrogenated Vanadium, Niobium, and Tantalum. 527-535A
Effects of Oxygen on the Mechanical Behavior of Hydrogenated Vanadium, Niobium, and Tantalum. 853-859A
The Effects of Interstitials and Hydrogen-Interstitial Interactions on Low Temperature Hardening and Embrittlement in Vanadium, Niobium, and Tantalum. 1179-1189A
- Vanadium, Solubility**
Alloying Behavior of Co_3Ti . 1433-1439A
Thermotransport of Carbon in Two-Phase V—C and Nb—C Alloys. 1955-1966A
- Vanadium base alloys, Diffusion**
Hydrogen and Deuterium Diffusion in Vanadium—Niobium Alloys. 645-650A
- Vanadium base alloys, Mechanical properties**
High-Temperature Plastic Deformation of Two V—Ga Alloys With A15 Structure. 519-525A
- Vanadium compounds, Thermal properties**
Standard Enthalpies of Formation of $TiSi_2$ and VS_2 by High-Temperature Calorimetry. 1217-1221A
- Vanadium steels**
See also Chromium molybdenum vanadium steels
- Vanadium steels, Mechanical properties**
Microstructure—Mechanical Property Relationships in Isothermally Transformed Vanadium Steels. 1191-1202A
- Vapor deposition**
See Vapor deposition coating
- Vapor deposition coating**
CVD Aluminide Nickel. 215-220A
- Vaporizing**
Thermodynamics of Gaseous SbS. 913-914B
- Vapors**
See Metal vapors
Water vapor
- Viscosity**
A Calculation of Viscosities for Iron—Metalloid Liquids. 901-903A
- Volatility**
The Formation of Volatile Corrosion Products During the Mixed Oxidation—Chlorination of Cobalt at 650°C. 1223-1228A
- Volatilizing**
See Vaporizing
- Warm working**
Superplasticity in a Thermomechanically Processed High-Magnesium, Al—Mg Alloy. 1035-1041A
The Influence of Thermomechanical Processing Variables on Superplasticity in a High-Magnesium, Al—Mg Alloy. 1043-1050A
- Washing**
See Gas scrubbing
- Water vapor, Environment**
Complex Defects in the Oxidation of Uranium. 911-914A
- Wear**
See Hot gas corrosion

Wear resistance

Wear resistance

- Wear Resistance of Quenched and Tempered AISI 4137H Steel. 295-306A

Weld defects

- Solidification and Solidification Cracking in Nitrogen-Strengthened Austenitic Stainless Steels. 727-737A
The Welding Metallurgy of Hastelloy Alloys C-4, C-22, and C-276. 2035-2047A
The Use of New PHACOMP in Understanding the Solidification Microstructure of Nickel Base Alloy Weld Metal. 2107-2116A

Weld metal

- A Model for the Silicon-Manganese Deoxidation of Steel Weld Metals. 1797-1807A

Weld metal, Crystal growth

- The Role of Transient Convection in the Melting and Solidification in Arc Weldpools. 735-744B

Weld metal, Microstructure

- The Use of New PHACOMP in Understanding the Solidification Microstructure of Nickel Base Alloy Weld Metal. 2107-2116A

Weldability

- Solidification and Solidification Cracking in Nitrogen-Strengthened Austenitic Stainless Steels. 727-737A
Resistance Spot Welding of Galvanized Steel. I. Material Variations and Process Modifications. 879-885B
Metal Vapors in Gas Tungsten Arcs. I. Spectroscopy and Monochromatic Photography. 1851-1863A
Metal Vapors in Gas Tungsten Arcs. II. Theoretical Calculations of Transport Properties. 1865-1871A
The Welding Metallurgy of Hastelloy Alloys C-4, C-22, and C-276. 2035-2047A

Welded joints, Crystal growth

- Computer Simulation of Convection in Moving Arc Weld Pools. 2271-2277A

Welded joints, Mechanical properties

- Discussion of "Fundamental Aspects of Formation and Stability of Explosive Welds" and Reply. 374A

Welded joints, Phases (state of matter)

- Inclusion Phases and the Nucleation of Acicular Ferrite in Submerged Arc Welds in High Strength Low Alloy Steels. 1611-1623A

Welded joints, Thermal properties

- Computer Modeling of Heat Flow in Welds. 587-600B

Welding

- See Arc welding
Diffusion welding
Gas metal arc welding
Gas tungsten arc welding
Laser beam welding
Plasma arc welding
Resistance spot welding
Spot welding
Submerged arc welding

Welding parameters

- Resistance Spot Welding of Galvanized Steel. I. Material Variations and Process Modifications. 879-885B
Resistance Spot Welding of Galvanized Steel. II. Mechanisms of Spot Weld Nugget Formation. 887-901B
Metal Vapors in Gas Tungsten Arcs. II. Theoretical Calculations of Transport Properties. 1865-1871A

Welds

- See Welded joints

Widmanstätten structure

- On the Formation of Widmanstätten Austenite. 741A

Wire, Crystal growth

- A Model for the Formation of the Non-Sag Structure of Potassium-Doped Tungsten Wire. 1455-1459A

Wolfram

- See Tungsten

Work hardening

- See Strain hardening

Work softening

- See Strain softening

Work strengthening

- See Strain hardening

Workability

- See also Formability

Workability, Heating effects

- Influence of Soaking Treatments on Hot Ductility of Al-4.85Mg Alloys Containing Manganese. 833-841A

Wustite

- On the Gibbs Energy of Formation of Wustite. 179-184B

Wustite, Reduction (chemical)

- The Gaseous Reduction of Solid Calcicowustites in CO/CO₂ and H₂O Gas Mixtures. 375-381B
The Effect of Sulfur on the Gaseous Reduction of Solid Calcicowustites. 383-393B
An Investigation of the Critical Influence of Potassium on the Reduction of Wustite. 657-663B

Yield strength

- Numerical Modeling of the Propagation of an Adiabatic Shear Band. 443-450A
High-Temperature Plastic Deformation of Two V-Ga Alloys With A15 Structure. 519-525A
Characterization and Modeling of the High Temperature Flow Behavior of Aluminum Alloy 2024. 2227-2237A

Yield strength, Alloying effects

- The Effects of Replacing the Refractory Elements Tungsten, Niobium, and Tantalum With Molybdenum in Nickel-Base Superalloys on Microstructural, Microchemistry, and Mechanical Properties. 651-661A
Effect of Aluminum Content on Low Temperature Tensile Properties in Cryogenic Fe/Mn/Al/Nb/C Steels. 2097-2098A

Yield strength, Cooling effects

- Microstructures and Mechanical Properties of Melt-Quenched Ferritic Stainless Steels. 261-269A

Yield strength, Deformation effects

- Unloading Yield Effects in Aluminum Alloys. 121-126A

Yield strength, Diffusion effects

- Effects of Nitrogen on the Mechanical Behavior of Hydrogenated Vanadium, Niobium, and Tantalum. 527-535A

Yield strength, Impurity effects

- Effects of Oxygen on the Mechanical Behavior of Hydrogenated Vanadium, Niobium, and Tantalum. 853-859A
The Effects of Interstitials and Hydrogen-Interstitial Interactions on Low Temperature Hardening and Embrittlement in Vanadium, Niobium, and Tantalum. 1179-1189A

Yield strength, Microstructural effects

- A Model for Yielding in Anisotropic Metals. 107-114A
Orientation and Temperature Dependence of Some Mechanical Properties of the Single-Crystal Nickel-Base Superalloy René N4: III. Tension-Compression Anisotropy. 507-512A
Microstructural Dependence of Iron-High Manganese Tensile Behavior. 537-547A
Effect of Microstructure on Strength and Toughness of Heat-Treated Low Alloy Structural Steels. 1203-1209A
A Rationalization of Stress-Strain Behavior of Two-Ductile Phase Alloys. 2209-2226A

Yield stress

- See Yield strength

Youngs modulus

- See Modulus of elasticity

Yttrium, Alloying additive

- A Relationship Between Indigenous Impurity Elements and Protective Oxide Scale Adherence Characteristics. 923-932A

Zinc, Diffusion

- Anomalous Fast Diffusion in the Fe-Zn System. 1523-1527A

Zinc, Extraction

- Electrochemical Determination of Thermodynamic Properties and X-Ray Diffraction Investigation of the Fe₃O₄-ZnFe₂O₄ System. 515-521B
Agglomeration of Particles During Roasting of Zinc Sulfide Concentrates. 647-656B

Zinc, Mechanical properties

- A Model for Yielding in Anisotropic Metals. 107-114A

Zinc, Ternary systems

- Estimation of Diffusion Path Slopes at Zero-Flux Plane Compositions. 362-364A

Zinc base alloys, Mechanical properties

- The C.L. m-δ Equation of Superplasticity. 679-684A
Superplastic Behavior of a Zn-22Al-0.5Cu Alloy. 1873-1875A

Zinc compounds, Ternary systems

- Electrochemical Determination of Thermodynamic Properties and X-Ray Diffraction Investigation of the Fe₃O₄-ZnFe₂O₄ System. 515-521B

Zirconium, Alloying elements

- Decomposition Characteristics of Al-Mn-Zr Alloys Rapidly-Quenched From the Melt. 799-806A
Precipitation and Ostwald Ripening in Dilute Aluminum Base-Zr-V Alloys. 2187-2198A

Zirconium base alloys, Welding

- The Diffusion Bonding of Zr-2.5Nb to Steel. 429-434A

